APPLICATION OF NANOPARTICLES AS PROPPANTS AND BREAKER ENCAPSULATING AGENTS

By

CHARLES CHEMPAKATHINAL BOSE

Submitted to the graduate degree program in Department of Chemical & Petroleum Engineering and the Graduate Faculty of the University of Kansas in partial fulfillment of the requirements for the degree of Master of Science.

_____

Dr. Reza Barati

(Chairperson)

_____

Dr. Paul Willhite

_____

Dr. Stephen Johnson

Date Defended: 06/10/2016

The Thesis Committee for Charles Chempakathinal Bose

Certifies that this is the approved version of the following thesis:

APPLICATION OF NANOPARTICLES AS PROPPANTS AND BREAKER ENCAPSULATING AGENTS

_____

Dr. Reza Barati (Chairperson)

Date approved: 07/26/2016

Abstract

Guar-based fluids are commonly used as fracturing fluids to form a filter cake, propagate the fracture and carry proppants during a typical hydraulic fracturing job. In order to achieve a conductive fracture, cross-linkers and breakers are added to the fluid to degrade the polymer gel and filter cake before the start of production. Enzymes and oxidizers are the two main classes of breakers. Enzyme breakers are preferred over oxidizers as they are cheap, non-corrosive, environmentally benign, easy to handle and since they are not consumed during the reaction.

Different methods of injecting high concentration breakers are still not capable of degrading the residues left after the fracturing jobs. Permeability reduction of the proppant pack caused by incomplete degradation of polymer gel is well known [1]. It has been previously proven that polyethylenimine-dextran sulfate (PEI-DS) nanoparticles can delay the release of enzymes and protect enzymes against alkaline environments [2]. This delayed release helps in injecting higher concentrations of enzymes by encapsulating them inside nanoparticles, thereby reduces the possibility of viscosity degradation during injection. Injecting higher concentrations of enzymes will help in better clean-up of proppant pack thus increasing the proppant pack permeability. However, performance of these nanoparticles in reaction with high concentration filter cakes has not been studied yet.

In this work, feasibility of using PEI-DS nanoparticles as enzyme breaker carriers and fluid loss additives for hydraulic fracturing applications was studied. Static fluid loss tests showed a significant reduction in both fluid loss coefficients and fluid loss volumes when PEI-DS nanoparticles were used as fluid loss additives with core samples having 0.1-10 mD permeability. The fluid loss reduction capabilities will help in generating longer fractures. Long term fracture

conductivity tests showed that fracture conductivity of the proppant pack increased, when enzyme was entrapped inside PEI-DS nanoparticles instead of using them directly. Hence the use of PEI-DS nanoparticles helps in injecting higher concentrations of enzymes (due to delayed release), generating longer fractures (due to reduced fluid loss) and generating more conductive fractures (proven by fracture conductivity tests).

Fracturing jobs in tight shale plays using slickwater fluids tend to generate or extend a large network of micro-fractures during the injection of fracturing fluids. Small fractures tend to close under closure stress unless a nano-sized proppant with significant stress resistance is injected to keep these micro-fractures opened. Proppants with different mesh sizes of 20/40, 30/50, 40/70, 70/140 and 80/200 with grain diameters ranging from 0.033 inch (0.8382 mm) to 0.0041 inch (104.14 μm) are used during hydraulic fracturing of tight shale formations. These proppants are large enough to create conductivity in the larger generated or existing fractures but not small enough to penetrate into the existing or generated micro-fractures. This will cause the closure of micro-fractures at the end of the fracturing job thereby reducing the length and conductivity of the complex fracture network.

An ideal proppant material should be hard enough to withstand the stress encountered in the formation and should form a conductive path for the flow of hydrocarbons while keeping the fractures open. Conventionally used sand proppants are tested for crush strength between 4000 and 12,000 psi and are designed to retain at least 90 % of their basic fracture conductivity under this pressure [3]. Brady sand and Ottawa sand are popularly used proppant types. Pure quartz has hardness of 7 Mohs (roughly 11.39 GPa) [4]. In order to be used as nano-proppants, particles, in addition to sphericity, hardness, reduced elastic modulus, and size must be tested. The ultimate

testing of nano-proppants is the so-called API conductivity testing, which is designed to measure the performance of particles under stress in keeping the fracture open to flow.

The second part of this work is focused on investigation of size, hardness, reduced elastic modulus, fluid loss prevention capabilities as well as the fracture conductivity induced by ‘fly ash nanoparticles’ when used as nano-proppants. Transmission Electron Microscope (TEM) images showed that fly ash nanoparticles are spherical in shape with particle sizes varying from 100 nm to 800 nm. Particles showed hardness and reduced elastic moduli of 1.3 GPa and 20 GPa, respectively, significant fluid loss reduction capabilities when tested with (1-10) mD permeability cores and showed good fracture conductivity results when used as proppants in an API fracture conductivity test. These properties show the potential of these nanoparticles to be used as proppants.

Acknowledgments

First and foremost, I would like to express my gratitude to Prof. Reza Barati for his unwavering trust and support without which this research would not have been possible. He is a great source of guidance and encouragement.

I greatly appreciate the time and effort put into this work by my committee members Prof. Paul Willhite and Dr. Stephen Johnson. Their valuable comments have helped me in improving the whole research. I would like to thank the Society of Petroleum Engineers (SPE), School of Engineering (New Faculty General Research Fund) and Kansas Interdisciplinary Carbonate Consortium (KICC) for funding my research work. I appreciate the help from Mr. Alan Walker, Mr. Scot Ramskill, and Mr. Jeff Curley in setting up the equipment in the laboratory. I would also like to thank Mr. Levi Swartz and Mr. Bader Alshatti, who helped me in conducting the fracture conductivity experiments.

Finally, I would like extend my appreciation to all my wonderful friends in the department who have supported me during the course of my student life.

I affectionately dedicate this work to my parents (Tessy K. Mathews and C.M Bose) who are my biggest source of inspiration and my sister (Christy C. Bose).

Contents

List of Figures

List of Tables

1. Introduction

1.1 Nano-Particles as Fracturing Fluid Additives in Hydraulic Fracturing of Conventional Reservoirs

Hydraulic fracturing is a commonly used practice in the oil industry for well stimulation and production enhancement. To create a fracture hydraulically, a fluid must be pumped at high enough pressure to overcome the tensile strength of the rock and at high enough rate to cause the extension of the fracture into the formation. Additives are added to the fracturing fluids to increase its viscosity so as to enhance its proppant carrying ability and hydrostatic potential. Guar gum is one of the most commonly used agents to viscosify aqueous based fracturing fluids [5].

During the injection and shut-in period, the fracturing fluids inside the fracture are acted upon by the overburden stress which causes the formation of filter cake with high polymer concentration on the two faces of the fracture and the resultant fluid filtrate leaks off into the matrix. The more the fluid is lost into the formation, the less is the pressure applied on the formation rocks thereby reducing the length and the width of the fractures propagated. The volume of the fluid loss into the formation increases with the decrease in viscosity of the fluid injected [5].

The formation of filter cake resists further fluid loss into the formation which in turn saves the operator from injecting huge volume of fresh water to generate the desired fracture parameters. The thickness of the filter cake formed depends on the type of fracturing fluid used, formation characteristics, difference between reservoir and fracture pressures and the erosional effect caused by the slurry pumped along the fracture face [6]. Unless the fracture is completely plugged, a small path in the middle of the fracture would retain the properties of the injected polymer [7]. Because

of the different exposure times to fracturing fluid and different proppant concentrations across the fracture, polymer concentration of the fluid residue and the filter cake, vary locally across the length of the fracture [8].

The filter cake and the concentrated polymer left in the fracture after the injection and shut in stage, reduces the fracture conductivity, and the hydrocarbons suffer significant pressure loss when they flow through the fracture during the production phase. Additives called breakers are added with the fracturing fluid to degrade the filter cake and gel residue just before the production stage. However, if these breakers degrade the polymer gel before the fracture propagation, fracturing fluids will lose their hydrostatic potential and proppant carrying abilities, which will impact the generated fracture dimensions and fracture conductivity. For this reason, encapsulating agents are used for the breakers, the purpose of which is to delay its activity during injection.

In spite of the wide usage of breakers, the effective producing fracture length after hydraulic fracture treatments is still shorter than the designed fracture length [9]. Polymer damage (gel residue) due to incomplete fracture clean-up is considered to be the major reason [9, 99]. It was also found that the concentrated polymer residue would cause significant yield stress for the hydrocarbons to overcome, when they flow through the fracture length into the well bore [10].

The fracturing fluid which leaks off into the formation during the injection and shut in stages causes physical and hydraulic damage in the invaded zone [7, 14]. Increase in water saturation in the invaded zone causes shift in capillary pressure and relative permeability curves in the invaded area. This is termed as hydraulic damage. Physical damage (permeability reduction in the invaded

zone) is caused by processes such as clay swelling, and invasion of fracturing fluid into the formation etc. [2]

1.2 Nano-Particles as Proppants in Hydraulic Fracturing of Unconventional Reservoirs

In the last decade or so, hydraulic fracturing has been used extensively to increase the productivity of ultra-tight shale oil and shale gas reservoirs. Non cross-linked fluids with relatively lower polymer concentrations have typically been applied for tight shale plays as these formations generally have lower permeability and higher brittleness. Fracturing jobs in tight shale plays tend to generate or extend a network of fractures rather than forming the bi-wing fractures typically observed in conventional reservoirs. This network of fractures includes a large network of micro-fractures opened during the injection of fracturing fluids. These small fractures tend to close under closure stress unless a nano-sized proppants with significant stress resistance is injected to keep these micro-fractures opened [11].

Proppants with different mesh sizes of 20/40, 30/50, 40/70, 70/140 and 80/200 with grain diameters ranging from 0.033 inch (0.8382 mm) to 0.0041 inch (0.104 mm) are currently being used in shale formations. Manufacturers subject them to crush testing between 4000 and 12,000 psi. Most commonly used sand proppants are Brady sand and Ottawa sand) [3]. Pure quartz has hardness of 7 Mohs (roughly 11.39 GPa) [4]. These proppants are large enough to create conductivity in the larger generated or existing fractures but not small enough to penetrate into the existing or generated micro-fractures. This will cause the closure of micro-fractures at the end of a fracturing job thus reducing the length and conductivity of the complex fracture network [12]. Use of nanoparticles prior to the placement of larger proppants is a good way to prevent fluid loss

into the formation, and also increase the conductivity of the fissures and micro-sized fractures by propping them [12].

Silica nanoparticles were found to show good resistance against compressive stress, and have been used successfully in drilling fluids to decrease water invasion into shale formations [13]. Fly ash nanoparticles obtained as a byproduct in power plants is a cheap waste material which includes nano-particles of silica, calcium oxide and aluminum oxide. Fly ash nanoparticles are waste materials and therefore have a cheap source. Since they have a high composition of silica (40-60%), it was worth studying their hardness and reduced elastic modulus in order to qualify as nano-proppants. Fly ash nanoparticles should be able to withstand the same values of stress at which conventional proppants are tested.

1.3 Thesis Statement

This thesis has two main objectives:

1. The polyethylenimine dextran sulfate nanoparticles have already been found to be capable of efficiently delaying the activity of enzyme breakers for an extended period of time [2]. The first objective of this project is to investigate the efficiency of these nanoparticles when used as enzyme encapsulating agents, in reducing the fluid loss to the formation during the injection and in maintaining long term fracture conductivity of the proppant pack.
2. The second objective is to study the potential of fly ash nanoparticles to act as fluid loss minimizing additives and nano-proppants in tight and ultra-tight formations with permeability values in the 0.00001-0.1 mD range.

2. Literature Review

The literature review of this thesis is divided into two parts: 1- Fracture conductivity improvement using polyelectrolyte complex nanoparticles as enzyme breaker carriers and fluid loss additives, 2- Application of fly ash particles as fluid loss additives and nano-proppants. It has been again subdivided into various other components to explain the background of the research.

In section 2.1.1 an attempt has been made to outline the process and objectives of hydraulic fracturing in conventional reservoir formations. In section 2.1.2, fracturing fluids and the most important additives in them have been explained. In section 2.1.3, fluid loss which is an important phenomenon that occurs during hydraulic fracturing and its impacts on hydraulic fracturing process has been explained. Section 2.1.4 and 2.1.5 tries to explain incomplete fracture clean-up and its detrimental effects on the production respectively. Section 2.1.6 contain information on the delivery agents for breakers used in oil industry. Sections 2.1.8 and 2.1.9 describe polyelectrolyte complex nanoparticles and Polyethylenimine-Dextran Sulfate system invented by Tiyaboonchai. Section 2.2.1 gives an idea about hydraulic fracturing in tight and ultra-tight reservoirs. 2.2.2 has information on the fracturing fluids and 2.2.3 has information on the proppant systems used in unconventional Reservoirs. Section 2.2.4 speaks about the potential of silica nanoparticles to act as nano-proppants and section 2.2.5 introduces fly ash particles, a waste material which is a significant source of silica nanoparticles. Section 2.2.3 summarizes the literature review.

2.1.1 Hydraulic Fracturing in Conventional Reservoirs

Hydraulic fracturing is currently the most commonly used process for stimulating oil and gas wells. It has contributed significantly towards making previously unrecoverable reserves exploitable and enhancing production rates from existing fields. The first hydraulic fracture treatment was carried out in Hugoton Gas field in Grand county, KS in 1947 [15].

The process consists of pumping a fracturing fluid into the pay zone at an injection pressure and rates high enough to generate and propagate fractures into the formation. The fracturing fluid used in the process is a blend of different additives like viscosifiers which aid in the creation of fractures which would then act as a conduit for the flow of hydrocarbons into the wellbore. Initially, fluid without additives called 'pad' is pumped to initiate the fracture. This is followed by injection of a 'slurry', which is a mixture of different additives and proppants, which would then continue to extend the fracture further into the formation. Once the injection pressure is removed and the well is 'shut-in', the fractures tend to close because of the overburden stress applied by the rocks. The proppants having been already injected into the fracture prevent the fractures from closing, ensuring a conductive path for the hydrocarbons to flow once the well is put into production. Before the production phase starts, the viscous fracturing fluid present in the fracture has to break down and flow back to the surface, to prevent it from causing hindrance to the flow of hydrocarbons during production. For this purpose, the 'slurry' contains chemicals termed breakers which would break down the highly viscous fracturing fluids into less viscous fluid which can flow back to the surface during the 'flow back' period after the shut in process. This process is termed 'clean-up'. After the flow back period, the well is put into production and the hydrocarbons flow into the wellbore through the highly conductive hydraulic fracture network.

2.1.2 Fracturing Fluids & Additives

It is a common understanding in the petroleum industry today that most wells drilled would not sustain a commercial production rate if not hydraulically fractured. For this purpose, fracturing fluids are injected into the underground formation (1) to create a conductive path from the wellbore extending into the formation and (2) to carry proppants into the fracture to sustain the conductivity of the created path for production of hydrocarbons [16].

The selection of a proper fracturing fluid involves several considerations. It starts with choosing the pad volume where one must consider what and how much pad is required to create the desired fracture geometry. This is followed by choosing how much viscosity the fluid is expected to provide, sufficient fracture width (to ensure proppant entry into the fracture), sufficient proppant carrying capability (to transport proppant from the wellbore to the fracture tip) and limit fluid loss. In cases where a gel filter cake cannot form, fracturing fluid viscosity is the main mechanism for fluid loss control.

When it comes to selecting the appropriate fluid system for a propped or acid fracture treatment, the considerations also include [17]:

- Safety – The fluid should expose the on-site personnel to a minimal danger.
- Environmentally Friendly – The composition of the fluid should be as “green” as possible.
- Breaker – The fluid must “break” to a low viscosity so that it can flow back and allow clean-up of the fracture.

- Cost Effective – The fluid must be economical and not drive the treatment cost to an unacceptable level.
- Compatibility – The fluid must not interact and caused damage to the formation mineralogy or formation fluids.
- Clean-up – The fluid should not damage the fracture conductivity of the fracture or change the relative permeability of the formation.
- Easy to Mix – The fluid system must be easy to mix even under very adverse conditions.
- Fluid Loss – The fluid need to help control fluid loss. An ideal fluid should have fluid loss control flexibility.

In short, an ideal fracturing fluid would be one that would "have an easily measured controllable viscosity, controllable fluid loss characteristics, would not damage the fracture or interact with the formation fluid, would be completely harmless and inert and cost less than $4.00 US/ gallon" [17]. Unfortunately, due to the lack of such an 'ideal' fluid, compromises have to be made [17].

Of these factors, fluid viscosity is the major fluid related parameter for fracture design. Excessive viscosity increases costs, raises treating pressure which may cause undesired height growth, and can reduce fracture conductivity since most chemicals used to increase viscosity leave residue which damages the proppant permeability. Insufficient viscosity leads to improper proppant distribution, increased fluid loss, inferior fracture dimensions and inadequate fracture conductivity [17].

There are several types of fracturing fluids and a wide range of fluid additives. The types of fluids include:

- Water based fluids
- Oil based fluids
- Energized fluids
- Multi-phase emulsions
- Acid Fluids

The additives include:

- Gelling agents
- Cross-linkers
- Breakers
- Fluid loss additives
- Bactericides
- Surfactants and Non-emulsifying agents
- Clay control Additives.

Although oil-based fracturing fluids were the first to be used, the environmental and safety concerns raised by their applications have prompted the industry to move towards developing an alternative. Today more than 90% of today's fracturing fluids are water-based [15]. Aqueous fluids are not only economical but the additives developed over the years to be used with them have helped in providing control over a broad range of the generated fracture parameters [16].

2.1.2.1 Guar and Its Derivatives

Guar gum is one of the most commonly used agents to viscosify aqueous based fracturing fluids. Guar is a long-chain, high-molecular-weight polymer, composed of mannose and galactose sugars [5]. Guar concentrations of 0.12-0.96% w/w have been conventionally used for fracturing different formations [18]. The polymannose backbone of guar is not soluble in water while the galactose branches cause solubility in water. The ratio of mannose to galactose sugars may range from 1.6:1, to 1.8:1 [5].

When the guar powder is exposed to high pH water at a high temperature for an extended period of time, the powder swells, generating guar derivatives. During this process, helices are broken thus exposing the backbone polymer to react with derivatizing agents like propylene oxide. Hydroxypropyl guar (HPG), containing about 2-4 wt. % insoluble residue, is formed when the guar reacts with propylene oxide [2, 5, 19].

Guar-based fluids are commonly used as fracturing fluids to form a filter cake, propagate the fracture and transport proppants during a typical hydraulic fracturing job in conventional reservoirs. It is used in its linear and cross-linked forms. They are relatively cheap and they have been found to perform well under shear and temperature conditions encountered in the wellbore and formation. The viscosity of the polymer solutions decreases with increasing temperature.

Experiments using enzyme breakers have shown that, breakers when allowed to react with the polymer chain for an extended period of time, causes residues as a result of helices made by inappropriate breaking of the polymer backbone [19]. These generated residues reduce the conductivity of the proppant pack.

Although the proppant pack damage caused by guar and HPG is more or less the same, HPG is more stable than guar at higher temperatures [5, 31].

When using guar or its derivatives, the fluid loss control mechanism is “wall-building – i.e. C-III” When the base fluid leaks off and the polymer is deposited on the rock face forming a filter cake, the initial leak off is quite rapid and is called “spurt”. Once a filter cake forms, the leak-off volumes are significantly reduced after which it becomes a function of the square root of time [20].

2.1.2.2 Cross-Linkers

Cross-linkers are used to increase the molecular weight of the polymer by crosslinking the polymer backbone into a 3D structure. This increases the base viscosity of the linear gel from less than 50 cP into the 100’s or 1000’s of cP range. This crosslinking also increases the elasticity and proppant transport capability of the fluid [20].

Borate and several metals including titanium and zirconium are used as cross-linkers for guar based gels. In addition to these materials, iron, chromium and aluminum can also crosslink guar although they are not commonly used. Each cross-linker has a unique reaction requirement and behavior. Borate in the form of boric acid, slowly soluble salts of Ca and Mg and organic borate complexes are some of the most common cross-linkers in use today [20]. Borate cross-linked fracturing fluids can be applied across a wide range of treating conditions and are resistant to shear degradation.

2.1.2.3 Cross-Linked Fracturing Fluids

It is very important that the fracturing fluids retain their viscosity so that they can apply adequate

hydrostatic pressure on the rocks to crack them open. One could think of increasing the polymer concentration as an immediate solution to meet this requirement but this would lead to more polymer residue remaining in the fractures even after the clean-up phase. Hence cross-linkers (like borate and zirconate) are added to enhance the viscosity of the gel [5].

Addition of cross-linkers to HPG solution increases the viscosity of the linear gel from less than 50 cP into the 100's or 1000's of cP range. The higher viscosity aids in generating wider fractures which can accept higher concentrations of proppant. Cross-linking helps in reducing the fluid loss to improve fluid efficiency. Fluid loss is controlled by a filter cake which builds on the fracture face as the fluid leaks off into the formation. Cross-linking also increases the elasticity and proppant transport capability of the fluid while simultaneously reducing the friction pressure [20].

2.1.2.4 Slickwater Fracturing Fluids

Development of unconventional (e.g. tight gas) reservoirs has encouraged the application of slickwater or hybrid treatments. Slickwater treatments are defined as "a fracture treatment that utilizes a large volume of water to create an adequate fracture geometry and conductivity to obtain commercial production from low permeability, large net-pay reservoirs" [21]. This treatment uses slickening agents like polyacrylamide or low concentration (~ 10 pptg or 1.2 g/L) guar solutions to reduce the fluid friction [21, 87].

The following are some of the advantages of slickwater treatments listed in the literature [21, 87].

1. Reduced cost as a result of less proppants and polymers used
2. Reduced gel damage within the fracture
3. Reduced fracture height growth as a result of lower viscosity

4. The generated fracture geometry is more complex due to the lower viscosity and higher injection rates [20], generating larger stimulated reservoir volume (SRV) [22].

Despite all the above mentioned advantages, some major disadvantages of using slickwater fracturing treatments were also found in the literature [21, 87]. Due to its reduced viscosity, proppant transport and suspension capability of slick water fluid systems are greatly inferior compared to cross-linked fluid systems. This forces the operators to rely on relatively lighter proppants (compared to conventional proppant sands) which are prone to crushing during the shut in stages. The reduced viscosity also implies that the operator has to use significantly higher fluid volume and pumping rates to generate adequate hydrostatic pressure and ensure proppant transport. This increase in injection cost can offset the gains in using lower gel concentrations unless there is a large water source available nearby.

Slickwater treatments do not generate thick filter cake on the walls of the fracture unlike cross-linked fluid treatments. This leads to higher leak-off volume which increases the impact of formation damage (both hydraulic and physical) due to fluid leak-off. Linear HPG solution (less than 2000 ppm initial concentration) along with breakers are also used as slick water fluids [23]. Slickwater jobs account for 30 – 40 % of the stimulation fracturing jobs pumped [24].

2.1.2.5 Breakers

The viscous fluid (both crosslinked and linear) and the filter cake formed on the face of the rock, must be broken to ensure high conductivity in the proppant pack. The polymers have to be cleaved into small molecular weight fragments using additives called ‘breakers’, added to the fracturing fluids for this purpose. This reduces the viscosity and facilitates the flow back of

residual polymer which allows for cleanup of the proppant pack. Ideally these materials "should be totally inactive during the treatment and then instantly spring to action when pumping stops, rapidly breaking the fluid back to almost water like viscosity" [20]. In this manner, the fracture and the formation will be prepared for flow and would not cause much pressure loss for the hydrocarbons flowing into the well bore [20]. This is very difficult to achieve as the breaker activity is very dependent on fluid temperature which varies with time. Oxidizers, enzymes and acids are the typical breakers used depending on different fracturing conditions, of which oxidizers are the most commonly used.

2.1.2.5.1 Oxidizers

Ammonium, potassium, and sodium salts of peroxydisulfate (persulfate) are the commonly used oxidizers. Persulfates are very strong oxidizers and form a free oxygen radical when the temperature exceeds 125°F [20]. These free radicals attack the backbone of the polymer strand and break it down into its constitutive sugars [20].

Since the generation of free radicals is based on the thermal decomposition of persulfates, the reaction rates are slow at temperatures below 125 °F [5]. On the other hand, at very high temperatures, the oxidizers degrade rapidly. Encapsulation of the breakers helps in delaying the breaking activity during high temperature applications. However, perfect encapsulation is yet to be achieved. Oxidizers also have a bad reputation of being corrosive to the field equipment and tubing [20]. Oxidizers are used as breakers in cases where there is a chance of reduced enzyme action due to temperature and pH conditions unfavorable for enzymes (more details in the next section).

2.1.2.5.2 Enzymes

Enzymes are protein molecules that act as organic catalysts. They can attach themselves to specific sites on the polymer backbone and help in cleaving the polymer links. Enzymes are unable to change the overall equilibrium of a reaction. However, they can dictate its rate of occurrence [20]. They can couple two reactions by using the energy from one reaction to affect the equilibrium of the other reaction. They catalyze reactions by introducing an intermediate step. In the first stage of the reaction, enzymes attach themselves on the substrate forming an enzyme-substrate complex. The product formation is accelerated as a result of the formation of this complex and in the final stage, enzyme and the product is separated thus allowing the enzyme to catalyze the cleavage at a different site [2, 88, 106].

Typical enzymes that are used include hemicellulase, cellulose, amylase and pectinase and they cause reduction in the guar molecular weight. Since they act as catalysts, they are not consumed during the reaction. However, there is a chance of them becoming non-functional at elevated temperatures and extreme pH values. The enzymes remain active only if they maintain a specific conformation. Increasing temperature and pH conditions alters the conformation of enzymes making them incapable of breaking polymer gel [25]. Enzymes can achieve increased lifetime at high pressure conditions.

A guar molecule is made of a linear backbone of β-1, 4 mannose units with α-1,6galactoseside chains [26]. Enzymes have the ability to attack several bonds of guar like the endo- andexo-β-1, 4 bonds between the D-mannose sugar units on the backbone and the α-1, 6 bonds between the

backbone and the galactose side chains. These sites can be cleaved by endo- and exo-mannanase and α-galactosidase enzymes respectively [26].

Enzyme breakers have many advantages over chemical oxidizers: they are cheap, are not consumed during their catalytic reaction with guar, react only with the polymer, are environmentally benign, easy to handle and do not damage wellhead equipment [5]. A big disadvantage associated with conventional enzymes is that their application is limited to mild temperatures below 150°F (66°C) and fluid pH's between 4 and 9 [5, 20, 88]. They tend to get deactivated and permanently degraded when exposed to very high or very low pH and temperature above 150°F. Degraded enzymes cannot help in fracture clean-up process. Hence, if the enzymes can be protected from such conditions, the application of enzymes in fracturing fluids can be extended to previously unsuitable reservoir conditions.

2.1.3 Fluid Loss

When the fracturing fluid is injected, a high polymer concentration filter cake forms on the two faces of the fracture and the fluid filtrate invades the matrix [27]. Carter demonstrated a linear relationship between the leak off volume and the square root of exposure time of rock to fracturing fluid [28].

The fluid which 'leaks off' into the reservoir causes hydraulic and physical damage to the reservoir. In the area invaded by the leaked off fluid, hydraulic damage is caused by the shifts in capillary pressure and relative permeability curves. Physical damage is caused by processes like clay swelling, invasion of fracturing fluid into the formation, etc. [14]. These effects will be more

prominent in shales because of their significant clay content; this is especially the case with shale rocks that contain smectite and montromorillonite clays [1].

The volume of the fluid lost into the formation has a direct relation with the permeability of the formation and also increases with decreasing viscosity of the fluid injected. Fluid loss also depends on the deference between fracture injection pressure and reservoir pressure, initial water saturation of the formation etc. The more fluid is lost into the formation, the less is the pressure applied on the formation rocks thereby reducing the length and the width of the fractures propagated **(Figure 1).**

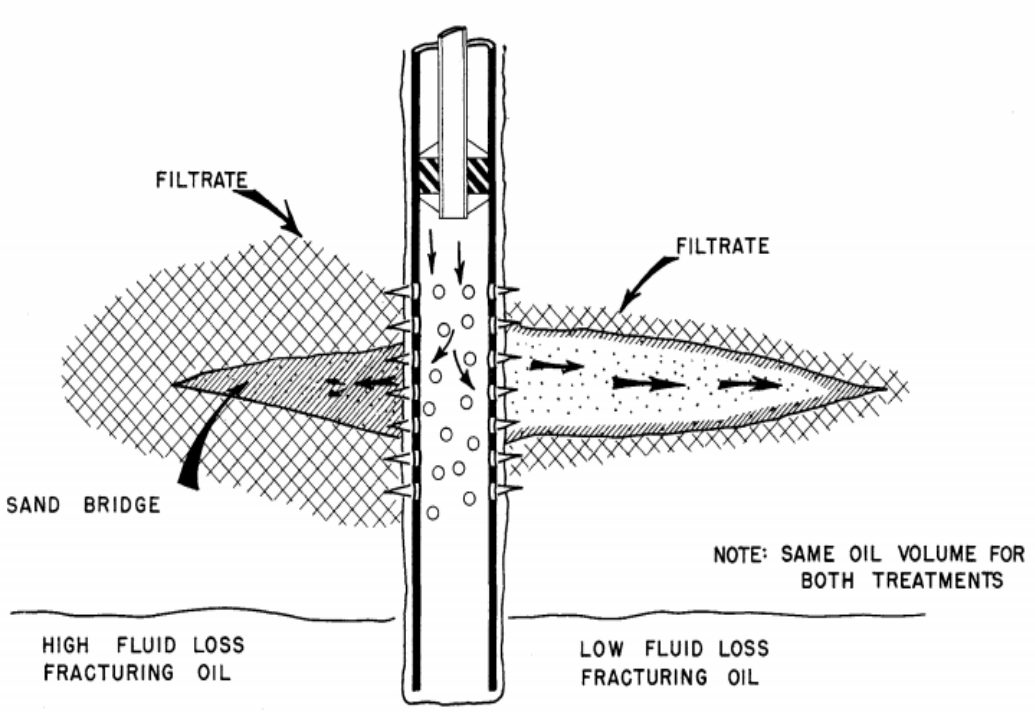

Figure 1: Effect of fluid loss on fracture propagation *[29]*

Damages due to the invasion of filtrate volumes are more significant in tight and ultra-tight formations, even though the fluid loss volumes are smaller for these very low permeability rocks

because of the inverse square root relation between capillary pressure and permeability. To further compound this problem, the system of naturally induced micro-fractures, from which the tight and ultra-tight unconventional hydrocarbon reservoirs typically produce, can cause significant fluid loss volumes [30]. Reducing fluid loss to the formation would help in creating longer fractures with more fracture contact area which would help in increasing production.

2.1.4 Incomplete Fracture Clean-Up

Hydraulic fractures usually fail to produce the desired conductivity. Proppant-pack conductivity determines the productivity improvement obtained after hydraulic fracture stimulation. The factors which effect proppant-pack permeability have commonly been divided into studies with and without fracturing fluids present [31]. In the absence of fracturing fluids, the factors which have been identified to impact proppant-pack permeability include parameters attributable to the proppant, the formation hardness, and the reservoir environment. These include proppant size and size distribution, proppant strength, proppant concentration within the fracture, proppant sphericity and angularity, closure stress, temperature, and time under stress [100, 38, 40, 37].

Cooke [32] in 1973 used short-term conductivity values to report that brine flow at elevated temperatures and closure stresses showed reduced proppant-pack permeability. Since then, many studies have focused on the area of long-term proppant-pack conductivity [38, 40, 37]. These studies have confirmed that proppant-pack permeabilities are dramatically reduced when exposed to long periods at temperature and stress. The long-term permeability of many of the proppants tested in these studies were found to be as much as 50% less than was indicated by the previously published short-term values [31].

Another type of permeability damage to proppant-packs is caused by the gelling agents commonly used in hydraulic fracturing fluids. The parameters known to affect the degree of damage due to hydraulic fracturing fluids include polymer type and concentration, crosslinking, breaker concentration, fluid loss additive concentration, and reservoir temperature [31, 39, 41, 100].

This is usually affected by factors such as incomplete cleanup of gels, non-Darcy flow effects, multiphase flow effects, gel distribution, crush, and embedment of proppants. Fracturing-fluid residue can reduce the proppant conductivity by about 90% or more, depending on the fracturing-fluid type, quality, and effectiveness, particularly of the breaker system [6]. The non-Darcy flow factor increases with damage, contributing to further reduction in the effective gas-well fracture conductivity. Two-phase flow effects also have a significant impact on reducing the effective fracture conductivity. Fracturing fluids cause reduction in proppant pack permeability because of their following disadvantages.

2.1.4.1 Filter Cake Buildup

During the fracturing operation, the high-pressure fracturing fluid leaks off into the formation. A polymer and fluid-loss additive filter cake is formed. The filter-cake thickness is determined by the kind of fracturing fluid used, the formation characteristics, the fracture-to-reservoir pressure difference, and the erosional effects caused by slurry being pumped along the fracture faces [6]. During fracture closure, the proppants are embedded into the filter cake, making it difficult to remove the filter cake during production. A typical filter-cake thickness of 0.5 mm [0.13 in.] on each fracture wall will completely block a thin fracture propped with two layers of 20/40-mesh proppant [6].

Filter cake is usually attacked by the injected breakers reducing its thickness during the clean-up period, but in most cases a thin layer of filter cake still remains during the production phase due to the inefficiency of the clean-up operation. The ratio of the filter cake to the fracture width determines the extent of resistance offered by the fluid, against the applied pressure difference

across the proppant pack [14, 27]. A thick filter cake reduces the width of the fracture available for the flow of hydrocarbons **(Figure 2)**.

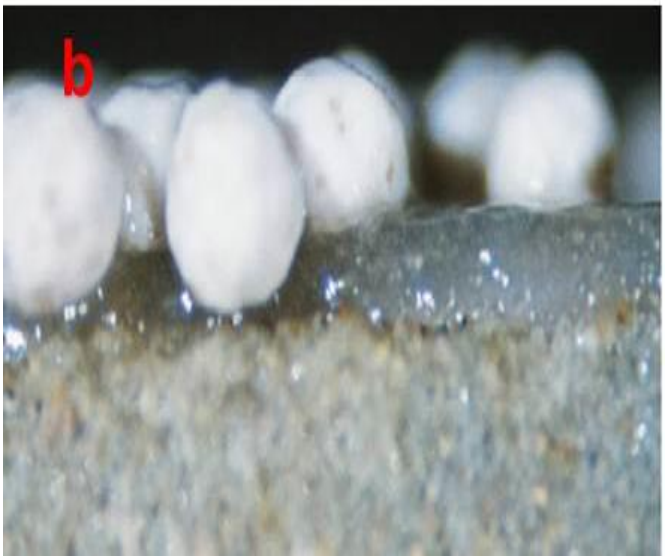

Figure 2: Filter cake reducing fracture width *[33]* ***Stimlab***

2.1.4.2 Gel Residue

Despite the usage of copious amounts of breakers, the usage of cross-linked fluids usually leaves a proppant pack containing a lot of fibrous material between the grains, which are then "glued" together [6]. Palisch et al. reported that gel damage is a significant factor which reduces proppant pack conductivity by different mechanisms [33]. The porosity and permeability of the proppant pack gets significantly reduced by the gel residue (**Figure 3**) left in the proppant pack due to incomplete fracture clean-up. Moreover, the unbroken fluids found mostly near the tip of the fractures cause loss in effective fracture length. The gel saturation is usually higher near the tip of the fracture as the drawdown pressure is weaker towards the tip. This causes the effective fracture

length available for production to be much less than the propagated fracture length as the yield stress required for the flow to start is harder to overcome near the fracture tip [9].

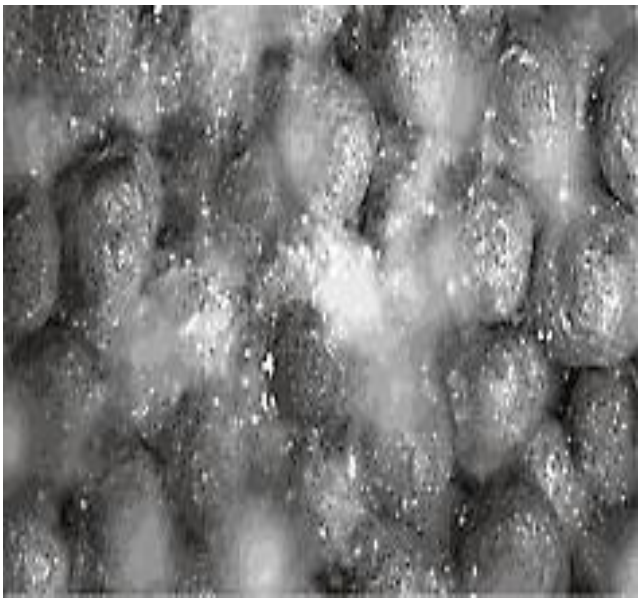

Figure 3: Gel residue in the proppant pack *[34]*

2.1.4.3 Non-Degraded Fracturing Fluid

If you consider the scenario just after the fracturing job, the propped fracture will be almost completely saturated with fluids with viscosity much greater than that of the injected fluid because of the fluid leak off into the formation. The fluid which leaked off reduces the oil/gas saturation in the invaded zone to their irreducible saturation. The deliverability of the well will continue to remain impaired until this fluid is at least partially removed from the formation and the fracture. Further reduction in productivity can occur due to the increased bottom hole pressure as a result of the dense liquid which is held up in the wellbore.

As soon as the well is allowed to produce, this viscous fluid will offer significant resistance to flow of hydrocarbons. Eventually the gas will finger through the fracturing fluid and reach the wellbore. This helps in fracture clean-up and in increasing the effective length of the fracture available for hydrocarbon flow. The gas saturation in the fracture will continue to increase thereby reducing the resistance to flow of hydrocarbons through the fracture. An idealized well would reach maximum productivity immediately after the fracturing treatment, but with the damage caused by inadequate cleanup, it would take the well several days to attain maximum productivity [35]. This effect has been found to be more prominent when the formation permeability is lower [1].

2.1.5 Incomplete Clean-Up Studies from Literature

Incomplete clean-up of fractures leaves partially broken fracturing fluids and residues even after the breakers have degraded the filter cake. The significant damage caused by partially broken fracturing fluids and filter cake to the fracture conductivity, and thereby to the cumulative oil production, has been shown by many researchers.

In 1975, Cooke published a study in which he numerically correlated the volume of residue observed from various lightly concentrated non-crosslinked fracturing fluids to the amount of permeability reduction observed in a 20/40 mesh sand-pack [32]. The results indicated a decrease in the permeability of the proppant-pack when the volume of gelling agent residue increased.

In 1985, Kim et al [36] reported the effects of lightly concentrated crosslinked fracturing fluids on the permeability of short-term stressed proppant packs in an API conductivity cell without leak-off. Permeability reduction in the order of 30 to 50% were reported for polymer concentrations ranging from 40 to 100 lbm per 1000 gallons.

Several fracture conductivity studies since then have sought to quantify the damage caused by concentrated treatment fluids when exposed to realistic environmental conditions. In 1986, Roodhart et. a1. [37], for the first time, carried out a reasonable simulation study of the damage caused by concentrated fracturing fluids. The authors observed substantial permeability reductions and recommended that only 10% of the permeability measured without fracturing fluid should be assumed when concentrated fracturing fluids are present in the proppant pack.

Penny, McDaniel, and others [38, 40] incorporated dynamic fluid loss, two core leak-off, and long-term exposure to temperature and stress into their sophisticated fracture conductivity tests and reported their results. They injected the proppant slurry manually into the cell after the dynamic filter-cake deposition. A static fluid-loss phase was conducted to simulate fracture closure, resulting in concentration of the fracturing fluid within the proppant pack. Subsequently, closure stress was applied and the cell was shut-in until the start of the flow back or cleanup phase. The measured permeability reduction was not only a function of the dynamically-formed filter cake but also of the concentration of the bulk fluid. Large reductions in the proppant-pack permeability were observed, especially in the case of crosslinked fluids. Assuming that all the polymer associated with the dynamic filter cake remained within the cell, the final polymer concentration within the proppant pack was estimated to be five to seven times the initial concentration [38].

In spite of the significant progress made in the efforts to realistically evaluate and quantify proppant-pack permeability damage due to concentrated fracturing fluids, only a few authors have done studies on reducing the permeability impairment. Breakers, both oxidative and enzymatic, have been in use for many years for degrading the viscosity of polymeric fracturing

fluids. Several studies [31, 36-41, 100] have illustrated that the permeability is significantly reduced by the polymer residues despite the usage of sufficient breaker concentrations to reduce the fluid viscosity.

Hawkins studied proppant pack permeability using a modified API cell (experimental procedures can be read in reference [41]). He conducted static fluid loss tests and generated filter cake using Ohio sandstones (0.75 mD). He reported that the concentration of filter cake formed was 25 times as much as that of the fluid he injected initially. According to his results, HPG crosslinked with borate, causes less damage to the permeability of the proppant pack as compared to the uncross-linked, and titanate or zirconate crosslinked HPG.

Ayoub et al. [27] postulated that the concentrated polymer would require a specific pressure gradient to flow through the proppant pack. They conducted a study measuring the Flow Initiation Gradient (FIG) and conductivity of proppants filled with filtered borate crosslinked guar and broken using encapsulated oxidizers [27]. They calculated the yield stress and FIG along the proppant pack and showed that flow along the fracture encounters significant yield stress due to concentrated gel residue. In order to study the effect of distributing breakers directly into the filter cake, they conducted two types of experiments. At first, they measured the yield stress caused by the proppant pack which was created by pouring well mixed fracturing fluid containing encapsulated breakers directly on to the cores. In the next experiment, they distributed the same amount of encapsulated breakers directly on the surface of the cores where the filter cake will be formed after the fluid loss. They noted that the yield stress caused by filter cake decreases significantly when breaker is delivered directly into the filter cake (second case) rather

than distributing in the slurry (first case). Better conductivities were recorded for the runs with encapsulated breakers located within the filter cake [42].

Barati et al. (2009) studied the impact of broken gel viscosity, yield stress, formation damage and fracture conductivity on low permeability gas reservoir production using a three phase 2D model [1]. The three phases were gas, water and fracturing fluid. They showed that ineffective fracture clean-up causes the conventional hydraulic fracture completions to show discrepancies between the placed propped length and the effective production fracture length. They observed that this effect increases when the formation permeability is reduced.

Assuming Newtonian-fluid behavior, Voneiff et al (1996) concluded on the basis of his results from modified numerical reservoir-simulators that unbroken fracturing fluids can decrease gas reserves in a tight gas well by 30% and initial production rate by 80%.

2.1.6 Encapsulation of Enzymes

In addition to denaturation of enzymes at higher temperature and pH conditions, operators face another problem while injecting enzymes along with the fracturing fluids. The enzymes, if used in high concentrations in the free state, causes premature degradation of polymer gels thus decreasing the viscosity and proppant carrying properties of the fracturing fluid. This leads to the generation of comparatively inferior fracture parameters and proppant placement. However, the use of insufficient concentration of enzymes cause incomplete fracture clean up and reduced fracture conductivity.

One practical solution to this problem lies in finding an encapsulating agent to entrap the enzymes in order to make sure they do not degrade the viscosity of the gel until the end of fracture

propagation. This same encapsulating agent should also be capable of releasing the enzymes after the fractures have been created, in time for fracture clean-up. Such an encapsulating agent would ensure high fracture conductivity and minimum gel residue without compromising on generated fracture parameters.

Encapsulation of breakers gives the flexibility of using higher concentrations of breakers for better clean up. A mixture of free and encapsulated breakers is usually used to achieve a better performance [5]. Barati et al proved that polyelectrolyte complex nanoparticles are capable of encapsulating enzymes and protecting them from temperature and pH conditions that are usually inhospitable to them when in free state [2].

2.1.7 Delivery Agents for Delayed Release of Breakers

Encapsulating the breakers during injection prevents the premature degradation of fluid viscosity and gives the operator the flexibility of using higher concentration of breakers for gel clean-up later. Various researchers have worked on encapsulating breakers to delay their release and the release mechanisms. Nolte (US patent 4506734) [43] proposed a method in which the breakers are coated during injection and are released when the coating ruptures due to crushing of breakers during fracture closure [25, 96]. Gulbis et al. studied the effect of encapsulating ammonium persulfate with a water-barrier polymer coating according to the idea conceived by Nolte [25, 43]. Their study involved two different stages- testing the effects of pumping equipment on encapsulated breaker and testing the effect of encapsulated breaker on well performance. They found the premature release of breakers during pumping to be less than 2% by weight. For field studies, they tested two cases on different wells in the same region. In the first set of wells

breakers were pumped without encapsulating them. In the second set of wells, they used a higher concentration of breakers encapsulated inside the coating [44]. After 90 days, the cumulative production from the wells with increased breaker concentration was found to be about 70% more than the other case [44]. The improvement in cumulative production is thought to have been the resultant of an improved fracture conductivity [44].

2.1.8 Polyelectrolytes

Polymers carrying multiple ionic groups are called polyelectrolytes. They exhibit a dual character of highly charged electrolytes and macromolecular chain molecules simultaneously. Hence they have the viscosity of a polymer and the electrical properties of an electrolyte, their ionic groups tend to dissociate in aqueous phase making the polymer charged [45]. Depending on their charge, polyelectrolytes can be divided into poly-anions (negatively charged ionic group), poly-cations (positively charged ionic group), and poly-ampholytes (carries both positively and negatively charged ionic groups).

Polyelectrolyte complexes (PECs) have been used as carriers for vaccines and anticancer drugs to limit their off-target tissue toxicity [46-49, 110]. PECs are the result of strong electrostatic interactions between two oppositely charged polyelectrolytes. Therapeutic agents are incorporated into them by encapsulation, covalent attachment, or surface adsorption [46]. Although electrostatic interactions are the main molecular forces for PECs, hydrogen bonding, hydrophobic interactions and van der Waals forces aid in completing their formation [46].

Koetz and Kosmella classified the polyelectrolytes into natural, modified natural, and synthetic based on their origin [45]. The polyethylenimine/dextran sulfate system (PEI-DS) introduced later in this work falls under the classification of synthetic system.

2.1.9 Polyethylenimine/Dextran Sulfate System of Tiyaboonchai

A polyelectrolyte complex nanoparticle system with polyethylenimine (PEI) as the cation and dextran sulfate (DS) as the anion was developed by Tiyaboonchai [47]. It was a solid colloidal particle system with diameters ranging from 1 to 100 nm, designed to act as a delivery vehicle for pharmaceutical applications [48]. PEI is widely used polymer in the pharmaceutical industry because of its water soluble nature and wide availability in linear and branched forms. Dextran sulfate, available in a wide molecular range of 5-500 kDa is soluble in water and insoluble in ethanol and ether [47-49]. Both PEI and DS are biodegradable and biocompatible [2, 47-49, 89].

Tiyaboonchai observed that the particle size of the generated nanoparticles was dependent on the ratio of PEI over DS [49]. As the ratio increased, the mean particle size decreased. She believed that this behavior was due to the colloidal protective nature of PEI which prevents the aggregation of the nanoparticles [48]. The structures of PEI and DS are shown in **Figure 4** and **Figure 5** respectively. PEI-DS nanoparticles show positive charge when the mixing ratio of PEI to DS is above 1:1 v/v [50].

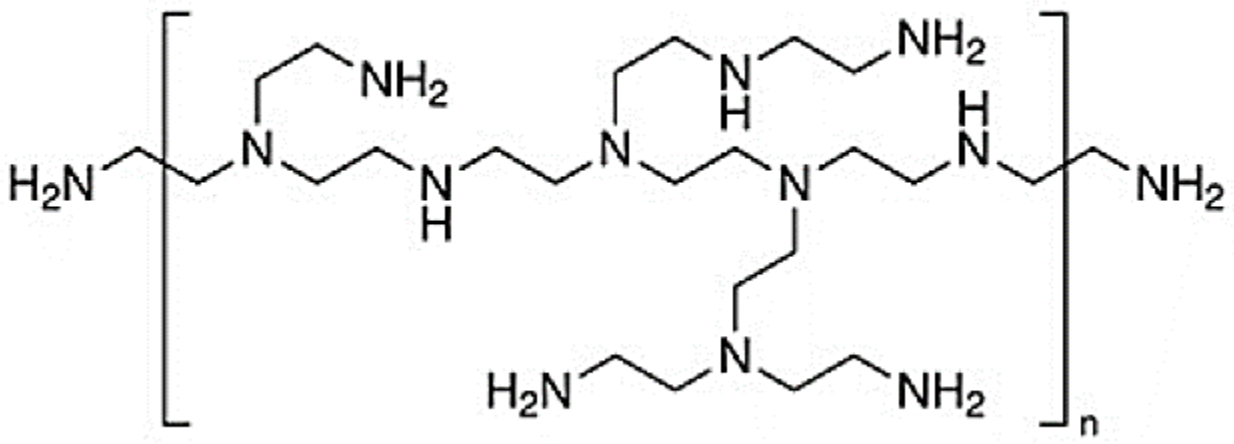

Figure 4: Chemical structure of PEI (Sigma Aldrich MSDS sheet) *[51]*

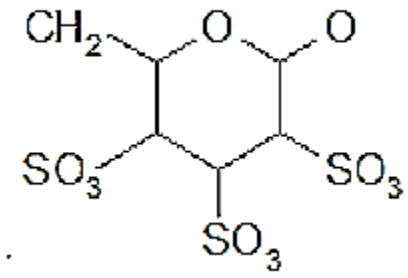

Figure 5: Chemical structure of DS (Drawn by Stephen Johnson: used with permission)

Table 1: Particle size and zeta potential measurement for polyelectrolyte complex nanoparticles with measurements done for 3 samples *[52]*

Polyelectrolyte complex Nanoparticles	**Mean size (nanometer)**	**Standard error size (nanometer)**	**pH**	**Mean zeta (mV)**	**Standard error zeta**
	545.43	10.57	8.7	37.16	4.93

2.1.9.1 Polyethylenimine/Dextran Sulfate System as an Encapsulating Agent for Delayed Release

Cordova et al. were the first to use the polyethylenimine/dextran sulfate system introduced by Tiyaboonchai in petroleum engineering applications [50]. To delay the gelation of hydrolyzed polyacrylamide (HPAM), they tried sequestering Chromium (III), the cross-linker ion inside this nanoparticle system [48, 50]. They were successful in preparing PEC nanoparticles with sizes less than 200 nm by adjusting both the concentration and ratio of PEI and DS. They suggested a mixing ratio above 1:1 v/v for PEI: DS to generate positively charged nanoparticles. They were also successful in generating negatively charged nanoparticles by decreasing PEI weight ratio.

Barati [2] sequestered pectinase (enzyme) inside the PEI-DS (PEC) nanoparticle system. After being entrapped by the PEC nanoparticles, pectinase retained its activity under the conditions of temperature and pH that denatured it previously. Barati optimized the enzyme-loaded nanoparticle system by varying the concentration and pH of PEI and DS. He observed that nanoparticle systems

with a 2:1 PEI: DS ratio showed the highest entrapment efficiency among the various system he prepared using 0.1 mL of pectinase (typical enzyme concertation used in field applications for cross-linked HPG system). The entrapment efficiency (EE) of the nanoparticles was found to decrease with increasing PEI: DS ratio. Nanoparticles which were prepared by adding pectinase to the PEI before addition of DS showed higher EE compared to the nanoparticles prepared by addition of pectinase to pre-formed PEI-DS nanoparticles. Based on his results he chose a PEI: DS ratio of 2:1 and chose the order of addition during the preparation as PEI followed by pectinase again followed by DS [2]. The PEI-DS system used in this work has a positive charge.

In order to prove the delayed release of enzymes from polyelectrolyte complex nanoparticles, Barati [2] performed rheometric studies with HPG gel solutions. He prepared two identical cross-linked HPG gel solution samples. While he employed unentrapped pectinase to degrade one sample of cross-linked HPG gel solution, he added pectinase entrapped in PEI-DS system to the other sample. A delay in the degradation of both elastic moduli (G') and viscous moduli (G'') was noted in the case of the gel solution with entrapped pectinase as compared to the unentrapped case [2, 90]. When left for an extended period of time (around 25 hours), the viscosity measurements showed that gels, containing pectinase solution entrapped inside PEC nanoparticles, reached the same viscosity values as those degraded using unentrapped pectinase. This confirmed that enzymes are released by the nanoparticles when left for an extended period of time [2]. Barati also observed that PEI-DS nanoparticles have the capability to degrade polymer gel. Their ability to degrade the polymer was very less as compared to that of pectinase (enzyme).

2.1.9.2 Polyelectrolyte Complex Nanoparticles as Fluid Loss Reducing Agents

Fluid loss control additives are agents applied to reduce the volume of filtrate lost to the formation during the propagation of a hydraulic fracture. The reduction in filtrate volume enables the propagation of longer networks of fractures. Fracture area has been found to increase when the fluid loss coefficient and volume decrease [53].

Fluid loss agents smaller than the ones used currently, could theoretically plug the nano-sized pore throat diameters and micro-sized fractures in shale oil and gas reservoirs. Additives with diameters larger than one third of the pore throat size cannot penetrate into the pores of the rock, and cause bridging [53]. Larger particles can result in external filter cakes and reduce the filtrate volume. Fluid loss additives having significantly larger sizes compared to the pore throat diameter will result in poor fluid loss prevention. Selecting the properly sized agent to plug fractures is therefore critical [52].

Pore throat sizes reported for different shale rocks are typically in the range of 10 nm – 1000 nm. Therefore, in order to plug the pore throats and reduce the filtrate volume, particles larger than 3 nm and 300 nm range must be used respectively, so as to cause only minimal damage to the rock [30]. Polyelectrolyte complex nanoparticles with particle sizes in nanoparticles were found to have a potential to act as fluid loss reduction agents. This potential acted as an impetus to carry out static fluid loss tests using polyelectrolyte complex nanoparticles [52].

2.2.1 Hydraulic Fracture Propagation in Unconventional Reservoirs-Concept of Stimulated Reservoir Volume (SRV)

Hydraulic fracturing is done in shale reservoirs to increase hydrocarbon production by connecting the already existing fissures and fractures and generating new small fissures. It is also believed to dilate the already existing systems of small fissures and fractures which are initially filled with calcite, quartz or other minerals [11, 56]. Re-opening of natural fractures occurs when the induced stresses inside the rock overcome formation in-situ stresses. Although the size of the induced cracks and re-opened parts of the pre-existing natural fractures are very small in comparison to the main hydraulic fracture, they can still tremendously increase the well-formation contact area if they are kept open during production using appropriate propping agents [54].

Hydraulic fracture growth can be divided into four categories [55]

- Planar coupled growth
- Planar de-coupled growth or fissure opening
- Complex growth (non-communicating and communicating)
- Network growth

Ultralow-permeability shale reservoirs are dependent on a large fracture network to maximize well performance. Micro-seismic fracture mapping has shown that large fracture networks can be generated in many shale reservoirs [56]. Pre-existing healed or open natural fractures and favorable stress-field conditions enhance the chances for creating large tensile-fracture networks **(Figure 6)**.

Such complex-fracture networks are desirable in ultra-tight shale reservoirs because they maximize fracture-surface contact area with the shale.

Conventional reservoirs are mostly reliant on single-plane-fracture half-length and conductivity for improving well performance. However, in shale reservoirs, where complex network structures in multiple planes are created, the concepts of single-fracture half-length and conductivity are inadequate to completely describe stimulation performance [56]. Hence, a concept called stimulated reservoir volume (SRV) was developed to be used as a correlation parameter against well performance [56]. The size of the created fracture network was approximated as the 3D volume (SRV) of the micro-seismic event cloud [56]. It has been observed that the volume of SRV increases with the fracture network size and complexity. Mayerhofer et. al has shown earlier that the cumulative production from the reservoir is directly proportional to the SRV [56].

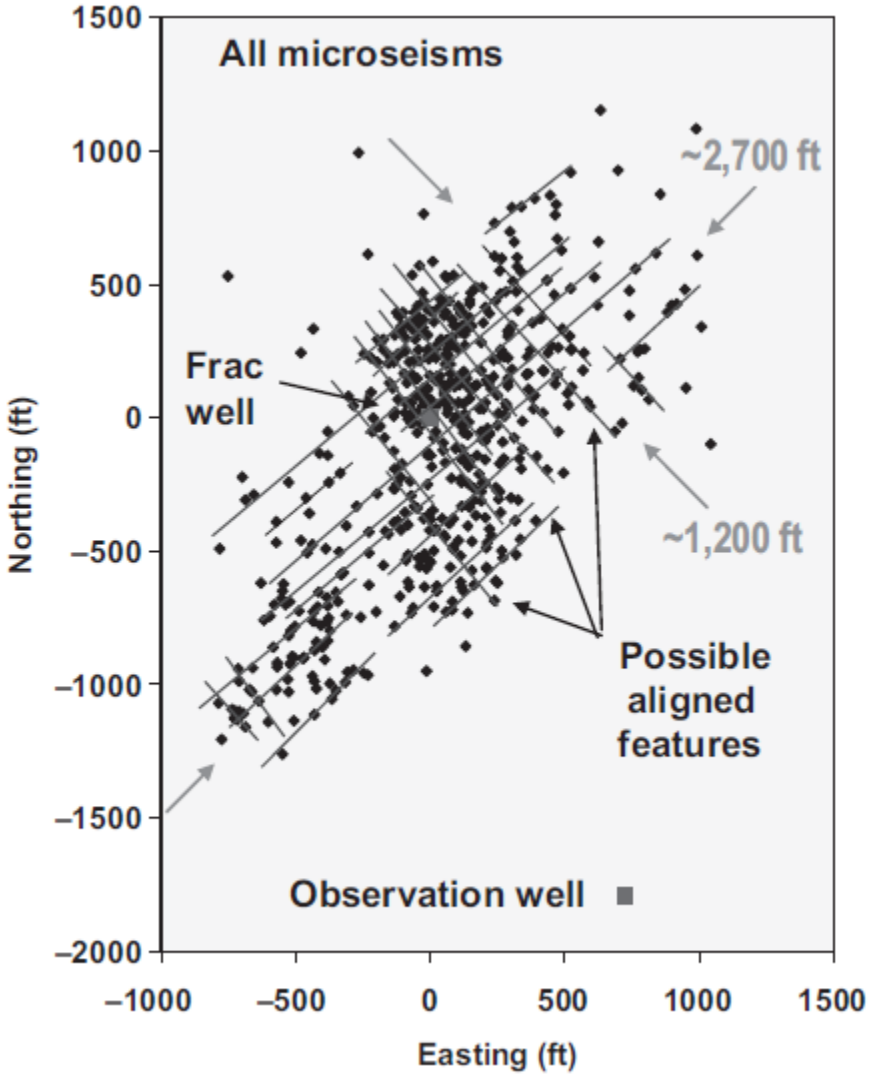

Figure 6: Micro-seismic fracture mapping shows complex-net-work growth in shales [57]

2.2.2 Fracturing Fluids Used in Unconventional Reservoirs

Fluid viscosity has a detrimental effect on fracture complexity. Laboratory tests have shown that both near-wellbore and far-field fracture complexity decrease during injection of high-viscosity fluids [58, 59]. Field data have also shown that high-viscosity fluids can reduce fracture complexity [60, 61]. It is more difficult for high-viscosity fluids to penetrate intersected natural

fractures or fissures [59]. Therefore, fluid viscosity could have a significant impact on fracture complexity and needs to be addressed in stimulation designs of unconventional reservoirs [55].

Slickwater fracturing fluids are less viscous than cross-linked fluids and aid in creating fractures with smaller width and longer fracture length. Slickwater fracture treatments connect the long hydraulic fractures to the natural fractures usually common in brittle shale formations and create a large stimulated reservoir volume. With the advent of shale gas plays, the use of slickwater fracturing has increased over the last decade due to their lower cost.

The main drawback of using slickwater lies in its inability to transport conventional proppants efficiently inside the fracture [62]. Use of higher concentration of gels can help in proppant transport but can introduce large formation damage by blocking pores in nano-Darcy shales [63]. A potential solution to this problem would be to use light weight proppants which can easily be transported by slickwater [31, 91, 102]. However there is no concrete evidence on whether these proppants can endure the stresses expected in various shale formations without compromising fracture conductivity [64].

2.2.3 Proppants for Unconventional Reservoirs

Proppants with different mesh sizes of 20/40, 30/50, 40/70, 70/140 and 80/200 with grain diameters ranging from 0.033 inch (0.8382 mm) to 0.0041 inch (104.14 μm) are conventionally used during hydraulic fracturing of tight shale formations [12]. These proppants are large enough to create conductivity in the larger generated or existing fractures but not small enough to penetrate into the existing or generated micro-fractures. This will cause the closure of micro-fractures at the

end of a fracturing job thus reducing the length and conductivity of the complex fracture network [12]. During fluid injection into the reservoir during hydraulic fracturing, the opening of the natural fractures and the pressure applied inside them decreases as the distance increases from the point of injection. Injecting nano-sized proppants after the injection of pad volume and prior to the placement of larger proppants, is a good way to prevent the closure of these micro-fractures and ensure their contribution to production. These nano-proppants should be able to prop the micro-sized fractures, withstand the pressure encountered in reservoir formations and provide a conductive path for the flow of hydrocarbons during production.

Although a very high conductivity is not required for very low permeability formations, an open fracture or micro-fracture performs better than a collapsed fracture [12]. A longer, more conductive hydraulic fracture or fracture network will deliver more production than a small, low-conductivity fracture. Most of the approaches used for economic optimization of fracture design vary parameters such as fluid and proppant volumes, concentrations and flowrates, but seldom consider changes in proppant type in any detail [65].

Injecting smaller proppants prior to the injection of larger ones may help in sequentially filling the widened natural fractures (widened during injection), allowing deeper percolation of proppants, thus propping a longer fracture length [66]. Similarly, injecting nano-sized particles which can withstand the overburden pressure, followed by the conventionally used larger proppants, may help in propping more of the SRV thereby increasing the seepage area and enhancing production [66].

Increasing the effective conductivity of the hydraulic fractures propagated in tight oil or gas plays by improving the type and placement of proppants will have the following results: [12]

- It will prevent the collapse of already existing micro and nano-sized natural fractures which are opened up during injection.
- Using very small proppants before the injection of the larger proppants will prevent the collapse of the fissures that are generated during the injection, after the injection is stopped.
- It will improve the production of oil and/or gas from the formation by reducing fluid loss and improving the total fracture conductivity.

Figure 7 demonstrates how the injection of nano-proppants will keep the small fissures open and extend the network of small fissures, while commercial proppants keep the main fracture open [12].

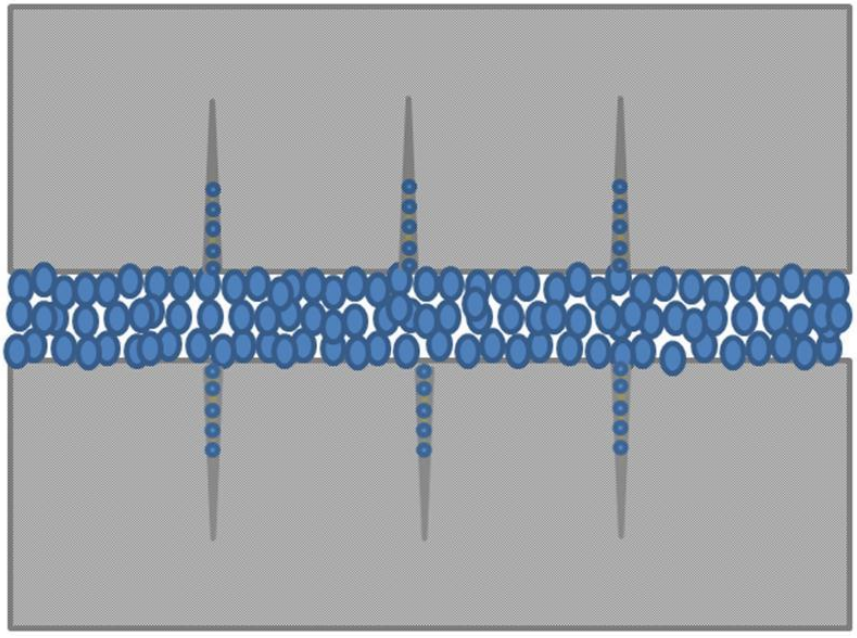

Figure 7: Schematic picture of proppants and nano-proppants distributed in fractures and micro-fractures, respectively (Drawn by Dr. Reza Barati: used with permission) *[12]*

2.2.4 Silica Nano-Particles

Silica nanoparticles show good resistance against compressive stress and have been used successfully in drilling fluids in order to decrease water invasion into shale formations [12, 13, 67, 92, 95]. Their hardness under stress and their size will potentially make them capable of penetrating into micro-fractures and fissures generated during a hydraulic fracturing job in tight shale plays. Their performance as fluid loss additives and proppants for micro-fractures is worth studying. Silica nanoparticles are very stable (colloidal stability) and do not coagulate at pH values above 8 [67]. Additionally, silica nanoparticles will not show precipitation problems during the injection since they are very light (suspension capability of the fracturing fluids depend on the weight of the proppants). If injected with water or linear gels before the injection of larger proppants they potentially can make the fractures longer and more conductive. Several research groups demonstrated the capability of silica nanoparticles in reducing the damage caused by fines migration [12, 92, 93]

2.2.5 Fly Ash

Fly ash is a byproduct of coal-fired power plants. After the coal gets burnt, the heavier ash particles fall to the bottom of the burning chamber and the lighter ash particles are carried away with the exhaust gas. The latter is known as fly ash and the former is known as bottom ash. Before getting expelled into the atmosphere, these fly ash particles are removed and collected by electrostatic precipitators [68]. Fly ash particles are generally spherical in shape as the particles solidify rapidly while being suspended in the exhaust gas [12, 103].

The chemical properties of fly ash are largely influenced by the chemical content of the coal burnt. Two classes of fly ash are defined by ASTM C618: Class C fly ash and Class F fly ash. Class F fly ash is produced when the harder, older anthracite and bituminous coal is burnt. Class C fly ash is produced from the burning of younger lignite or sub-bituminous coal. The main difference between these classes is the amount of calcium, silica, alumina, and iron content in the ash [69]. Fly ash is a heterogeneous material. Though SiO_2, Al_2O_3, Fe_2O_3 and CaO are the main chemical components present in fly ash, other components like MgO, TiO_2, arsenic, etc. are also present [12]. **Table 2** gives a list of constituents and their typical compositions in class F fly ash. Fly is a cheap waste product and it has significant silica content.

Table 2 : Constituents and their typical compositions in Class F fly ash (Alliant energy, MSDS, 2005)

Constituent	***Typical Composition ranges***
SiO_2	40-60 %
Al_2O_3	18-31 %
Fe_2O_3	5-25 %
CaO	1-6 %
MgO	1-2 %
TiO_2	1-2 %
Inorganic arsenic	16-210 ppm

2.3.1 Experimental Methods from Literature

2.3.1.1 Static Fluid Loss Cell

To study the formation of filter cake statically, tests are conducted by making fracturing fluids filter through a core sample by applying pressure on the fluid loaded over the core sample. The fluid which leaks off through the core is recorded against the square root of exposure time to study the filtration process. API Recommended Procedure 39 talks about the standardized procedures for static fluid loss tests. However the type of filter cell and core have not been specified [70]. The

most commonly used cells are the modified Baroid cell and the Halliburton cell. The core thickness of 1” is recommended. The general test procedures adopted are given below [70].

1. The test fluid should be well mixed with the additives before loading it in the cell.
2. Heat the cell to the required temperature for starting the experiment.
3. Nitrogen is used to supply the differential pressure required for the experiment.
4. Open the outlet valve to collect filtrate.
5. Filtrate should be collected for a minimum period of 36 minutes.

McGowen and Vitthal used Halliburton’s high pressure, high temperature static fluid loss cell for their studies. They recommended creating a repeatable procedure for mixing the fluids for obtaining accurate results. They also recommended keeping the core length constant for different tests and opening the leak-off valve immediately after the application of differential pressure [71].

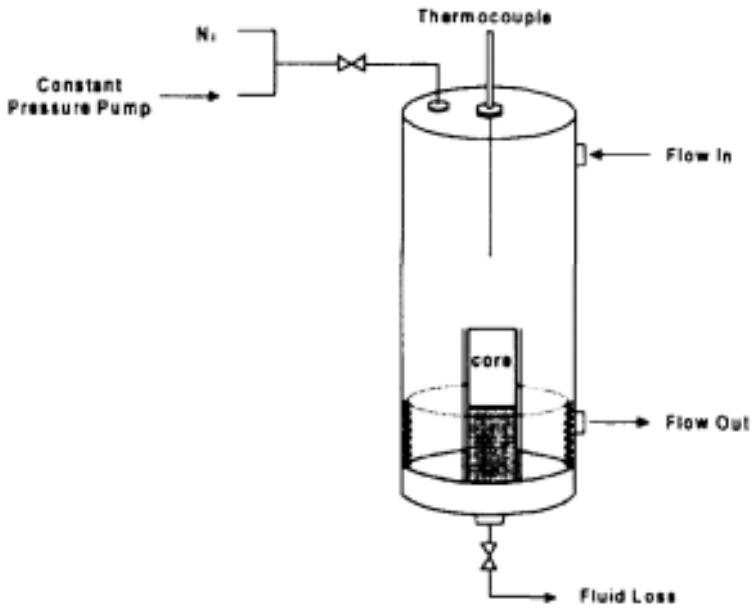

Figure 8: Schematic picture of high pressure high temperature cell used by McGowen and Vitthal *[71]*

2.3.1.2 Long Term Fracture Conductivity Cell

A test setup for evaluating short term proppant pack conductivity was recommended by API. This system was designed to measure the closure stress under which proppants crush. Core samples could not be used in this test set up and the proppants were placed between two pistons. The contact area between the proppants and the pistons was 10 square inch. The cell is shown in **Figure 9**. API gave the following recommendations [72].

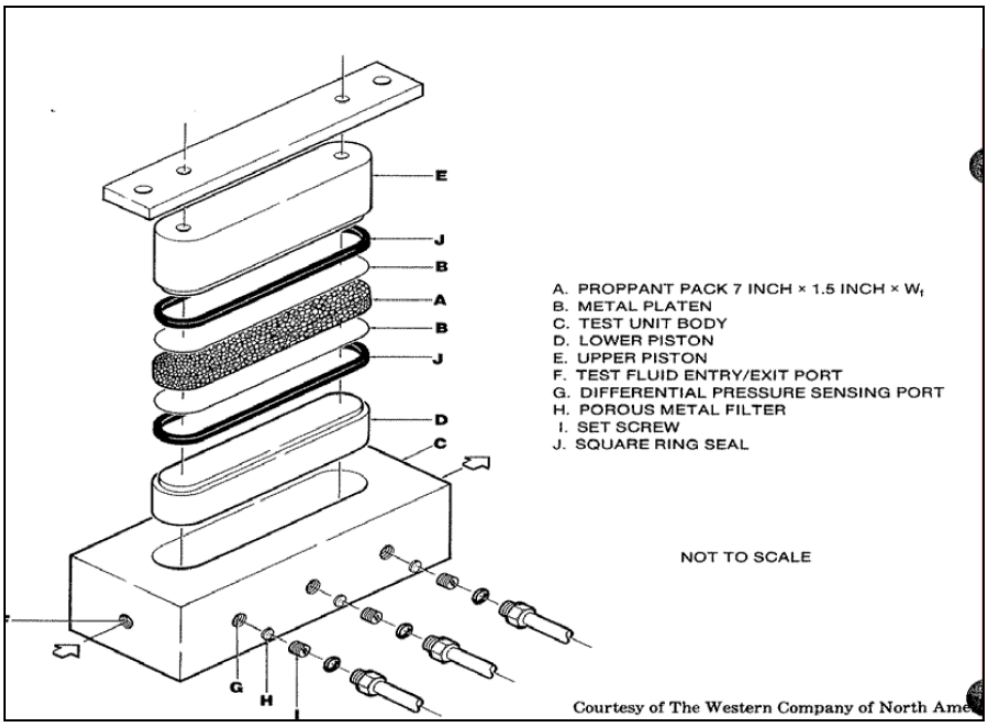

Figure 9: Dissembled API Conductivity Cell *[72]*

1. Hydraulic load frame used to apply closure stress should be capable of applying 150,000 pounds force preferentially with loading rate of 5000 lbf/min. This would apply 15000 psi pressure on the proppant pack which is the equivalent of closure stress acted upon the proppants at a depth of 20,000 ft., assuming a closure stress gradient of 0.75 psi/ft.
2. Constant flow rate pumps which can keep the flow rate constant within a range of 1-10 mL/min with pressure fluctuations less than 2%, is recommended.
3. Differential pressure transducers with a range of 0-1 psi are deemed satisfactory.
4. Back pressure regulators should be capable of keeping the downstream pressure 50 psi more than the vapor pressure of the test fluid to prevent the vaporization of the fluid which would plug the pores. API recommends deoxygenation and saturating with silica.
5. API recommends a proppant pack loading of 2 lbm/ft^2 or more.

6. After applying different values of closure stress on the proppant pack, fracture conductivity is calculated after measuring the width, pressure gradient and flow rate at each stress level. It can be estimated from the proppant crushing sound whether or not the proppant pack has reached the semi-steady state condition [72].

2.4 Summary

Industry is currently reliant on enzymes and encapsulated oxidizers to achieve fracture clean-up. However, gel damage continues to be one of the main mechanisms reducing the permeability of hydraulic fractures. Industry is still craving for a more sophisticated encapsulating agent which can release the breaker after the shut-in time and uniformly distribute them to target the filter cake [1, 14, 27].

Polyelectrolyte nanoparticles have been found to be capable of protecting the enzymes from temperature and pH conditions otherwise inhospitable to enzymes. Their ability to delay the release of enzymes, thus preventing them from breaking down the viscosity of fracturing fluids during the injection period has been already proved in laboratory experiments [2]. Taking advantage of high surface area and delayed release, polyelectrolyte nanoparticles have the potential to release high concentrations of breakers in the filter cake. In the absence of these encapsulating agents, which also act as fluid loss reducing agents, the breakers could be lost into the formation as a part of the fluid leak off, as their molecular size is small enough to leak through the pore throats. A small volume of unentrapped enzymes in the system can also be used along with the entrapped enzymes to degrade the polymer that could have leaked into the formation along with the initial fluid loss. PEI-DS nanoparticles can also release the breakers within a controlled time

period to remove the filter cake [2]. It is worth studying the proppant pack conductivity of the fracturing fluid system which uses PEC nanoparticles as encapsulating agents for enzymes and also its fluid loss reduction capabilities for ultra-tight formations.

Tight and ultra-tight reservoirs are dependent on large stimulated reservoir volume involving a large network of micro-fractures for their economical depletion. Injection of nano-proppants prior to the conventionally used proppants, will help improve the production by propping more micro-fractures thereby increasing their fracture conductivity. It will also help in extending the length of the generated small fissures during propagation [12]. The size and hardness of silica nanoparticles encourages their application as nano-proppants. Fly ash particles, a waste product from the thermal power plants (much cheaper) is a significant source of silica.

3. Materials

3.1 Fly Ash

Two samples of fly ash were donated by Alliant Energy; Class 'C' and Class 'F', with slight differences in their constituents and compositions. Class ‘C’ fly ash is reddish brown in color while class ’F’ is greyish dark. After being washed with 2% KCl, they were imaged using a transmission electron microscope (TEM) followed by nano-indentation tests to measure their ability to withstand compressive stress. Class F fly ash samples were found to show better fracture conductivity results and hence were used as fluid loss additives in the fluid loss tests and as nano-proppants for the conductivity tests [12].

3.2 Core Materials

In order to test the fluid loss reduction capability of polyelectrolyte complex nanoparticles, API static fluid loss tests were carried out using Indiana Limestone, Kentucky and Crab Orchard core samples. These three types of cores represented the properties of high permeability reservoirs, low permeability reservoirs and tight reservoirs respectively. Core samples used in fluid loss experiments were approximately 1", both in length and diameter. For testing the fluid loss reduction capability of fly ash nanoparticles, Indiana limestone core samples were used with the same dimensions. The suppliers for the cores were Kocurek Industries, Caldwell, TX.

Parker sandstone and Scioto sandstone core wafers were used in the fracture conductivity tests for testing the conductivity of polyelectrolyte complex nanoparticles while only Scioto cores (low permeability) were used to test the conductivity of fly ash nanoparticles (to simulate unconventional reservoir formations). Both kind of cores were again supplied by Kocurek

Industries. The cores were shaped with high precision, i.e. the dimensions were within 0.03" of the cell body dimensions. The upper core dimensions were 7" in length, 1.44" in width, and 0.70" in thickness, whereas the bottom core dimensions were 7.25" in length, 1.8" in width, and 0.625" in thickness. Kocurek industries reported porosity and permeability of the cores to be 12% and 0.01-0.1 mD (gas) for the Scioto sandstone and 17% and 8-10 mD for the Parker sandstone**,** respectively [14, 60, 90].

3.3 Sealant

734 Dow Corning RTV flowable sealant was used to seal the sides of the core samples used for API long term fracture conductivity testing to make sure that that liquids flow only through the upper and lower surface of the cores.

3.4 Guar Products

Hydroxypropyl guar (HPG) gum blend (Jaguar® 415, Rhodia, Paris, France, Lot#H0904166E) was used for all the experiments reported here. Jaguar® 415 is a high viscosity chemically modified polysaccharide, which disperses readily and then hydrates, to form a smooth and viscous solution [73].

3.5 Borate Cross-Linker

Sodium tetraborate decahydrate (J.T Chemical Co. reagent, Philipsburg, NJ, lot NO# 110M0107V) was used as the source of borate ions to cross-link guar polymer and generate guar gel.

3.6 Proppants

The proppants which have been used in the hydraulic fracture conductivity experiment were

CARBO Ceramic's 20/40 Econoprop. The median particle diameter is 635 microns. The reference conductivity value for 2lb/ft.^{2} proppant pack at 250 ° F under 2,000 psi closure stress is 6500 mD.ft. The data given by the supplier is listed in **Table 3** [74].

Table 3: Proppant properties (Carbo Ceramics)

Proppant properties (Carbo Ceramics co.)	
Type	CarboEconoprop
Size (mesh)	20/40
Roundness	0.9
bulk density (lb/cu.ft.)	96
apparent specific gravity	2.7
absolute volume (gal/lb)	0.044
solubility in 12/3 HCL/HF acid (%weight loss)	1.7
crushing pressure (psi)	7000
median diameter (microns)	635

3.7 Enzymes

Pectinase from Aspergillus aculeatus (Sigma-Aldrich, St. Louis, MO, Catalogue # P2611) was used for all the tests. In the test in which the cross-linked gel was used with just pectinase, the pectinase was diluted to 0.1 volume percentage in a 45 ml solution. In the test in which pectinase was entrapped inside the nanoparticles, it was used in 0.1 volume percentage, in a solution of a diluted mixture of enzymes and nanoparticles of 45 ml volume [52]. The activity of 0.1 % pectinase solution is 13 hour^{-1} [2].

3.8 Polyelectrolytes

A polycation (polyethylenimine branched with M_W 25 kDa from SIGMA, Batch# MK13L7852V) and a polyanion (dextran sulfate sodium salt with M_W 500 kDa, Lot No. 116614) were obtained from Fisher Scientific (Pittsburgh, PA).

3.9 pH Modifiers

Sodium hydroxide (1 M, LOT No. 120837A) and hydrochloric acid (6 N, LOT No. 122818) were used as pH modifiers. They were both obtained from Fisher Scientific (Pittsburgh, PA).

4. Methods

4.1 Potassium Chloride Solution

All solutions were made in 2% KCl solution as the base fluid. 20 g of potassium chloride (SIGMA ALDRICH P code: 1001404659 Lot# SLBH1238V) was added to 980 g of water, purified by reverse osmosis, and stirred using a magnetic stirrer (Thermo Scientific Cimarec) to obtain a homogeneous 2% KCl solution. The density of brine was measured as 1.0105 g/cm3 and viscosity was 0.95 CP at 25 °C [12].

4.2 Preparation of HPG Solution

In a 400 ml beaker containing 150 ml of vigorously stirring (600 rpm) solution of 2% KCl, 0.75 gram polymer (guar) was added slowly to the shoulder of the vortex, to create 5000 ppm HPG solution. The solution was left to stir at the same rate for 5 minutes, after which the stirring rate was reduced to 400 rpm. After an hour, stirring rate was reduced to 200 rpm after which it was kept for 12 hours to hydrate [12].

4.2.1 Cross-Linking of HPG Solution

The HPG was cross-linked using borax (cross-linker). In order to produce thick cross-linked HPG gel, 45 ml of 2000 ppm borax aqueous solution was added to the 5000 ppm HPG solution.

4.3 Preparation of Guar and Fly Ash Solutions

Two solutions were prepared using guar: one containing fly ash, and another one without it with the same guar concentration to use as a control fluid system [12]. Guar solutions of 5000 ppm concentration were prepared by carefully measuring out 0.75 g of guar (Rhodia Inc.) and mixing it

in 150 g of 2 % KCl solution. During the addition of the guar powder, the brine solution was stirred rapidly at 600 rpm using a magnetic stir bar inside a 500 ml beaker. Guar powder was added to the shoulder of the vortex while the solution was stirred in order to prevent clumping. Five minutes after the addition of guar, the stirring rate was lowered to 400 rpm and it was allowed to stir for about an hour [12]. A 6 ml sample was removed from the solution to make the volume 144 ml. After the solution was prepared, 45 ml of 2% KCl was added along with 45 ml of borate cross-linker, to make up a final volume of 234 ml crosslinked HPG gel.

For guar samples containing fly ash, fly ash required to form a final 1% concentration of fly ash in the 234 ml of final solution was weighed and added to the solution along with the 2% KCl solution. For the fly ash sample without guar, fly ash was simply added to 2% KCl, to yield a 1% by weight suspension, in order to produce another control system. The class F sample, which showed more promising results with conductivity tests, was used for all the fluid loss tests [12].

4.4 Preparation of Polyelectrolyte Complex Nanoparticles

The ratio of PEI (1% w/w): Enzyme (25% w/w): DS (1% w/w) used in the preparation of enzyme loaded PEI-DS nanoparticles was 2:0.1:1. 0.2 mL of pectinase, already diluted in R.O. water to 25%w/w ratio, was added drop-wise to 4 mL of a 1% w/w aqueous solution of PEI (pH adjusted to 8 using 4N HCl) while stirring. Then 2 mL of a 1% w/w aqueous solution of DS (pH 7.8) was added in the same manner while the solution was stirred at 600 rpm. The solution was allowed to stir for another 20 minutes. pH of the entrapped enzyme nanoparticle system was 7.5. In the experiment, which uses the nanoparticles without the enzyme, same volume of R.O. water was added instead of the enzyme [2, 60, 93].

4.5 Core Saturation and Porosity Measurement

The dimensions of the cores were measured and recorded in a research notebook. They were dried in a 70 °C oven for at least 48 hours till they reached a constant weight. The cores were then weighed and the weight was recorded as W_D. Cores were evacuated to 30'' Hg vacuum pressure for 20 minutes using a desiccator connected to a vacuum pump. The valve to the vacuum pump was closed and inlet valve was opened to allow the flow of 2% KCl in to the saturation vessel. Inlet lines were filled with the saturation fluid before opening the inlet valve to prevent air bubbles from entering the desiccator. **Figure 10** is the schematic of the core saturation setup. The cores were left immersed in the brine for 2 hours. The cores were then wiped with a paper towel before weighing them again to record W_S. Using W_S, W_D (recorded earlier) and the density of 2% KCl at room temperature (1.013 g/cm^3), porosity was calculated using the Equation 1 given below [2, 14, 60].

PV = Pore volume, cm^3

W_D= Dry weight of core, g

W_S = Saturated weight of core, g

ρ = Density of saturating fluid, g/cm^3

$$PV=[W_D-W_S]/\rho \quad \text{.....Eq. 1}$$

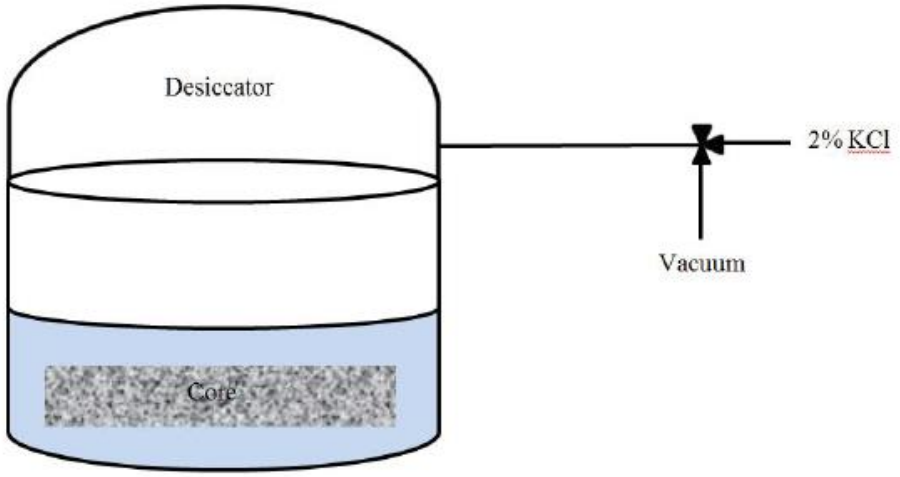

Figure 10 : Schematic figure of the core saturation setup used for the conductivity cell cores *[2]*

4.6 Permeability Measurements for Fluid Loss Experiments

The apparatus used to measure the permeability of the cores used for fluid loss experiments is shown in Bose et al., 2014 [52]. An ISCO pump filled with SOLTROL-130 was connected to a transfer cylinder filled with SOLTROL-130 and 2% KCl. In order to apply confining pressure, a Hassler-type core holder connected to a hydraulic pump, was connected to the transfer cylinders. The differential pressure transmitter (Honeywell) connected to the inlet and outlet of the core and the tubing, connecting the transmitter to the flow line was filled with SOLTROL-130. The whole setup was placed in a constant temperature chamber. Permeability measurement for the cores used for fluid loss tests were conducted using this setup. Pressure drop, temperature of cabinet, viscosity and calculated permeability using Darcy's law were recorded during each test [2, 14, 60].

4.7 Transmission Electron Microscopy (TEM)

Samples were prepared by suspending the particles in ethanol and agitating in an ultrasonic bath for 15 minutes. Samples of 5 µL were placed onto copper mesh grid with a lacey carbon film. The wet

grids were allowed to air-dry for several minutes before they were examined under a TEM. The particle size and morphology of the fly ash particles were examined by using a FEI Technai F20 XT field emission transmission electron microscope (**Figure 11**) at an electron acceleration voltage of 200 kV. High resolution TEM images were captured using a standardized, normative electron dose and a constant defocus value from the carbon-coated grid [12].

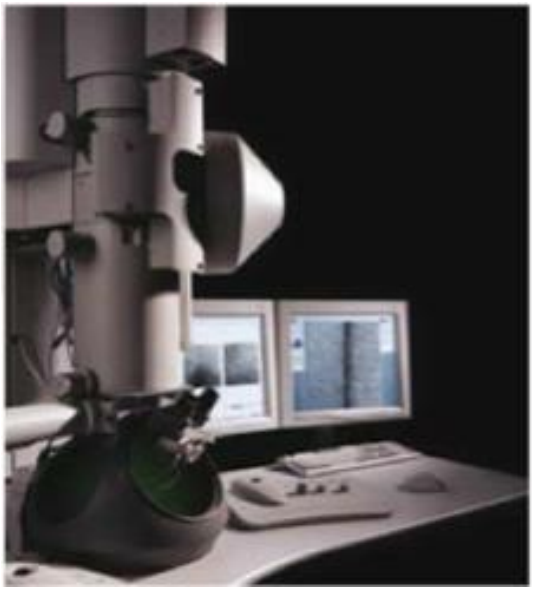

Figure 11: FEI Tecnai F20 XT Field Emission Transmission Electron Microscope *[75]*

4.8 Nano-Indentation

Nano indentation tests were carried out on fly ash samples to study if they can withstand the stress they would encounter in the fractures if used as proppants. Due to the unavailability of a nano-indentation set up in our lab, we had to outsource it to a private lab (Ebatco) who carried out the experiments according to our requirements and reported back the results.

The testing instrument that was used by Ebatco for performing the nano-indentation tests is a nano-mechanical test system (manufactured by Hysitron, Inc., USA). This high-resolution nano-

mechanical test instrument performs nano-scale quasi-static indentation by applying a force to an indenter tip while measuring tip displacement into the specimen. During indentation, a load-displacement curve was created for each indent by continuously controlling and measuring the applied load and tip displacement. From this load-displacement curve, by making use of pre-calibrated indenter tip area function and pre-determined machine compliance value, hardness and reduced elastic modulus values were determined using Oliver and Pharr method [76]. The instrument also has the capability to provide in-situ SPM (scanning probe microscopy) images of the specimen before and after indentation. Such nanometer resolution imaging function is accomplished quickly and easily by utilizing the same tip for imaging as for indentation. The in-situ SPM imaging capability is critical in positioning the indenter probe for indentation tests and also for measuring the size of nanoparticles [77].

Hardness and reduced elastic modulus values can be determined using nano-indentation. The reduced elastic modulus has a relationship with the Young's modulus as shown in Equation 2. If Poisson's ratio for the material to be tested is known, then the Young's modulus can be easily calculated. The Poisson's ratio for the diamond indenter is 0.07 and the Young's modulus of the indenter is 1141 GPa [77].

$$\frac{1}{Er} = \frac{(1-V^2 material)}{Ematerial} + \frac{(1-V^2 indenter)}{Eindenter} \quad \text{Eq.2 [77]}$$

Figure 12 illustrates the major components of the nano-mechanical testing system [77].

Figure 12: The full-feature, multi-technique nano-mechanical test system; Left: main unit; Right: transducers mounted on a granite platform inside the environmental enclosure *[77]*

In order to conduct nano-indentation and particle size analysis, the particle specimens were sparsely dusted onto a steel disk surface with strong and fast curing adhesive. **Table 4** summarizes the test conditions and parameters used in the hardness and modulus tests. To obtain the hardness and reduced elastic modulus values, 10 indents, were made onto 10 particles. All indents and images of particles were performed through in-situ SPM imaging. Class C was tested under a load of 70 N while Class F was tested under a load of 50 N. The loads were selected to reach contact depths at maximum of 50 nm, to restrict the indenter from indenting too deep into the smaller particles [12].

Table 4: Hardness and modulus testing conditions and parameters *[77]*

Specimens	**2 Kinds of Fly Ash Powder Specimens**
Test instrument	TriboIndenter
Indenter Probe Tip	Diamond Berkovich indenter tip
Indentation Loads	50, 70 μN
Temperature	70°F
Humidity	16% RH
Environment	Ambient air

4.9 Static Fluid Loss Tests

Polyelectrolyte complex nanoparticles and fly ash nanoparticles were used in fracturing fluids in order to study the fluid loss prevention effect of the nanoparticles on cores with different permeabilities. Filter cake was allowed to be formed first and a graph of filtrate volume versus square root of time was prepared for a period of 90 minutes.

The fluid loss cell, available at Tertiary Oil Recovery Project (TORP) labs, has six grub screws (shown in **Figure 14**) to secure the end-caps to the cell body. Leakage is prevented by O-ring seals and a rubber core holder which prevent any possible overpass of the core. Special attention must be paid to ensure that the cell is cool and all pressure has been relieved before loosening the grub screws. The cell must not be operated above 1000 psi at any circumstances.

The flow schematic of the setup is shown in **Figure 13**. A nitrogen supply provides the pressure applied for the fluid loss and the back pressure required to prevent vaporization of water in the outlet. Pressure is recorded at the inlet and the outlet. The fluid loss cell is placed inside a cabinet equipped with valves used to set the inlet and backpressure **(Figure 16**). All tests were carried out at room temperature.

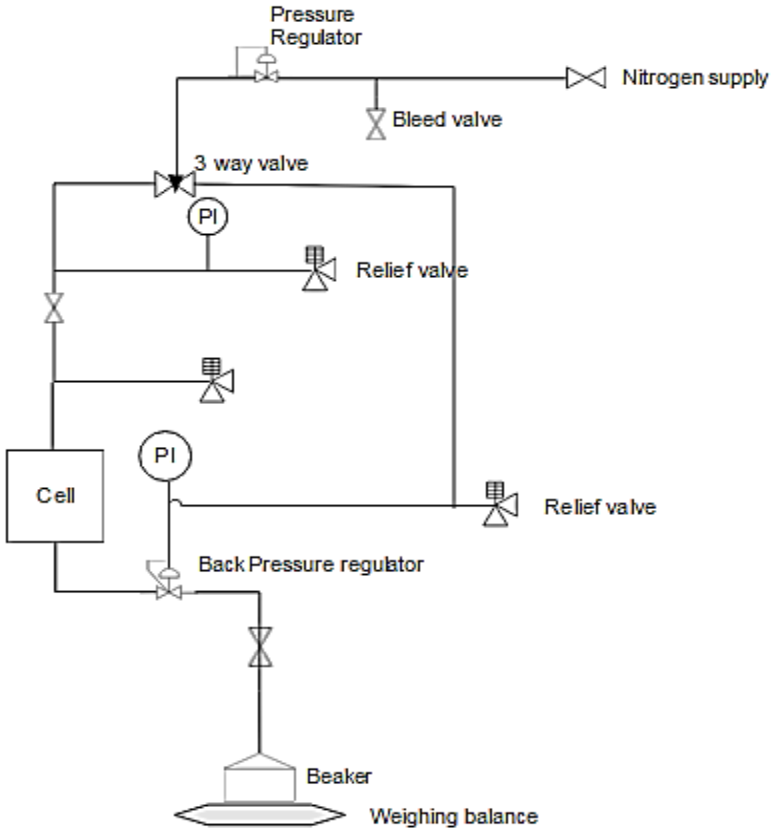

Figure 13: Schematic Picture of API Static Fluid Loss Cell

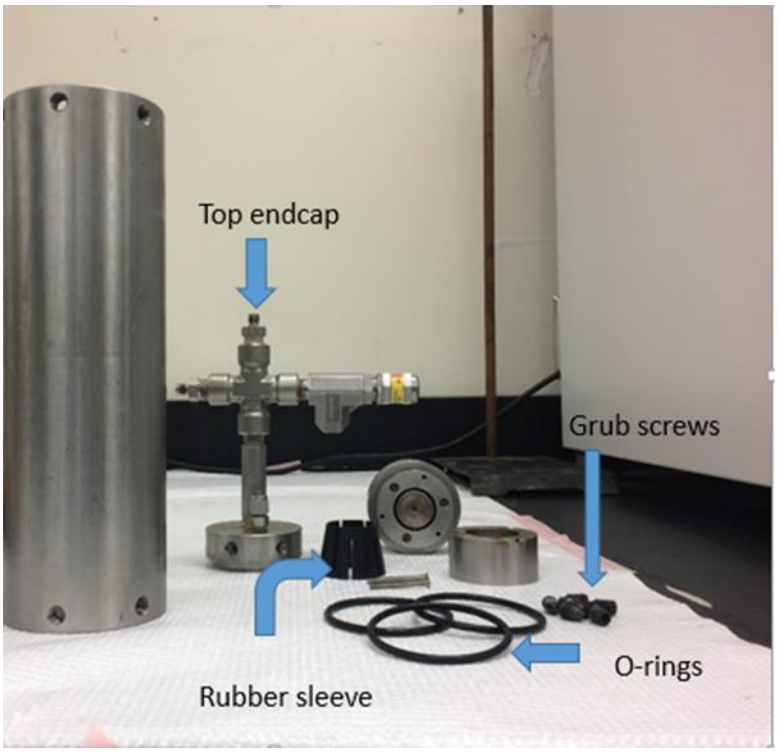

Figure 14: Parts of API Static Fluid Loss Cell Dissembled

The parts of an API static fluid loss cell are shown in **Figure 14**. In order to use a core in the fluid loss cell, rubber sleeve with plastic collet, a stainless retainer, a tapered stainless receptacle and an endcap having a tapered cone for sealing inside the rubber sleeve were used. The one-inch by one-inch core was inserted into the rubber sleeve. One end of the rubber sleeve was attached onto the endcap with tapered cone. The core was pushed against the tapered cone. The thin stainless retainer was screwed using small screws into the endcap to secure the sleeve against the tapered cone. The plastic collet was inserted over the rubber sleeve. The large stainless shaped-receptacle was placed onto the collet and secured into the small retainer using the long screws. Screws were tightened evenly. Space was left to accommodate the filter cake above the surface of the core. The core assembled inside the endcap is shown in **Figure 15** [2].

Figure 15: Bottom end-cap with core assembled in place *[2]*

The following procedure recommended by Schlumberger for loading the static fluid loss cell was followed [78]. Firstly, bottom endcap was inserted into cell with either 1 or 2 O-rings. The screws for securing the end cap were checked for deformation, and if found to be deformed, were replaced immediately. All six screws were tightened. After securing the bottom endcap, the cell was inverted and filled with the desired fluid combination. The top endcap was attached with O-rings and the six grub screws were tightened. The cell with endcaps attached was placed into a pressure control cabinet supplied with a nitrogen tank (**Figure 16** and **Figure 17**). The inlet nitrogen was attached to the upper quick connect. With a syringe filled with the base fluid, the bottom exit assembly was flushed and filled with 2% KCl and quick connect was attached. This ensures that the first drop of liquid coming out will be collected in the measuring balance kept under the outlet line of the cell. The inlet pressure regulator was increased to 550 psi. The back pressure regulator was set at 50 psi. The outlet valve was opened and data collection started. Leak-off fluid was collected on the balance and the weight versus time was recorded using appropriate data acquisition equipment. The test must be stopped before the cell is completely empty to prevent the entry of air into the core sample. The cell and endcaps were cleaned thoroughly before reuse [78].

Figure 16: Fluid loss cell placed inside a pressure control cabinet supplied with a nitrogen tank *[2]*

Figure 17: Close view of the cell assembled inside the cell holder *[2]*

The wall building coefficient C_w is related to the cumulative fluid leak off volume by the following equation.

$$V_L = 2C_w * \sqrt{t} + S_P \quad \text{.....Eq. 3}$$

Where:

V_L = Total fluid loss volume (mL)

C_W = Fluid loss Coefficient (ft./min$^{1/2}$)

S_P = Spurt loss coefficient (mL)

t = Total time duration of experiment (min)

C_w is calculated from the slope of the straight line in the fluid loss curve using the equation given below [79]:

$$Cw = 0.0164 * m/A \quad \text{Eq. 4}$$

Where:

m = slope of volume versus $t^{1/2}$, $ml/min^{1/2}$

A = core cross sectional area, cm^2

C_w = wall building coefficient, $ft./min^{1/2}$

4.10 Long-Term Hydraulic Fracture Conductivity Measurement Tests

4.10.1 Modified API Conductivity Tests

The cell body has three ports on each side where one side has three pressure access ports for pressure measurement and the other side is for temperature. 150 micron Monel screens are placed in all ports, including the inlet and outlet flow inserts in order to prevent solids from flowing out through the ports. The cell has a fixed bottom piston and a floating top piston. The upper and bottom piston cross-sectional areas are 10 in^2 and 13 in^2, respectively. Side pistons with O-ring rubber seal are used to apply closure stress on the cores and maintain the stress inside the cell during the experiment. The side pistons have three access ports for leak off fluid through the cores wafer when a desired stress is applied. The total weight of the cell is about 80 lbs. (without cores and fluid). The cell can take normal loading of proppant (1 to 4 lb. $/ft^2$) and up to 250 mL of fluid, which is enough to create adequate amount of filter cake for study purposes [80]. **Figure 18** shows a picture of the conductivity cell.

The equipment used in the API long term fracture conductivity tests are explained below followed by the procedure that was adopted.

Figure 18: Picture of the fracture conductivity cell provided by Schlumberger

4.10.2 Hydraulic Press

A desired stress is applied on the conductivity cell by a hydraulic press. The load system consists of two 19” by 19” stainless steel plates, a two stage press hydraulic cylinder, load cell, gauge pressure, and hydraulic oil reservoir. The load system is capable of producing a force up to 50,000 pound-force (lbf). A hydraulic jack is used to pressurize the hydraulic oil in two stage cylinders to lift the bottom plate. The amount of force applied is recorded through the load cell. The load cell composed of a strain gauge and was calibrated first through the pressure being applied on the slave cylinder. When stress is applied over the conductivity cell, only the top piston and the top rock are moved down [81].

Hydraulic Press Properties

- Maximum Capacity: 75 tons

- Width Between Uprights (inches): 44
- Width Between Table Channels (inches): 8.25
- Min Ram To Table (inches): 6
- Max Ram To Table (inches): 36
- Ram Travel (inches): 4.5
- Cylinder: 75 ton
- Weight (pounds): 1245
- Dimensions (L* W * H): 55” * 36” * 87”

4.10.3 Test Fluid Drive System

A Dual ISCO Pump was used as the test fluid drive system. Pressure fluctuations during differential pressure and flow rate measurements should be less than 1%. Considering the small pressure drops across the sand pack even small fluctuations can cause significant errors.

Dual ISCO Pumps

Technical Specifications of Dual ISCO pumps are given in **Table 5.**

Table 5: Technical Specifications of ISCO pump (Tele-dyne ISCO pump manual)

Cylinder capacity	102.93 ml
Flow rate range	.01 µl/min to 50 ml/min
Flow rate accuracy	±0.3% (maximum .25 µl/min seal leakage)
Refill or depressurization rate	.01 µl/min to 60 ml/min
Pressure range	10.1 psi to 10135.6 psi
Pressure accuracy	± .5% of full scale at constant temperature
Ambient temperature range	5 to 40˚C
Dead volume	1.3±.02 ml

Continuous flow procedure:

After purging air from the system, total volume was reset to zero. Pressure limits were set by setting the limits of pump. One of the pumps was refilled and constant flow rate option was set for both pumps. Same settings were set for both the pumps under refill option on the menu. Refill rate had to be same or higher than the desired flow rate to avoid time lag or different flow rates. It was ensured that auto refill options are on. The pumps were run in continuous flow mode. It was ensured that the time lag between switching the pumps was less than 8 seconds [82].

Cylinder washing procedure:

A thin film of liquid wets the inside of the cylinder each time the piston travels up the cylinder. The lower flow rates (such as the 4ml/min used in conductivity tests) cause more corrosion since the liquid is in contact with cylinder wall for longer time. For this reason a wash fluid has to be selected that will best flush the cylinder of all liquid residue. The pumps have to be filled and emptied with flushing fluid twice after each use [82].

4.10.4 Pressure Transmitter

In this experiment Honeywell's ST800 Smart Line differential Pressure Transmitter with the Optional3-Button Assembly was used to calculate the pressure difference. The measurements of the transmitter are accurate up to 0.0375 of the calibrated span maximum pressure which is 200 inches of water. **Figure 19** shows the major assemblies.

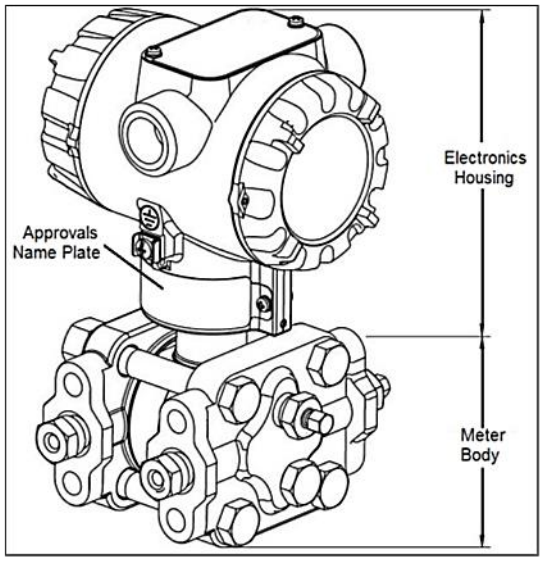

Figure 19: Honeywell Pressure Transducer (Honeywell Transducer Manual)

Optional3-Button Assembly provides the interface, which allows zero correcting. There are increase, decrease and the enter buttons on top of the transmitter's body. In order to set the correct zero the "zero correct" tab should be selected from the interface options. By double pressing on the enter button, the zero would be corrected. Also, the interface option allows changing the range of the reading, the units and the number of the scientific figures [83].

To zero correct the pressure transducer, U shaped lines, manifold and pressure transmitter should be refilled with oil. Then all the valves should be opened widely to the atmosphere and the value on the screen should be permitted to stabilize [83].

4.10.5 Back Pressure Nitrogen Tank

Ultimate pressure in the back pressure nitrogen tank is 2500 psi. It should be stable at all times and be used with caution. The first gauge is the main valve pressure indicator and the second gauge is

the line pressure indicator. To open the back pressure nitrogen tank to the back pressure regulator, first open the main valve to increase the pressure. Then increase the middle valve to desired pressure and open the last valve to the back pressure regulator line. Back pressure should never be applied without having flow in the system so as to avoid breaking back pressure regulator's diaphragm. To check for leak, apply soapy water to all connections.

For removing the pressure, the first step is closing the main cylinder's valve. After that, decrease the pressure using the second valve. Then open the line to the atmosphere and close the valve to the line widely.

A Standard Lab Protocol was prepared for the long-term fracture conductivity measurements based on the standard procedure published by ISO [12]. Long-term hydraulic fracture conductivity measurements were conducted using this procedure detailed below.

4.10.6 Sealing the Cores

734 Dow Corning RTV flowable sealant was used to seal the cores. Core holders (**Figure 21)** were cleaned properly, dried and then release agent was sprayed all over them by keeping them inside the flame hood. They were left for drying for about 15 minutes.

The conductivity cell provided by Schlumberger requires upper and lower cores of different dimensions. The core holders have been made according to core dimensions. The dimensions of the smaller sized core to be used as the upper core, were measured and noted down for porosity calculations. The upper and lower surfaces were covered with transparent plastic tapes and the edges were trimmed just enough to make sure that the sealant doesn't affect the surface **(Figure 20).**

Figure 20: Covering the surface of cores with transparent tape (Picture taken by Reza Barati-used with permission)

A newspaper was folded in the shape of the core holder to act as a cover to prevent sealant from flowing out. The paper was fully covered with transparent tape to ensure that paper is not exposed anywhere. The newly prepared paper cover was kept inside the core holder frame and sealant was applied uniformly all around it. The core was kept above the paper cover and the cover was pushed inside all the way out using the core. It was ensured that the sealant is uniformly distributed all around and that there are no gaps and air bubbles inside. The same procedure was repeated for the larger sized lower core. Cores were left it inside the oven for at least 4 hours at a temperature of 40 degree Celsius. The sealed and dried core is shown in **Figure 22**.

Figure 21: Core Holders *[81]*

Figure 22: Sealed and dried Core inside the core holder

4.10.7 Saturation of Cores and Calculation of Core Porosity

The cores were weighed before saturation and the weight was noted down as W_D. It was made sure that the saturating vessel is clean and dry. The weighed cores were kept inside the vessel. The

vessel was closed and it was also made sure that all the flow lines to the vacuum pump are closed and are tight enough. It was ensured that there was adequate volume of oil inside the pump for the proper functioning of the vacuum pump. The vacuum pump was started and kept running for 20 mins after the gauge reading went all the way to 30 " Hg vacuum. Meanwhile the inlet tube of the saturation vessel was filled with 2% KCl using a syringe. The valve connecting the saturation vessel to the vacuum pump was closed just before the pump was stopped.

Once the chamber was evacuated completely, the end of the inlet tube was kept in a beaker filled with 2% KCl solution. The inlet valve connecting the inlet tube to the saturation vessel was opened to start the flow of 2% KCl solution into the saturation vessel. The valve was kept open until the cores were completely immersed in brine. The core was kept immersed in 2% KCl solution for at least an hour to make sure that the cores are completely saturated with the brine. The cores were taken out, weighed again and weight was noted down as W_S for porosity calculations. The porosity of the core was calculated using the porosity calculation method explained earlier in section 4.5 and 4.6 and also using Eq. 1.

4.10.8 Parts of the Conductivity Cell

The main parts of the conductivity cell are shown in **Figure 23**-**Figure 26**. The dimensions of the cell are included in **Table 6**. Two core wafers with proppants and fracturing fluids loaded between them are assembled together with the upper and lower pistons within the cell body. Parts of upper and lower pistons will remain outside the cell body.

Table 6: Cell Dimensions

Upper piston height (in.)	3.56
Lower piston base (in.)	0.91
Lower piston body (in.)	1.02
Lower piston height total (in.)	1.93
Contact area of upper piston with hydraulic press (sq.in)	9.78
Distance between pressure transducer outlets (in.)	5
Cell block height (in.)	4.77

Figure 23: Inlet and outlet valves

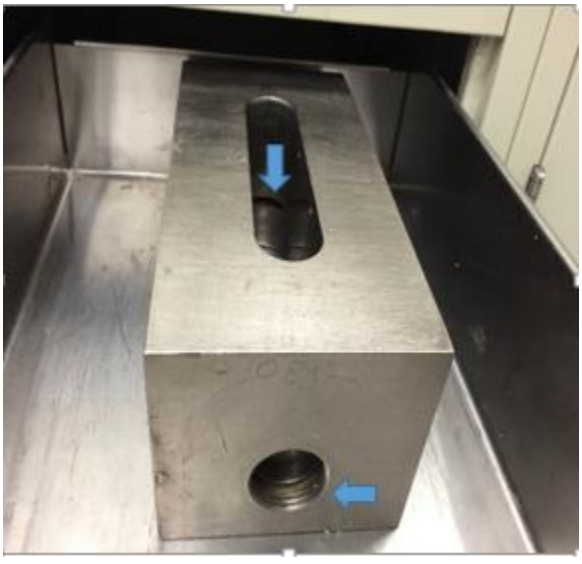

Figure 24: Dissembled cell main body with arrows showing outlets

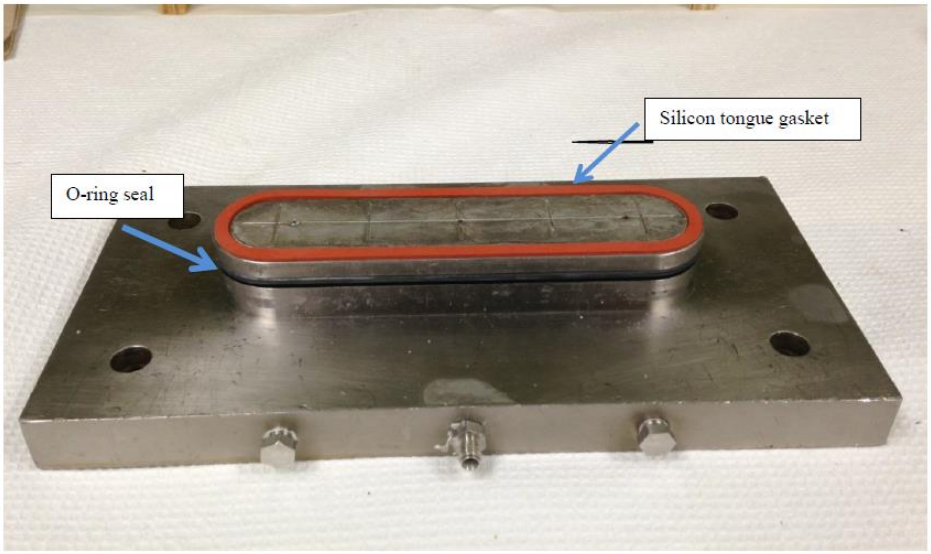

Figure 25: Expanded view of the lower piston [2]

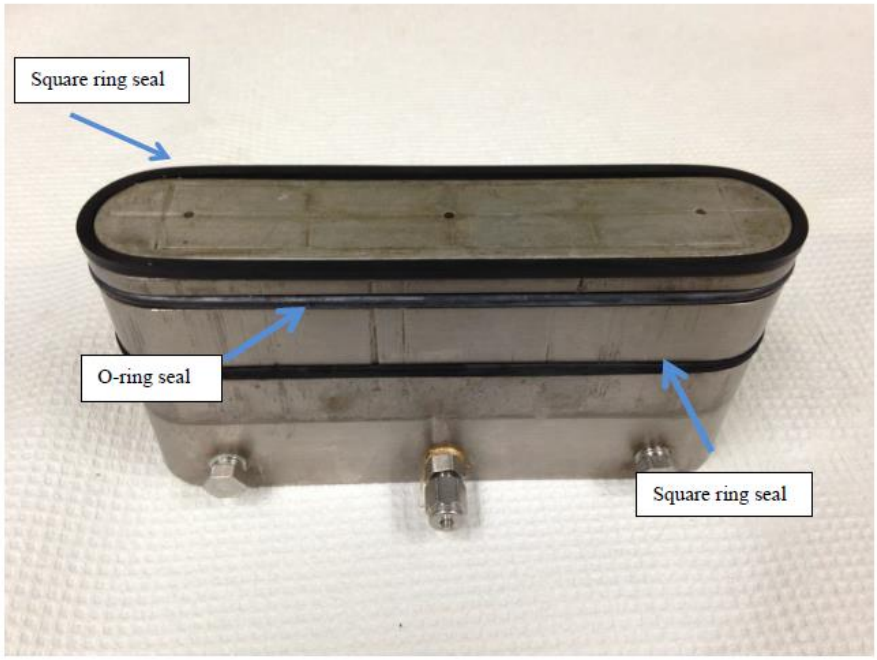

Figure 26: Expanded view of the upper piston [2]

4.10.9 Loading the Cell

Bottom core was loaded first applying a thin layer of sealant to the cell wall to have a better sealing.

A silicon lip gasket was fixed using glue on the gap around the lower piston to have a level surface

(**Figure 25**). The bottom piston was mounted on the top of the core and screwed tightly to the cell body. The cell loaded with the lower piston is inverted. Since there is a gap between top of the bottom core and the cell body, a silicon tongue was placed on the top of the bottom core. After screwing lower piston to the cell body, excess silicon tongue was cut and taken out of the cell.

Distance between bottom core and the top of the cell body was measured. The already prepared solutions were mixed in the calculated proportions to make the fracturing fluid combination for the respective test to be carried out. A 92.3 gram sample (refer to Appendix 9.1 for calculation) of 20/40 Carbo Econoprop proppant was used to get the total loading of 3 $^{lb}/_{sq.ft}$. The proppants were distributed uniformly on the surface of the bottom core.

The fracturing fluid slurry was poured on to the top of the bottom core after closing all the cell valves to prevent undesired fluid loss. The upper piston was prepared by attaching the O-ring and square ring seals (**Figure 26**). The upper core was placed in the cell followed by the top piston. The assembled cell was positioned on the middle of the lower platen of the hydraulic press.

The first stage, fluid leak off, happens through the outlets in the upper and lower pistons. Since differential pressure does not have to be recorded for the fluid leak off, the connecting valves (**Figure 23**) on the inlet and outlet side were kept closed.

4.10.10 Fluid Loss Procedure

All lines were kept closed at the beginning. Force was slowly applied on the cell until the press gage started showing increasing load. Force was applied continuously until the upper core touched the slurry. Before opening upper and lower piston outlines, distance between upper piston and

upper plate were measured to be used for calculating exact polymer concentration. Fluid loss valves were opened at this stage and the fluid leak off was collected in a cylinder kept on a weighing balance. Press load was increased with constant rate of 100 psi/min until 2000 psi final closure stress was reached. Every 30 s, balance reading was recorded to obtain the fluid loss rate. The final volume of fluid leak off was recorded.

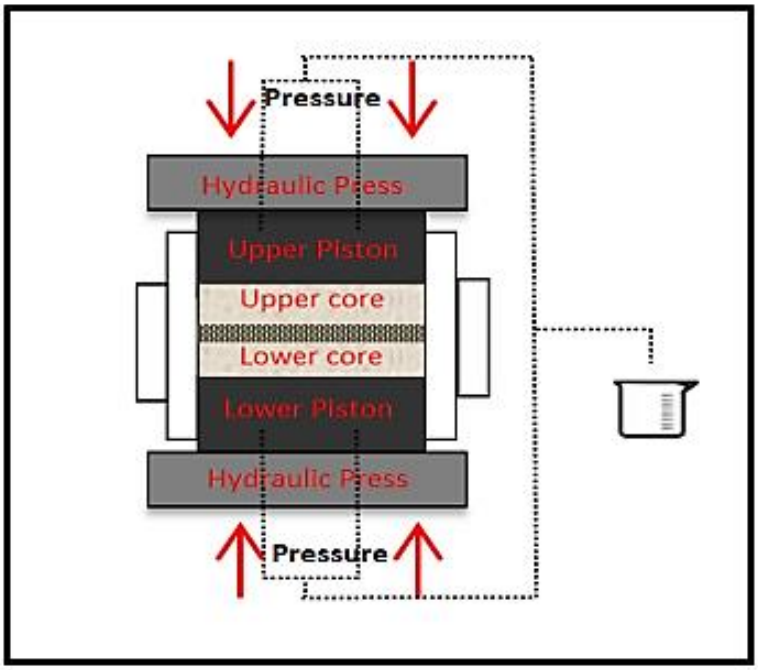

Figure 27: Schematic of Fluid Loss procedure Using Fracture Conductivity Cell [60]

4.10.11 Shut-In Time

Shut-in time had to be exactly 12hrs. During this stage all valves have to stay closed to simulate shut-in time in the actual well.

4.10.12 Clean Up

The inlet of the conductivity cell was connected to the ISCO pump and the outlet valve was connected to a waste container using flow tubes. 2% KCL was used as the cleanup fluid with the constant injection rate of 4ml/min. Closure stress remained at 2000 psi during the injection. 2% KCl solution was pumped through the proppant pack (**Figure 28**). The back pressure regulator was opened and a back pressure of 500 psi was applied. After 6 hours, the ISCO pump was connected to the top and bottom pistons so as to make the flow direction through the cores (**Figure 29**) perpendicular to the proppant pack for the next 6hrs. Both the steps were repeated one more time to complete a total clean up period of 24 hours.

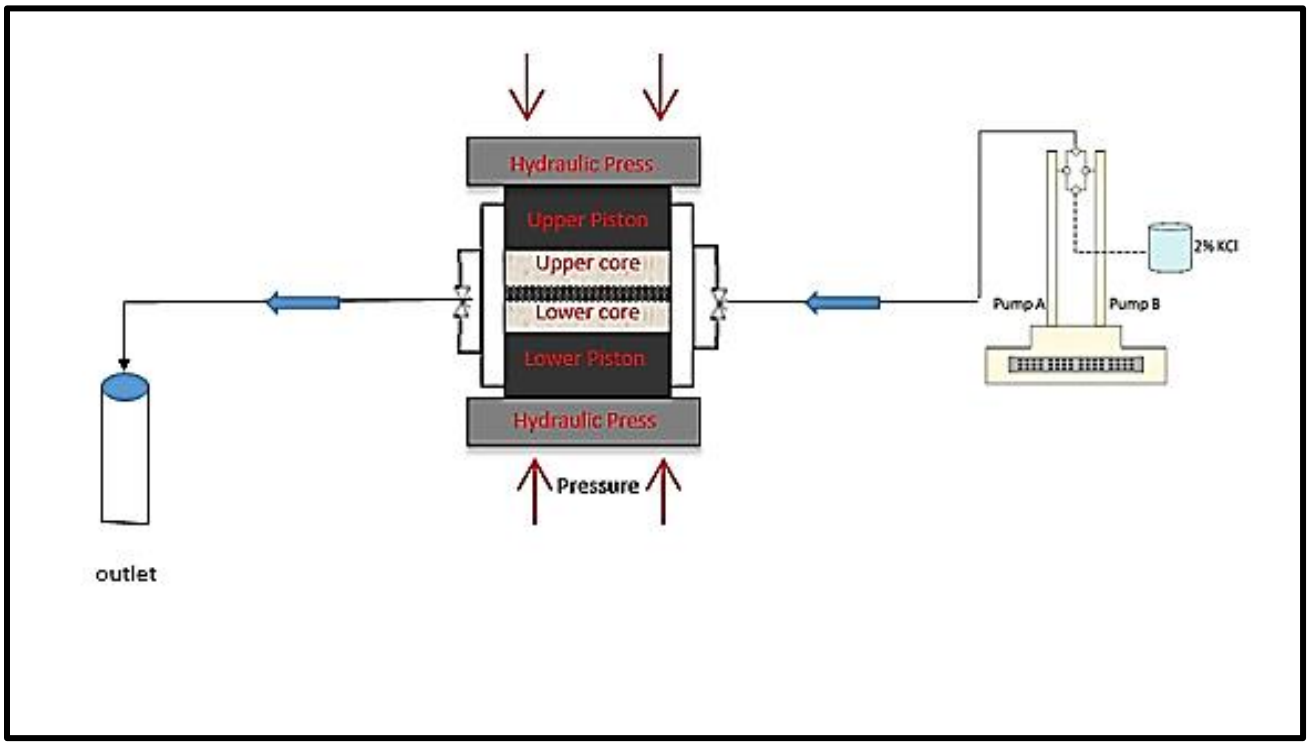

Figure 28: Clean-up through the proppant pack

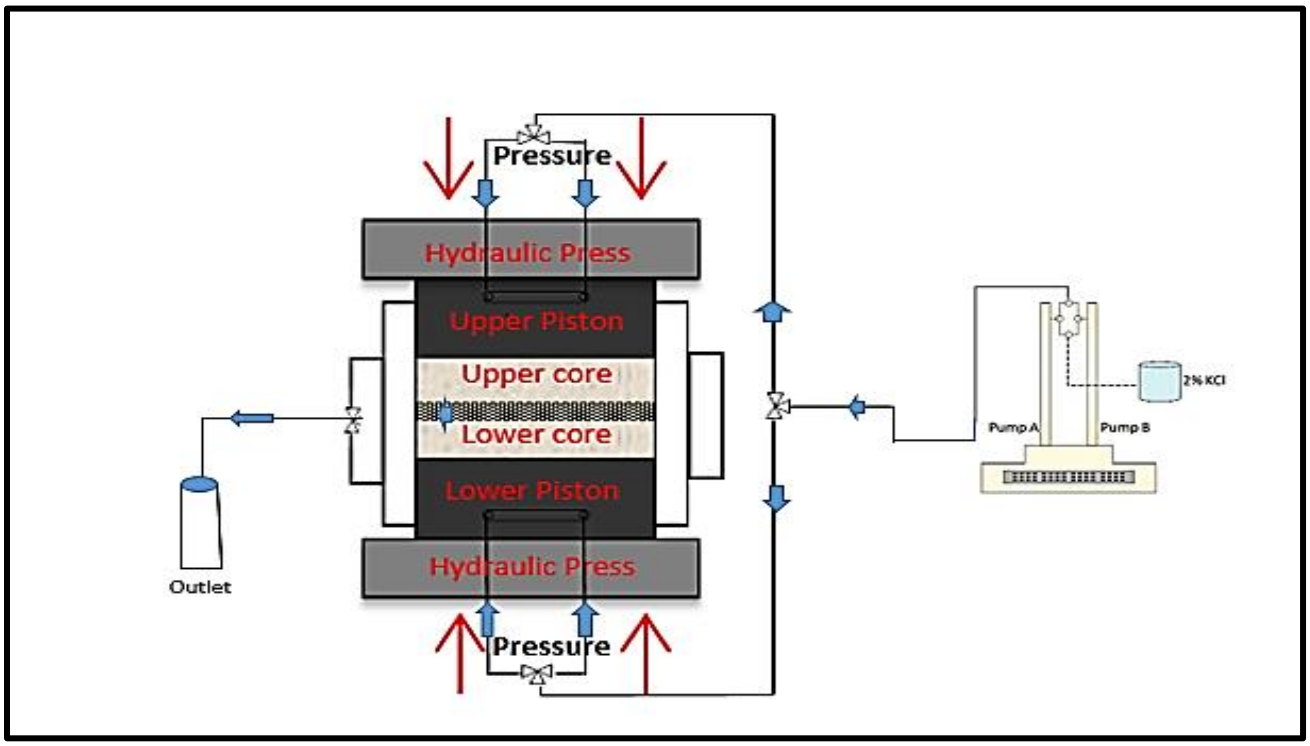

Figure 29: Clean-up through the cores

4.10.13 Differential Pressure Measurement

Transducer was calibrated using the procedure explained earlier in **4.10.4**. At the end of clean-up, flow direction was switched again to flowing between the cores and the flow lines to the transducer were filled first to get rid of the air. The lines were then connected to the differential pressure transducer as shown in **Figure 30**. Differential pressure values were recorded against time and injection pressures. Long term fracture conductivity was measured using the method described in Appendix 9.2.

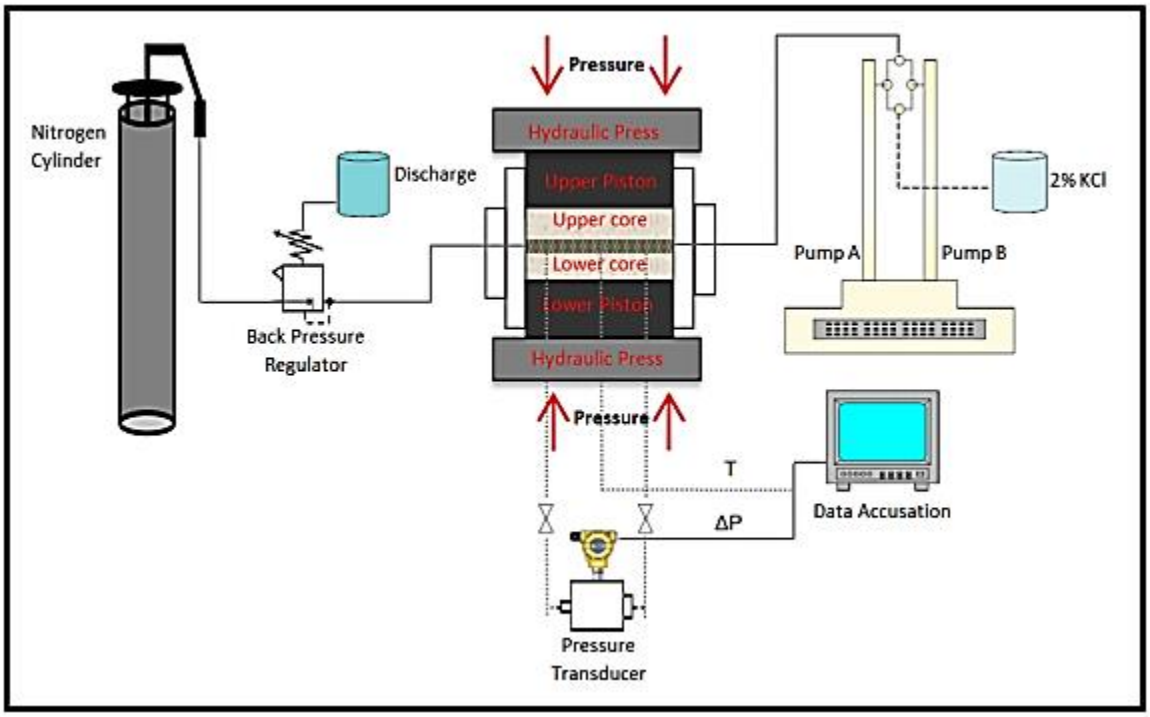

Figure 30: Schematic of API Long Term Fracture Conductivity Cell [60]

The fracture conductivity cell with all the attached flow lines assembled in the hydraulic press looked like **Figure 31**.

Figure 31: Fracture conductivity cell with the flow lines during the test

4.10.14 Disconnecting the Cell

The valves to the transducer are closed and the pump is stopped immediately. Next, the valve to the back pressure regulator was closed. Then the valve of the nitrogen cylinder was closed completely the pressure was leaked off using the procedure given in **4.10.5**. All the connections were disconnected and the stress load applied by the hydraulic press was released by lowering the lower platen of the hydraulic press. The cell was inverted to have the bottom piston on the top. The screws on the bottom piston were loosened to take the bottom piston off. The cell was inverted to take off the upper piston. The cell was moved back on to the press and the cores were pushed out using a wooden plug taking care not to disturb the proppant pack in between. The cell was cleaned carefully and kept for drying.

The cores with proppant pack bed after the conductivity test are shown in **Figure 32**.

Figure 32: Cores with the proppant pack after the conductivity test

5. Results

5.1 Polyelectrolyte Complex Nanoparticles

5.1.1 Imaging of Polyelectrolyte Complex Nanoparticles Using Transmission Electron Microscope (TEM)

The polyethylenimine-dextran sulfate nanoparticles were analyzed under a TEM to study its structure and attempts were made to see the difference in structure between the nanoparticles entrapping the enzyme (pectinase) system and the nanoparticle system without enzyme.

5.1.1.1 PEI-Pectinase-DS System

The series of oval shaped rings seen in the image are the carbon layers attached to the grid. The images were taken in the beginning without zooming in so as to get a general idea about the distribution density of the nanoparticles on the carbon layer on the grid. Later, the electron beams were focused on the high dense region and an image was taken (shown in **Figure 33)**.

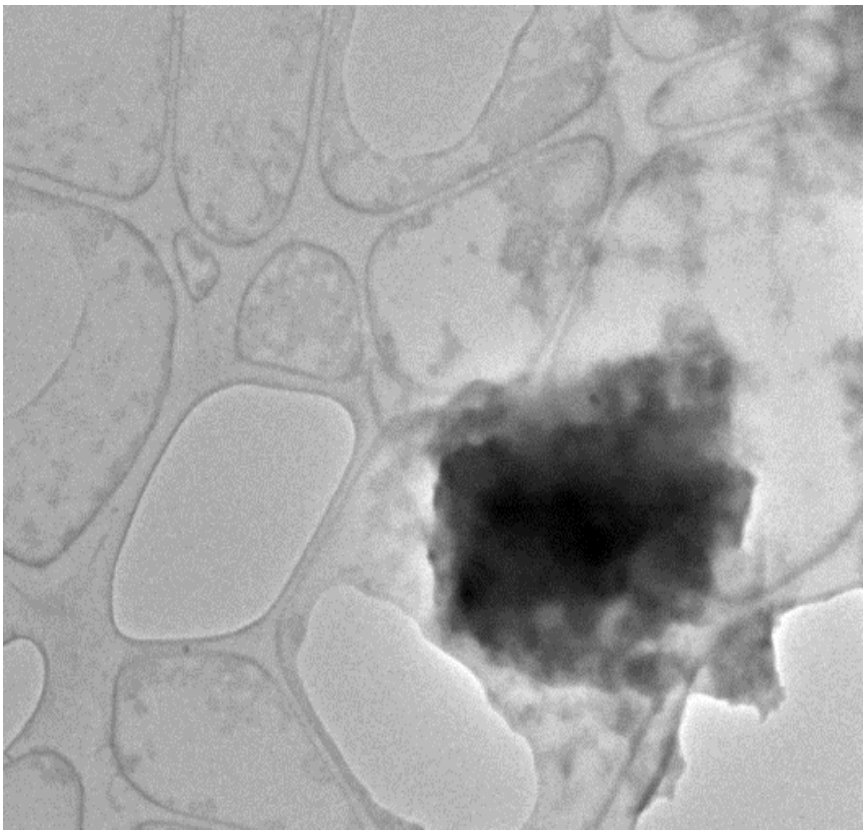

Figure 33: PEI-pectinase-DS System

After learning about the distribution of nanoparticles on the grid, an attempt was made to identify the more dense regions by zooming in to see inside the nanoparticles. The size of the images were found to be close to 500 nm. The images captured at this resolution are shown in **Figure 34** and **Figure 35**. They are different images of the same system taken at the same magnification.

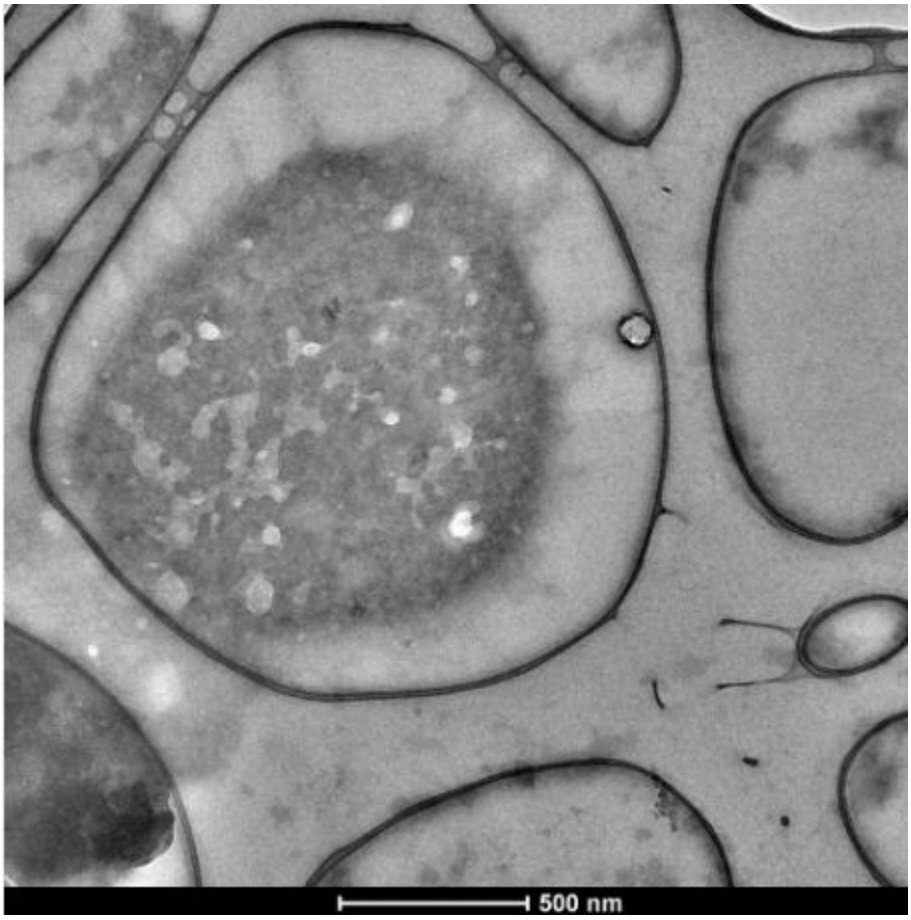

Figure 34: Images of PEI-pectinase-DS System

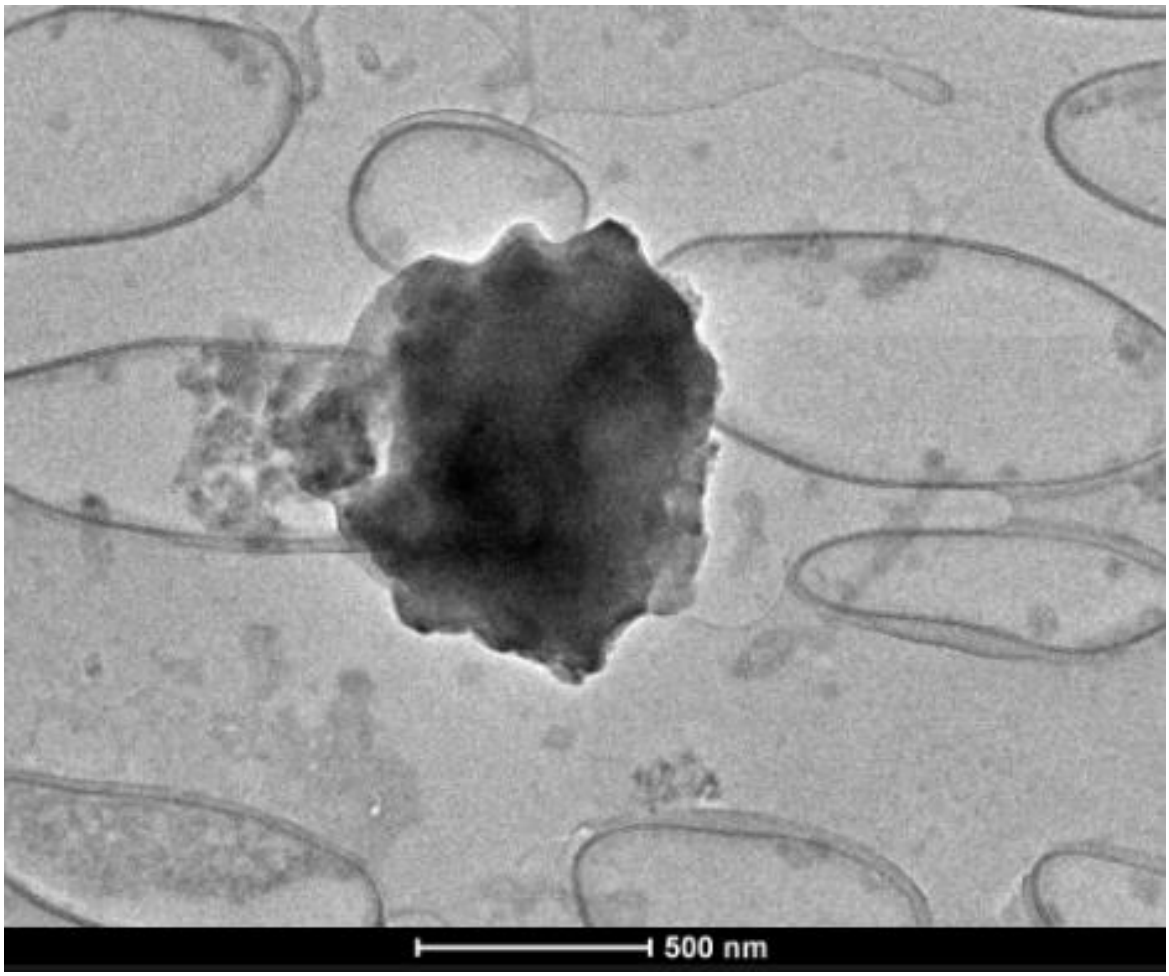

Figure 35: Images of PEI-pectinase-DS System

When the electron beam passes through several layers of the sample, the intensity of the images formed reduces. The color density of the image can be taken as a measure of the layers of particles stacked on each other. **Figure 34** shows an individual distinct nanoparticle of the size range around 500 nm. To study the internal structure of the nanoparticle, the magnification level was further increased. The images obtained helped in forming an idea of the internal structure of the nanoparticle system (**Figure 36 -Figure 39**).

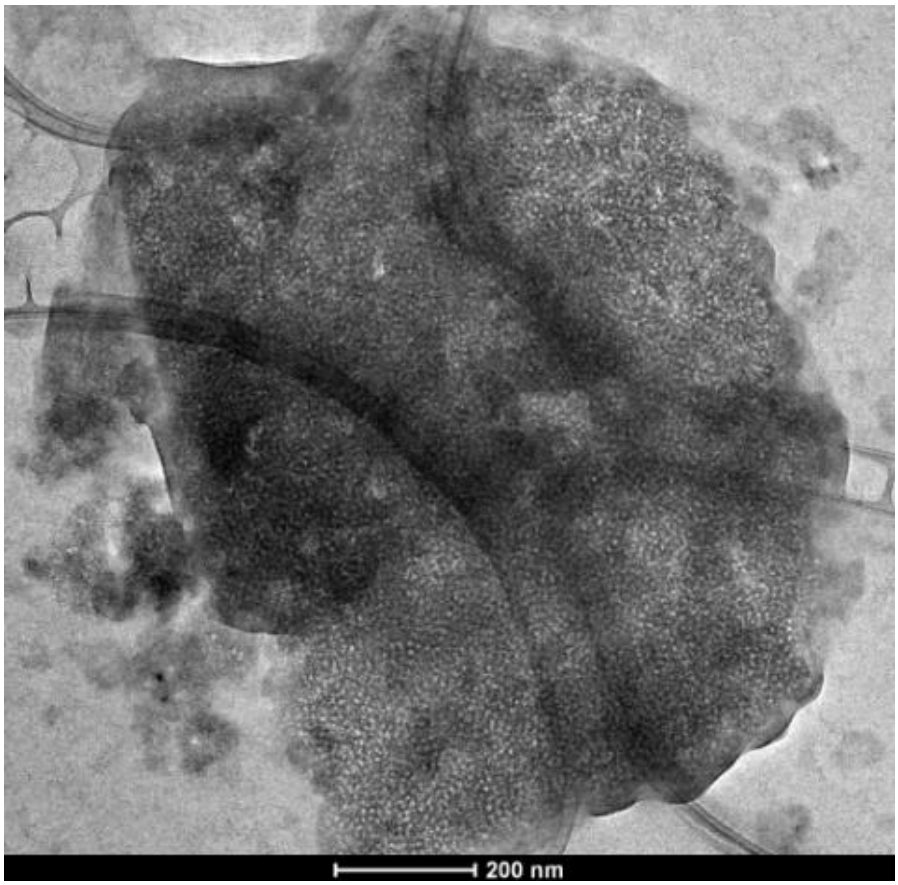

Figure 36: PEI-pectinase-DS System

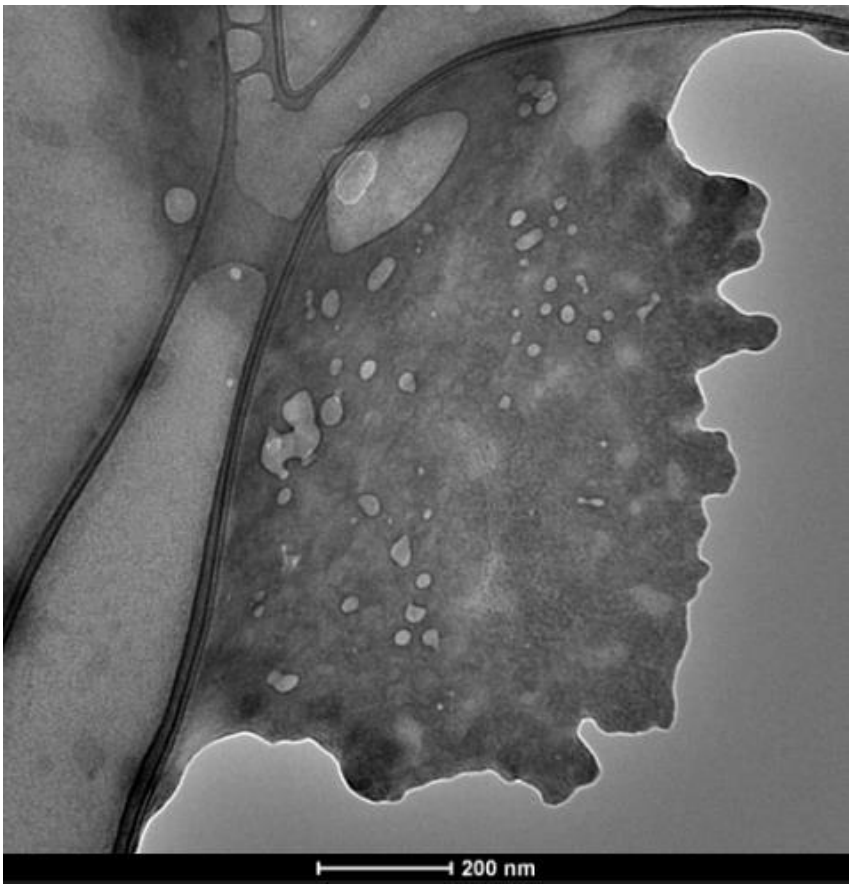

Figure 37: PEI-pectinase-DS System

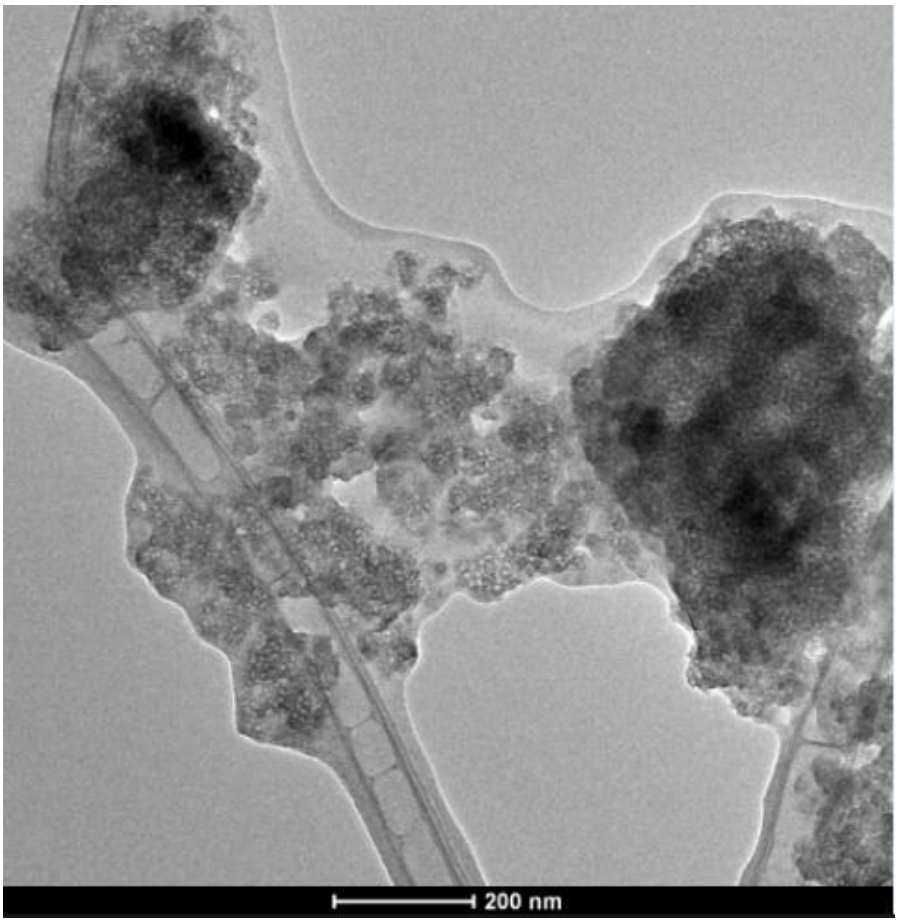

Figure 38: PEI-pectinase-DS System

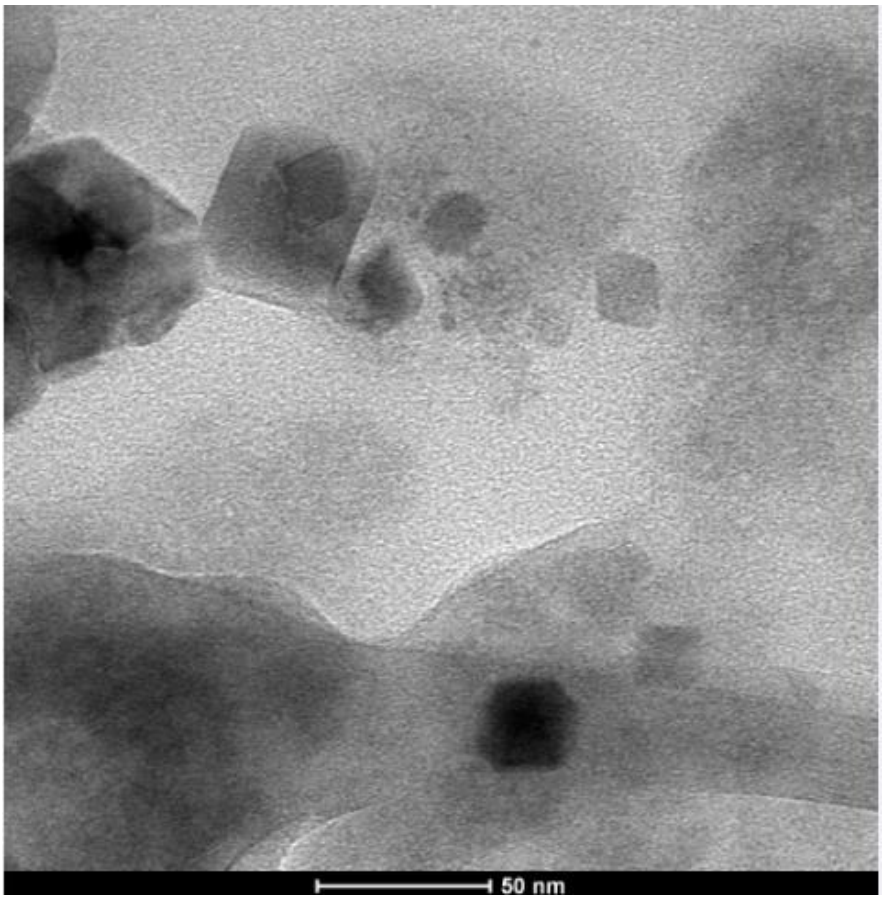

Figure 39: PEI-pectinase-DS System

5.1.1.2 PEI-RO-DS Nanoparticles

The procedure adopted for scanning was same as before and the images obtained were divided according to the type of copper grid used and the range of magnification. The imaging started with the similar type of copper grids used for the PEI-enzyme-DS nanoparticles. The images obtained are shown in **Figure 40**.

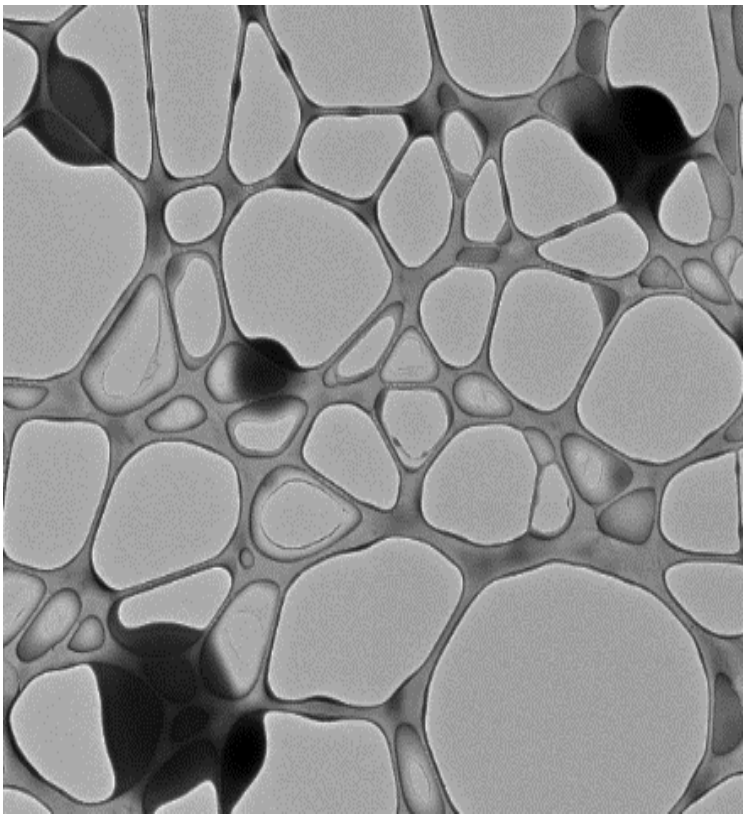

Figure 40: PEI-RO-DS system

The image clarity wasn't as good as it was for the previous case. The type of copper grid was changed to a different one which didn't have the carbon layer. Imaging was continued with the same resolution and it now looked like **Figure 41.**

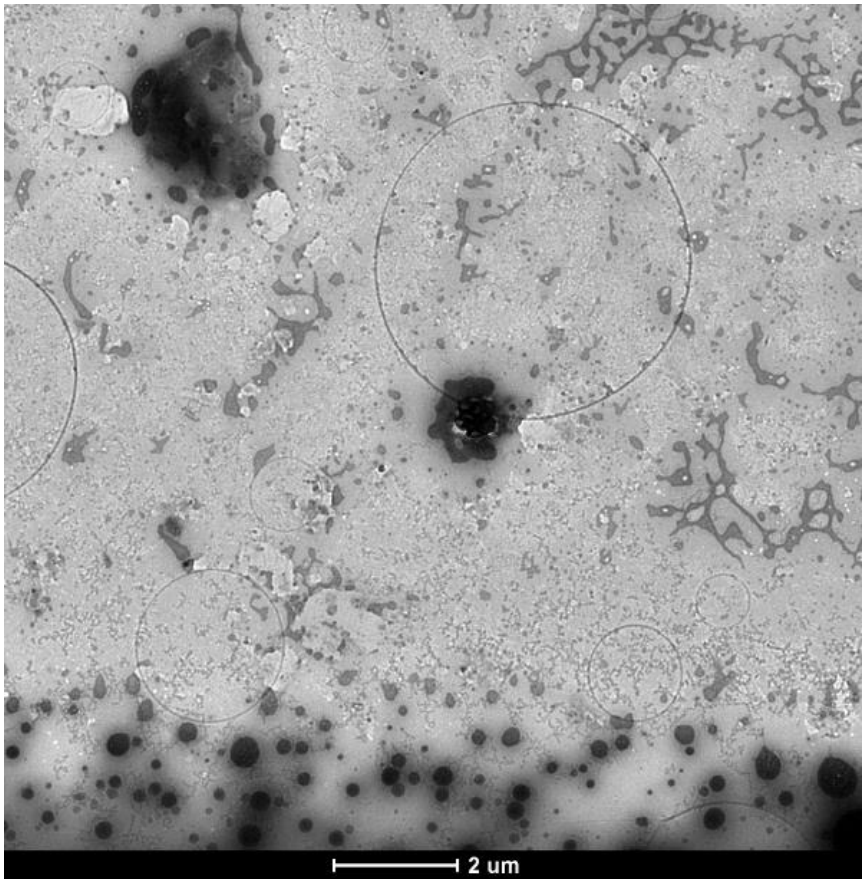

Figure 41: PEI-RO-DS system on new grid system

The scanning continued with higher magnification to look closer in the structure of the nanoparticle system (**Figure 42** and **Figure 43**).

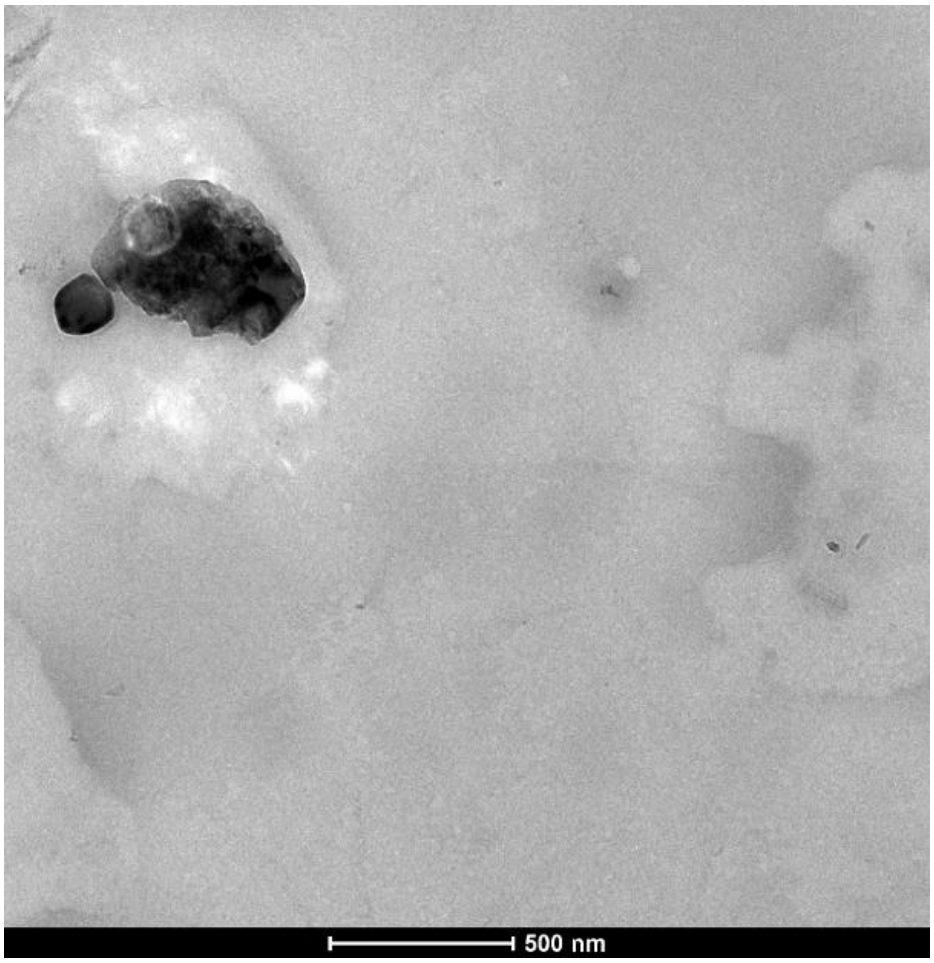

Figure 42: PEI-RO-DS system

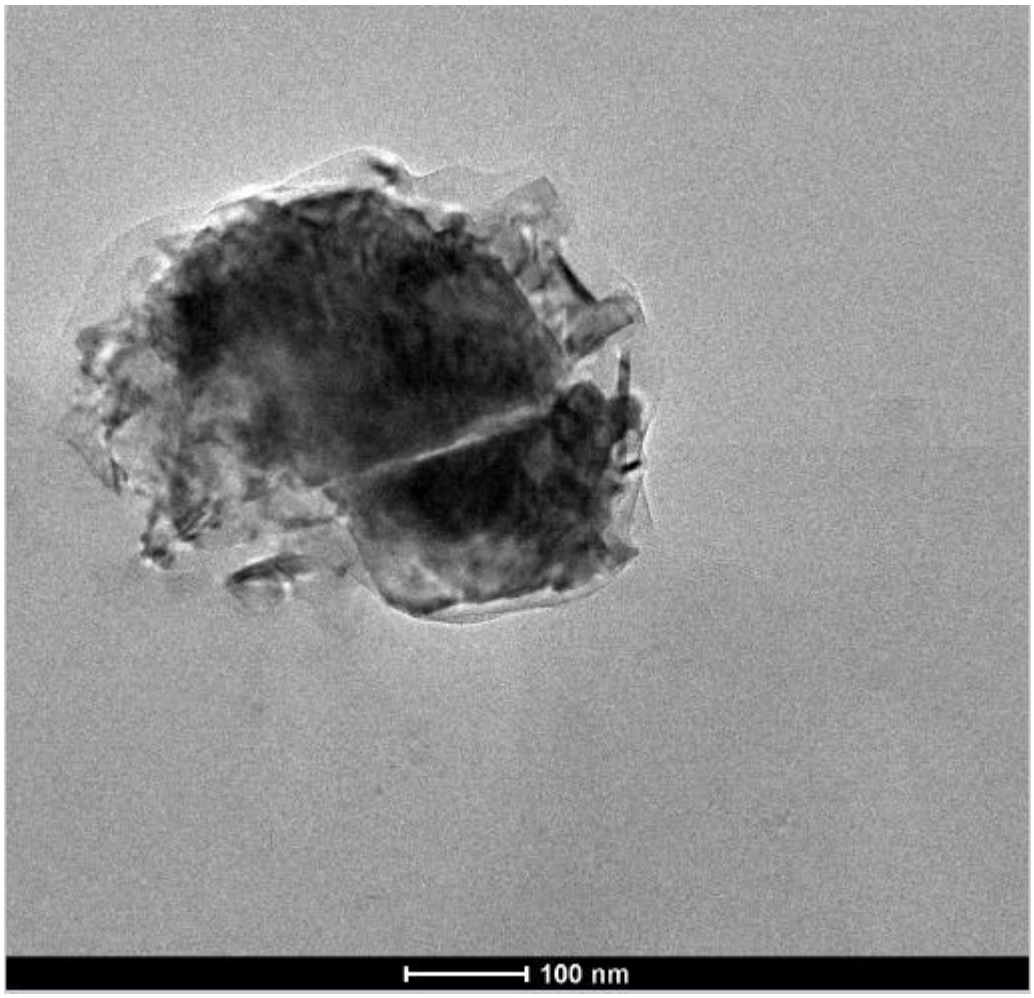

Figure 43: PEI-RO-DS system

5.1.1.3 Summary

The size of the nanoparticle systems were found to be around 500 nm. Similar shape and structure was observed for the nanoparticle system carrying enzyme and the one carrying R.O. water. The pectinase entrapped inside the nanoparticles showed no major visible change in the shape or structure. The PEI-pectinase-DS nanoparticle system was found to be more dispersed on the copper grid.

5.1.2 API Fluid Loss Tests

Three sets of core plugs with different measured brine permeability values categorized as "high permeability", "low permeability" and "tight" cores were used for fluid loss tests using PEC nanoparticles. **Table 7** summarizes all the core plugs used for API static fluid loss tests and their properties.

Table 7: Properties of the cores used for fluid loss tests using Polyelectrolyte Complex nanoparticles

Core Type	**Approx. Porosity (%)**	**Approx. Permeability (mD)**
Indiana Limestone	14	3
Kentucky (Sandstone)	14	0.1-1
Crab Orchard (Sandstone)	7	0.01-0.1

Core samples were flowed with 2% KCl solution before and after each test to measure the permeability of the core. The fluid combinations used for the fluid loss tests using polyelectrolyte complex nanoparticles are given in **Table 8**.

Table 8: Fluid combinations and volume for fluid loss tests

No	**Fluid combination**	**HPG Sol. (ml)**	**Borax (ml)**	**2% KCl (ml)**	**NP sol. (ml)**	**Total Vol. (ml)**
1	HPG Baseline	144	45	45	0	234
2	HPG + NP	144	45	0	45	234
3	NP + 2% KCl	0	0	189	45	234

5.1.2.1 High Permeability Cores

The fluid loss of polyelectrolyte complex nanoparticles when used with Indiana limestone cores of (1-10) mD and cross-linked gels (3077 ppm) were studied for different combinations of fluids. The wall building coefficient C_w was calculated from the slope of the straight line curve (fluid loss curve) after the spurt volume using Equation 4 [79].

Total fluid loss volume, and fluid loss coefficients related to each test are reported in **Table 9.**

Table 9: Results for Fluid Loss Tests with Indiana Limestone Tests

Core	Fluid (total vol. =234 ml)	Total fluid loss volume (ml)	C_w (ft./min$^{1/2}$)	Total time, minutes
IL-4	144 ml HPG+45 ml Borate + 45 ml 2% KCl	8.15	0.00187	90
IL-5	144 ml HPG+45 ml Borate +45 ml NP	7.31	0.00197	90
IL-7	189 ml 2% KCL+45 ml NP	182	NA	1.5

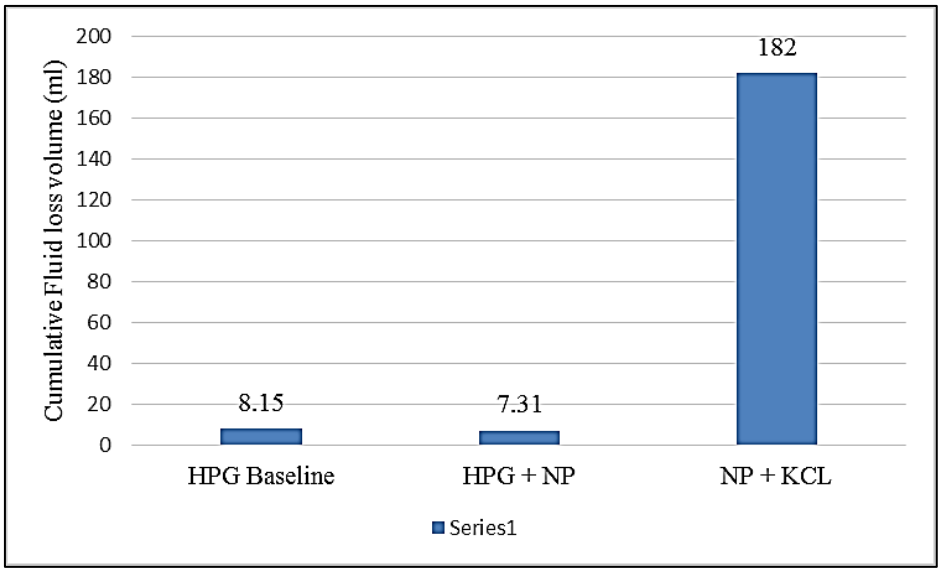

Figure 44: Cumulative fluid loss volume for Tests with Indiana Limestone Cores

Figure 44 shows the fluid loss volume obtained for different fluid loss tests using Indiana Limestone cores.

1) *HPG baseline test*

The fluid loss curve obtained for the HPG baseline experiment is shown in **Figure 45**.

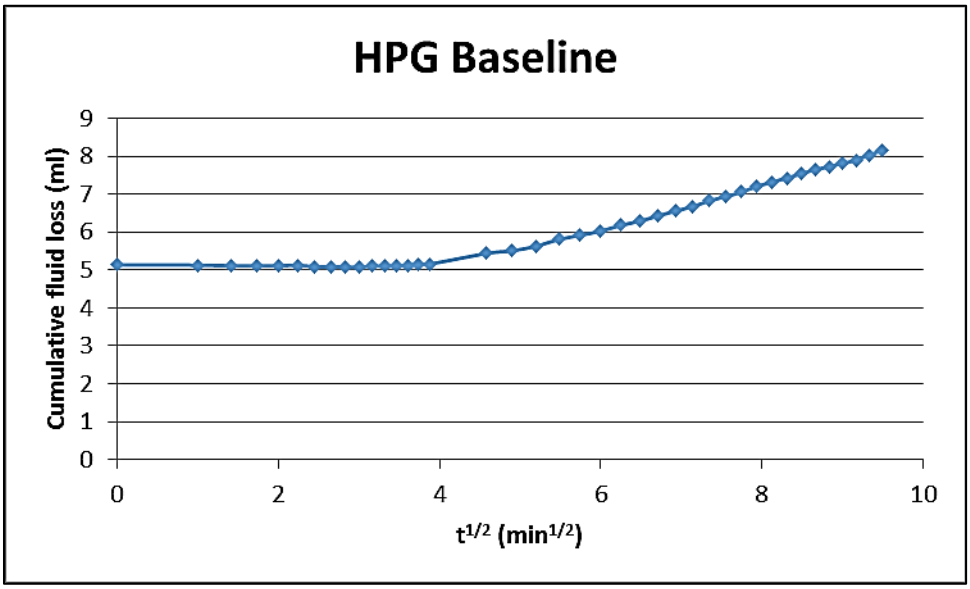

Figure 45: Fluid loss curve for HPG Baseline test

HPG +NP

Fluid loss curve obtained for HPG + NP test is shown in **Figure 46.**

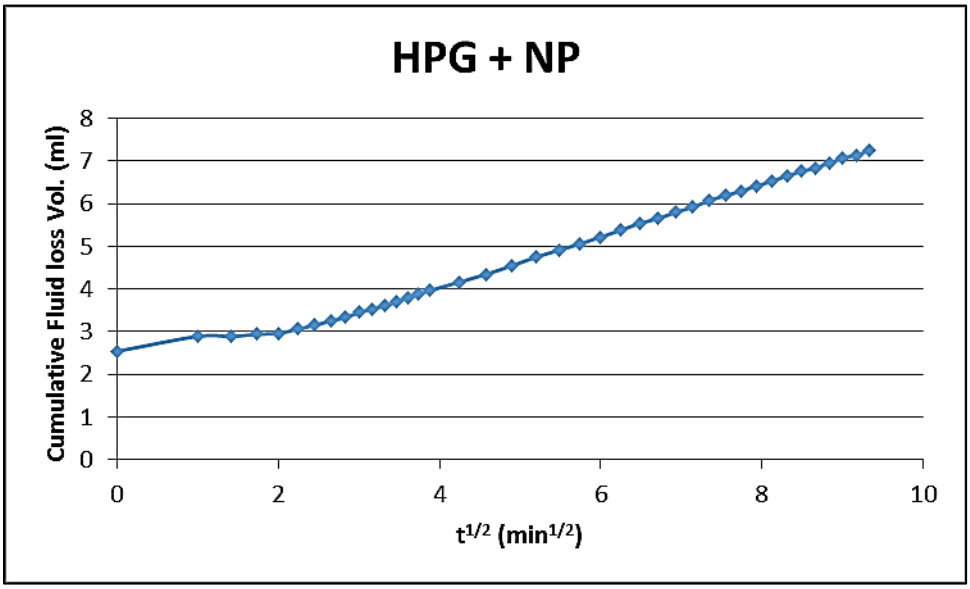

Figure 46: Fluid loss curve for HPG + NP test

NP + 2% KCl solution

The experiment without cross-linked HPG solution leaked out through the core in a just a couple of minutes and hence did not generate a fluid loss curve. 182 ml of fluid leaked off through the core sample. This test was discarded as it does not represent a realistic case as viscosifiers are a necessary component in hydraulic fracturing fluids.

The cores were tested for permeability before and after the fluid loss tests and the values are shown in **Table 10**. It was observed that the nanoparticles reduce the permeability of the cores after the fluid loss test. In case of IL-4, where the nanoparticles were absent, the cores regained their permeability during permeability measurement. The core samples with which nanoparticles were used never regained their former permeability despite flowing brine through them for several pore volumes which shows the presence of nanoparticles inside the pore throat diameter.

Table 10: Test: Permeability of Cores Before and After API Fluid Loss

Core	$K_{\text{Before the test}}$ (mD)	Fluid (total vol. =234 ml)	$K_{\text{After the test}}$ (mD)
IL-4	7.48	144 ml HPG+45 ml Borate + 45 ml 2% KCl	7.81
IL-5	6.60	144 ml HPG+45 ml Borate +45 ml NP	3.91
IL-7	5.23	189 ml 2% KCL+45 ml NP	4.79

The HPG baseline test and HPG+ NP tests were repeated to ensure reproducibility of results. The results are shown in **Table 11** and **Figure 47**.

Table 11: Results for Repeated Fluid Loss Tests with Indiana Limestone Tests

Fluid Type	Total Volume (mL) Case 1	Total Volume (mL) Case 2	Average vol. (mL)
HPG Baseline	8.15	9.37	8.76
HPG + NP	7.31	6.82	7.06

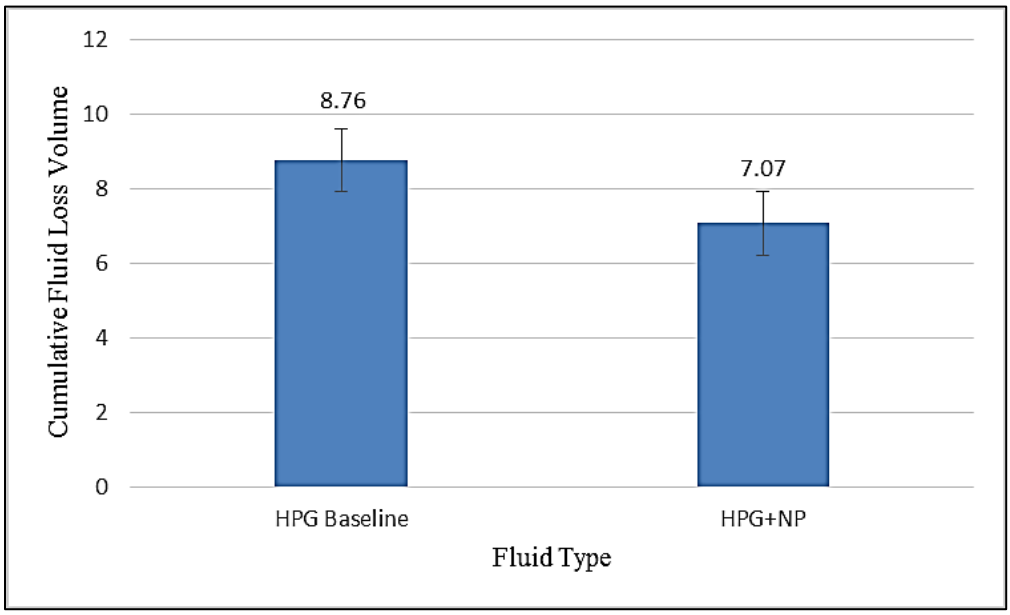

Figure 47: Fluid loss volume obtained with Indiana Limestone cores for multiple tests showing standard deviation: n=2

The results shown in **Figure 44** indicate that the PEC nanoparticles reduced the fluid loss volume by approximately 20% for 1" diameter cores. The PEC nanoparticles were proved to be effective fluid loss reducing agents in high permeability formations while causing only little permeability reduction to the core samples. This would help in reducing fluid loss to high permeable zones which usually account for most of the fluid loss (1-10 mD).

5.1.2.2 Low Permeability Cores

Kentucky cores are low permeability cores with the permeability range of 0.1-1 mD. Polyelectrolyte complex nanoparticles were used with slickwater fluids (lower concentrated non crosslinked HPG solution) for fluid loss tests. The final HPG concentration in the 234 ml of fluid used was 769 ppm.

Table 12: Summary of total fluid loss volume and fluid loss coefficients related to each test

Core	Fluid (total vol. =234 ml)	Total fluid loss volume (ml)	Cw ($ft./min1^{/2}$)	Total time, minutes
KC-1	144 ml HPG+ 90 ml 2% KCl	3.9	0.0025	90
KC-2	144 ml HPG+45 ml 2% KCl +45 ml NP	2.54	0.0018	90
KC-3	189 ml 2% KCL+45 ml NP	156.02	NA	1.5

Table 12 gives a summary of the fluid combinations used for fluid loss testing using different core samples. Total fluid loss volume and fluid loss coefficients related to each test are also shown.

1) HPG baseline

The fluid loss curves obtained for the experiments HPG baseline and HPG + NP (PEI-DS) are shown in **Figure 48** and **Figure 49** respectively.

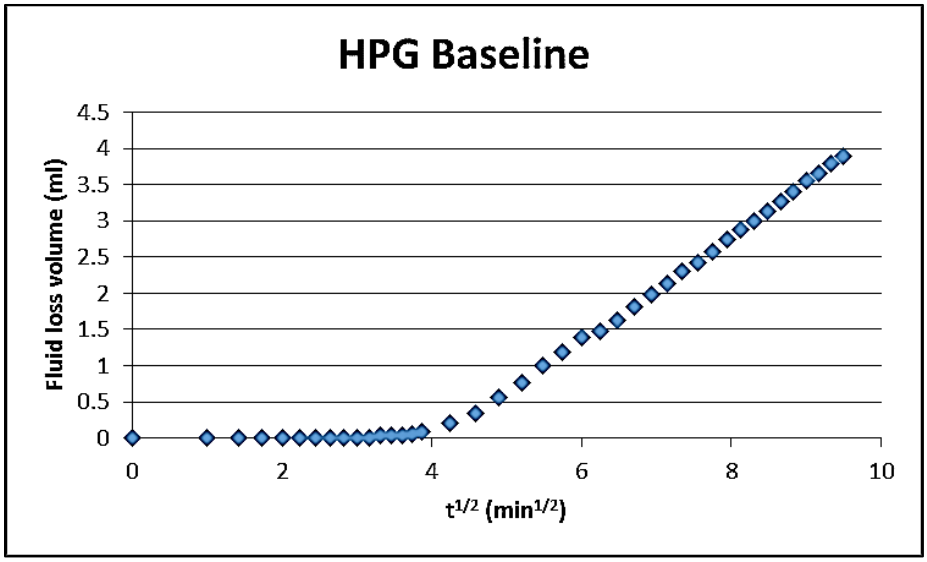

Figure 48: Fluid loss curve for HPG Baseline test

HPG +NP (PEI-DS)

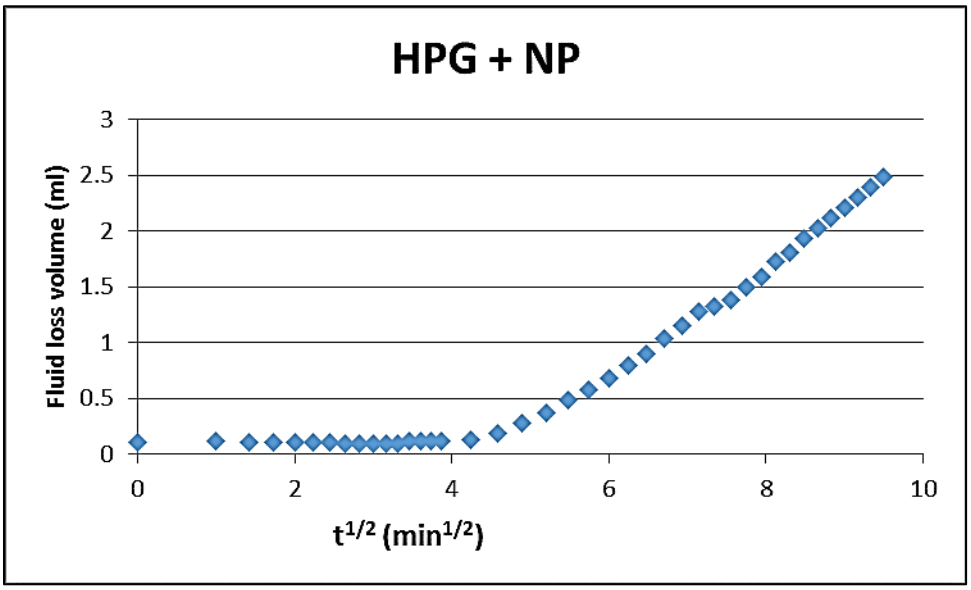

Figure 49: Fluid loss curve for HPG + NP test

PEI-DS NP + 2% KCl solution

The experiment without HPG solution showed a much higher rate of leak off and the final leak off volume collected was 156.02 ml.

Table 13: Core Permeability Before and After the API Fluid Loss Tests

Core	**K Before the test (mD)**	**Fluid (total vol. =234 ml)**	**K After the test (mD)**
KC-1	0.16	144 ml HPG+45 ml Borate + 45 ml 2% KCl	0.16
KC-2	0.31	144 ml HPG+45 ml Borate +45 ml NP	0.21
KC-3	0.18	189 ml 2% KCL+45 ml NP	0.19

The permeability of core sample before and after the fluid loss tests are shown in **Table 13**. It was observed that the PEI-DS nanoparticles reduce the permeability of the cores after the fluid loss

test. In case of KC-3 where the PEI-DS nanoparticles were absent, the core was found to regain its permeability during permeability measurement. The core sample with which the PEI-DS nanoparticles were used with HPG solution, never regained their former permeability despite flowing several pore volumes of brine through them.

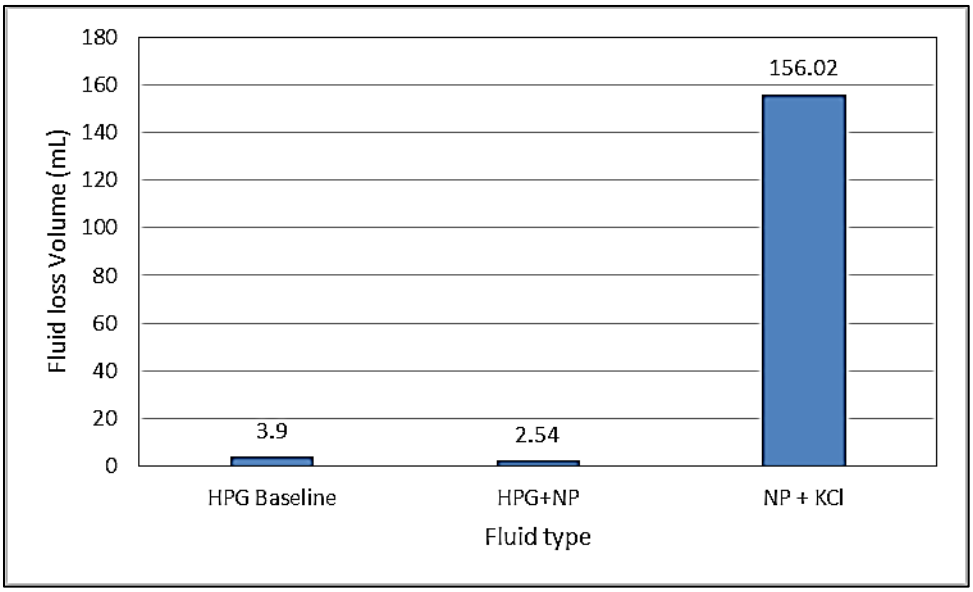

Figure 50: Fluid loss Test Results for Kentucky Cores

The permeability reduction of the Kentucky cores in experiments were PEI-DS nanoparticles were used shows the contribution of nanoparticles in forming an internal filter cake.

The HPG baseline and HPG + NP tests were repeated to ensure reproducibility and results are shown in **Table 14** and **Figure 51**.

Table 14: Repeated Fluid Loss Test Results for Kentucky Cores

Fluid Type	Total Fluid Volume (mL)- Case 1	Total Fluid Volume (mL)- Case 2	Average vol. (mL)
HPG Baseline	3.9	4.37	4.13
HPG + NP	2.54	2.17	2.35

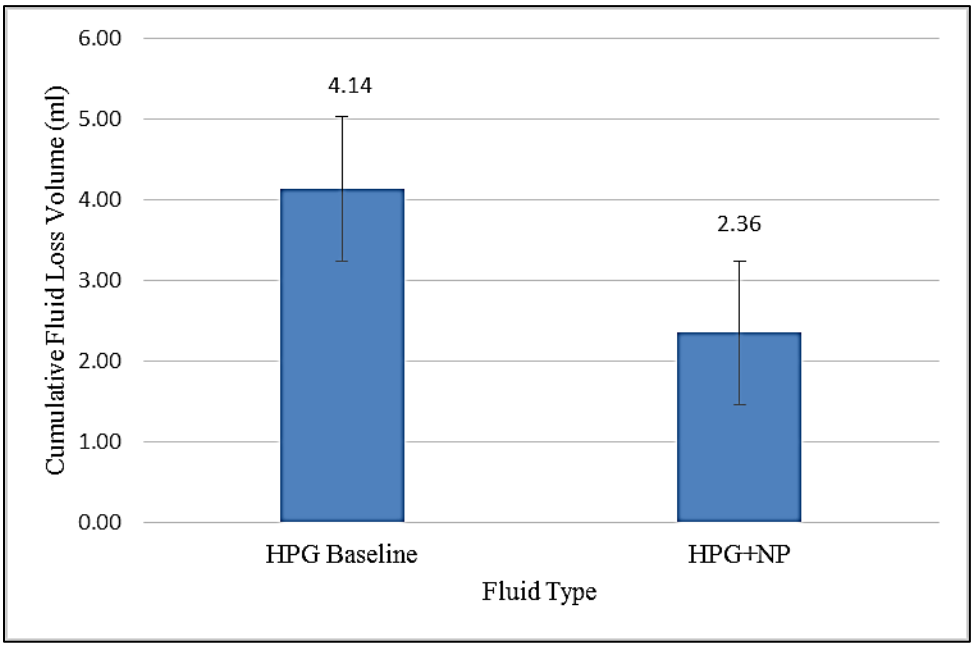

Figure 51: Average fluid loss volume for multiple tests with Kentucky cores showing Standard deviation: n=2

The results shown in **Figure 50** indicate that the fluid loss volume was reduced by the PEI-DS nanoparticles when tested on Kentucky cores. The PEI-DS nanoparticles are effective fluid loss reductive agents in low permeability formations.

5.1.2.3 Tight Cores

Crab orchard cores with permeability (0.01-0.1 mD) were used as tight cores to do fluid loss tests. Slickwater solution was used as the test fluid.

The volume of fluid loss obtained is shown in **Figure 52.** The fluid loss volume reduced to zero when PEI-DS nanoparticles were added to HPG solution. This shows the impact of PEI-DS nanoparticles as fluid loss additives in tight reservoirs.

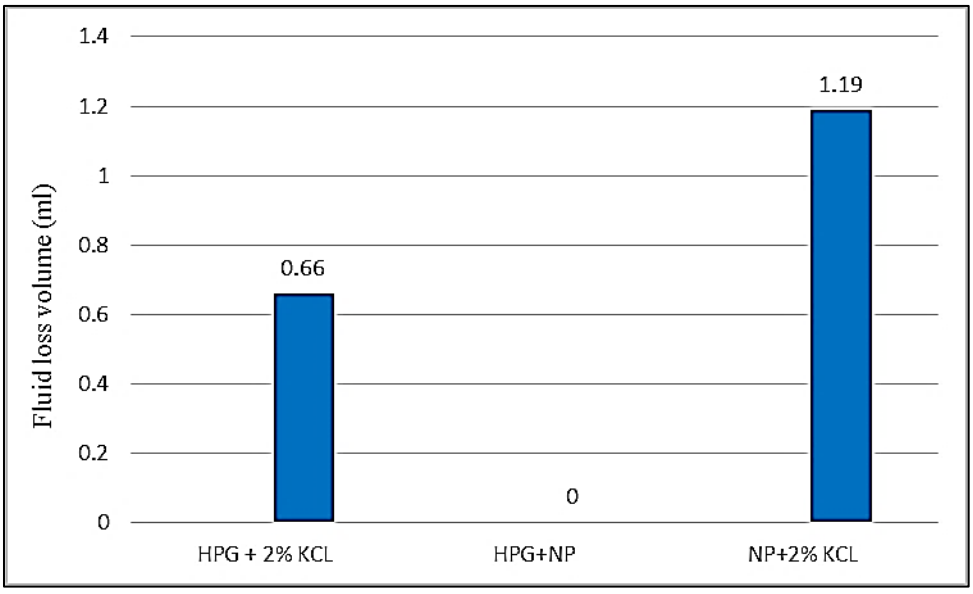

Figure 52: Fluid loss test results for Crab Orchard cores

The fluid loss volumes obtained were too small with tight cores to show reproducibility in results and calculate fluid loss coefficients. However, the results shown in **Figure 52** indicate that PEI-DS Nanoparticles have the potential to act as fluid loss reducing additives in tight cores.

5.1.3 Hydraulic Fracture Conductivity Tests

API long term fracture conductivity tests were conducted using the fracture conductivity setup using cross-linked fluid system on high permeability cores (Parker) and slick water fluid system on low permeability cores (Scioto).

In order to test the conductivity of the proppant pack formed with the PEI-DS nanoparticle system, the conductivity of various fluid combinations inclusive and not inclusive of nanoparticles were measured.

5.1.3.1 Proppant Baseline Conductivity Test

As a first step, the conductivity of the proppant pack (3 lb. /sq. ft. of Carbo econoprop 20 40), without adding fracturing fluids, was measured for different overburden stress values. The results are shown in **Figure 53**. The proppant conductivity was found to decrease as a function of closure stress.

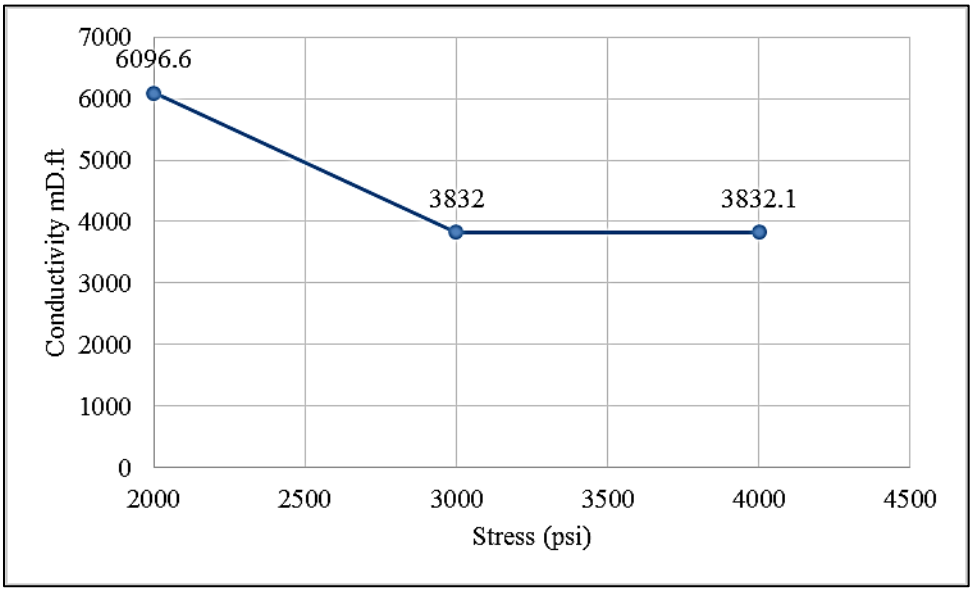

Figure 53: Proppant Conductivity (Carbo econoprop 20 40) vs. Stress

5.1.3.2 Cross-Linked Fluid Tests

The final concentration of the guar in the HPG solution is 3077 ppm and the HPG solution was crosslinked. Parker sandstone core wafers were used for this test. The fracturing fluid combinations used for different tests are shown in **Table 15**.

Table 15: Fracturing fluid combinations used in fracture conductivity tests *[52]*

Experiment Type	**HPG solution (5000 ppm)**	**Enzyme Solution (Pectinase) 0.1%**	**Enzyme entrapped in Nanoparticle system (PEI:PI:DS=2:0.1:1)**	**Nanoparticles with RO Water (PEI:RO:DS=2:0.1:1)**	**2% KCl solution**	**Borax solution (2000 ppm)**
Baseline	0	0	0	0	234	0
HPG Baseline	144	0	0	0	45	45
HPG + free enzyme sol (HPGE)	144	45	0	0	0	45
HPG + enzyme entrapped nanoparticle system (HPGEE)	144	0	45	0	0	45
HPG + Nanoparticle system (HPGNP)	144	0	0	45	0	45

The differential pressure across the fracture length was measured using a differential pressure transducer. Maximum pressure drop was observed for HPG baseline, which could be attributed

to the non-degraded polymer gel. The conductivity values obtained in different experiments are shown in **Figure 54.**

As expected, the baseline test (proppant baseline), having the proppants in between the cores with no polymeric fluids, showed the maximum value of conductivity. Guar (HPG) baseline, which used only the proppants and the cross-linked guar, showed the smallest conductivity, due to the high viscosity of the unbroken filter cake.

HPGE fluid system showed higher values of conductivity, which was expected due to the degradation caused to the crosslinked guar by the free enzyme. HPGEE, which used an entrapped enzyme, showed a conductivity value almost equal to but slightly higher than HPGE. This proves the fact that the nanoparticles which entrap the enzyme for a period of time during the injection give slightly higher values of conductivity as reported by the free enzyme. This also implies that the enzyme is being released after a period of time after which it acts as in the case of the free enzyme. The slightly higher value of conductivity obtained may be due the fact that the nanoparticles could distribute the enzyme more evenly in the filter cake and because the enzymes were not lost to the formation [52]. It can also be because of the fact that the nanoparticles themselves are capable of degrading guar gel as shown by Barati [2]. HPGNP gave a conductivity value less than that of HPGE and HPGEE because of the absence of the enzyme to break down the gel, but it still gave a higher conductivity value than that of HPG baseline. This shows that the nanoparticles help in the formation of a relatively weaker filter cake, which can be easily cleaned up as compared to that of HPG baseline, in which a tight filter cake was formed by the polymer gel which resulted in a very low conductivity [52]. The tests were repeated multiple times to ensure reproducibility of results (**Figure 55**). Statistically,

HPGNP and HPGE cases belong to the same population and therefore are similar but HPGEE results belong to a different population. Hence, there is a significant difference in fracture conductivity results between the HPGEE and HPGE results.

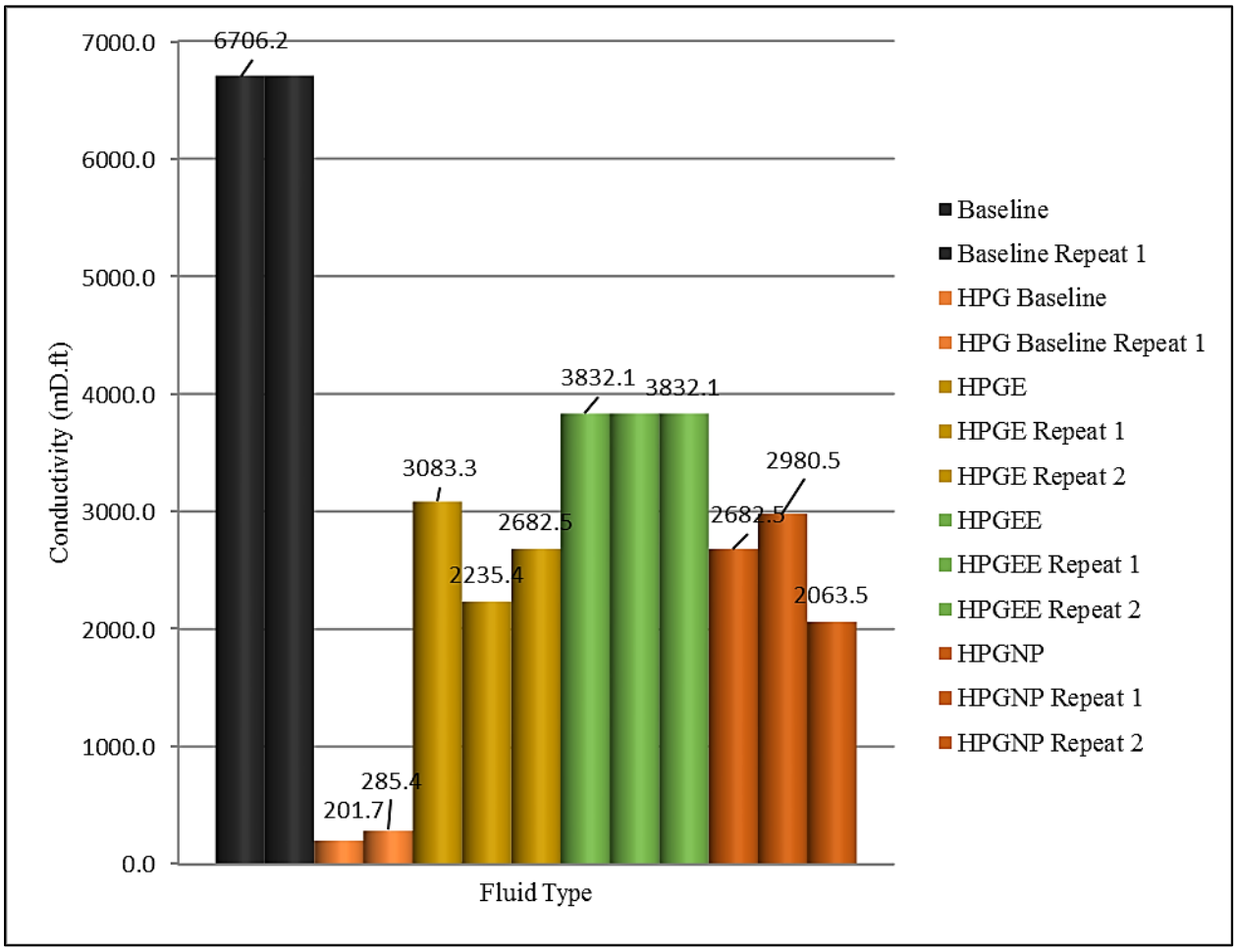

Figure 54: Fracture conductivity results obtained for cross- linked tests [60]

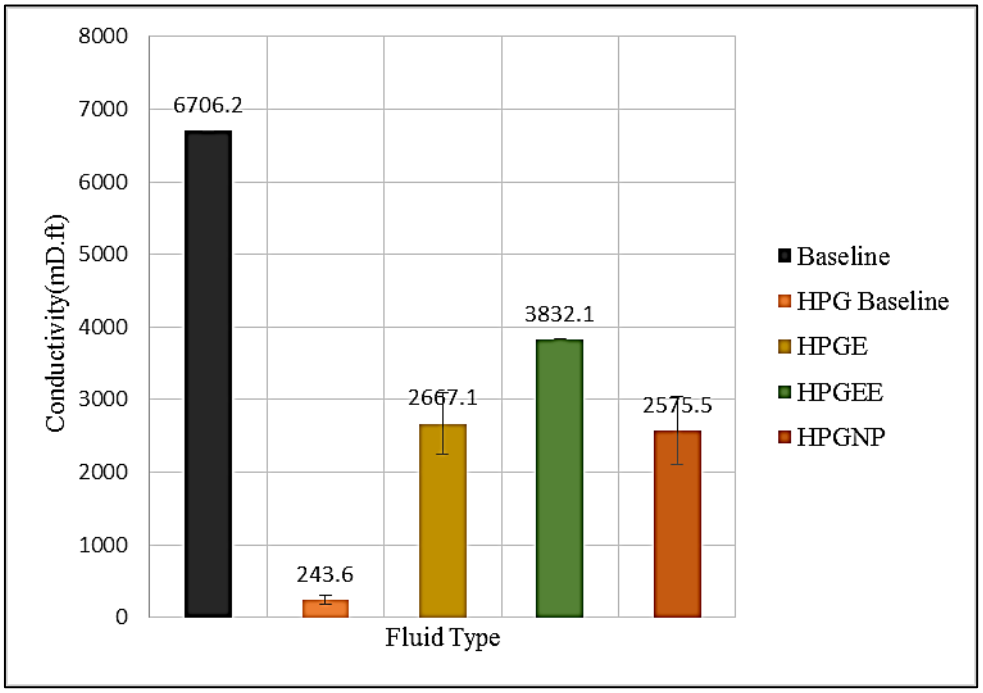

Figure 55:Cross-linked fluid Results with Standard Deviation

5.1.3.3 Slick-Water Fluid Tests

The fracturing fluid tests were repeated for the same fluid components using slickwater HPG concentrations (769 ppm). The gel was not cross-linked and Scioto sandstone core samples were used for this test. Brine solution was used in place of borax cross-linker in slick water fluid system.

In the initial tests, enzyme concentration used was same as that of the cross-linked fluid (0.1%). The conductivity values were similar to that of free enzyme case and entrapped enzyme case. The possible reason could be that the enzymes are degrading the filter cake before the differential pressure readings could be recorded. The enzyme concentration was stepped down to 0.025% to account for the reduced HPG concentration used in the slick water tests.

The test results showed similar results (**Figure 56**) to that of the crosslinked tests. Enzymes entrapped in nanoparticles showed the best value of fracture conductivity followed by the case when enzymes were added directly to the cross-linked HPG solution. Interestingly, nanoparticles when added directly to the gel solution without enzymes also showed remarkably higher fracture conductivity results as compared to that of guar baseline.

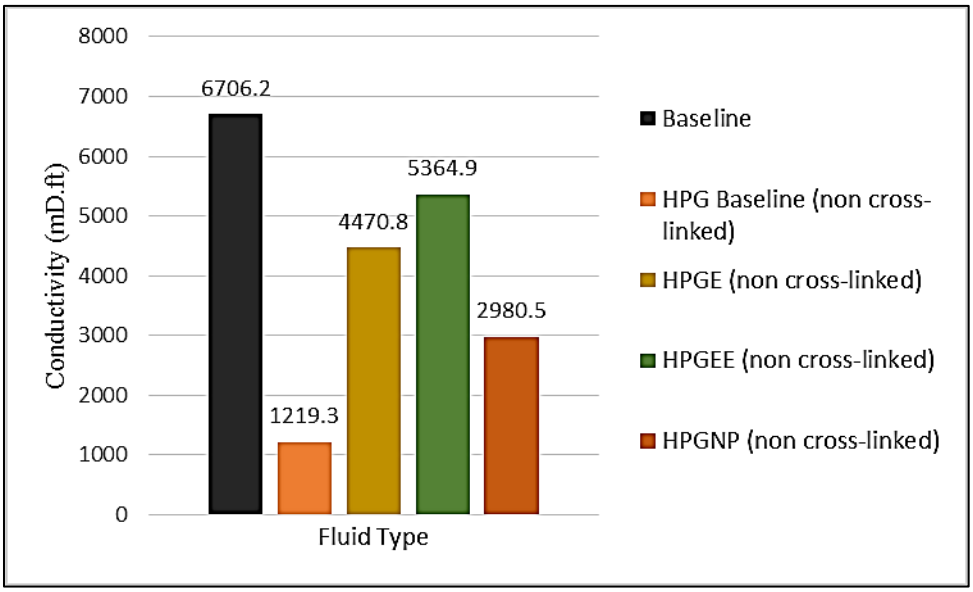

Figure 56: Conductivity Results for Slick Water Fluids

5.2 Fly Ash Nanoparticles as Nano-Proppants

Fly ash particles were tested for their size, hardness, reduced elastic modulus, and fluid loss prevention capabilities as well as for the fracture conductivity generated when they were used as proppants.

5.2.1 Particle Size and Shape Determination Using Transmission Electron Microscope (TEM)

TEM images of both types of fly ash particles were obtained to measure the size. Round shape nanoparticles between 100 nm and 800 nm were observed in addition to some residue that remained, despite washing the particles with 2% KCl and separating the lighter particles using a centrifuge, prior to imaging them. The images in **Figure 57** were captured from two different types of fly ash particles selected from two different power plants. The image in the left side of **Figure 57** shows the nanoparticle within the 200-800 nm range from the class C sample. The right image in **Figure 57** shows the nanoparticles from class F sample with particle sizes within the 100-300 nm range. Such nanoparticle sizes are suitable to be used as fluid loss additives for reservoir rocks with average pore diameters of 3 μm and 1 μm, respectively [12].

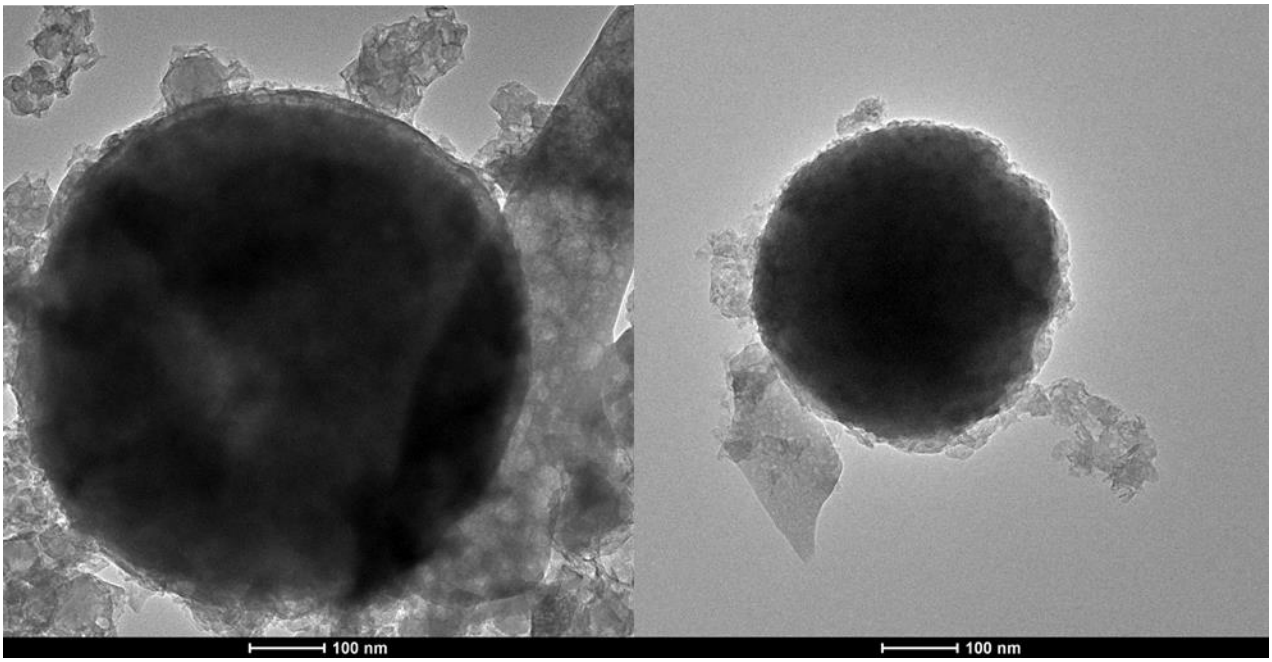

Figure 57: TEM images of fly ash nanoparticles collected from two different power plants. The left image presents a particle from the fly ash class C and the right image shows the different size of the fly ash particle from the class F

The sphericity of the proppant particles has a direct relation to the conductivity of the fracture propped by the respective proppants. The higher the sphericity, the better the conductivity of the fracture and vice-versa. Most of the samples were found to be spherical in shape, which shows the potential for creating a highly conductive fracture when placed inside the micro fractures which are naturally present. Further modifications may be done in the future to optimize the shape of fly ash particles to be completely spherical shaped particles having a uniform size distribution [12].

More images are shown in Appendix (section 9.4). All the images showed spherical shape and dimensions in nanometer range.

5.2.2 Measurement of Hardness and Reduced Elastic Modulus

Table 16 and Table 17 shows the numerical data of hardness, H, and reduced elastic modulus, E_r, and contact depth, h_c, of each test. **Figure 58** and **Figure 59** are plots of average hardness and reduced elastic modulus for all tested specimens. Because the particles have different shapes and sizes, based on the images it is difficult to quantify their dimensions. It was decided to use two parameters to define the particle dimensions, the diameter for the circle that would just fit the particle in, and the maximum height from the level plane [77]. It is worth noting here that the particles were held in place by a substrate which causes them to lump together. Therefore the sample diameter values mentioned in **Table 18** and **Table 19** are not the actual diameters of the individual particles but that of the sample which is a cylindrical clump formed by individual particles lumped together. The actual size and shape of the individual particles could be estimated only using TEM images and the values obtained have been reported in section 5.2.1.

From **Table 16** and **Table 17**, it can be understood that Class C had higher hardness and modulus at 1.36 GPa ($1.9* 10^5$ psi) and 33.10 GPa ($4.8 * 10^6$ psi) respectively. Class F had hardness and modulus of 1.23 GPa and 18.35 GPa, respectively. The average particle diameters for Class C and Class F were calculated to be 5.74 μm and 9.16 μm, respectively (**Table 18** and **Table 19)**. The average particle heights for Class C and Class F are 427.67 nm and 354.09 nm, respectively.

Table 16: Hardness and Reduced Elastic Modulus Test Results for Class C

Test Under 70 µN	H (GPa)	E_r (GPa)	h_c (nm)
1	1.26	22.41	37.03
2	1.51	42.91	32.96
3	1.80	43.53	29.34
4	1.43	23.14	34.14
5	0.91	38.46	45.36
6	1.37	31.44	35.08
7	1.66	26.52	30.92
8	1.22	28.26	37.81
9	1.33	29.75	35.61
10	1.08	44.61	40.77
Average	**1.36**	**33.10**	**35.90**
S. D.	0.26	8.57	4.70

Table 17: Hardness and Reduced Elastic Modulus Test Results for Class F

Test Under 50 µN	H (GPa)	E_r (GPa)	h_c (nm)
1	1.37	19.41	28.22
2	1.01	14.29	34.23
3	1.36	17.22	28.33
4	1.18	15.77	31.11
5	1.20	18.26	30.72
6	1.09	22.43	32.76
7	0.70	16.34	43.19
8	1.15	18.40	31.50
9	1.71	21.54	24.28
10	1.54	19.87	26.12
Average	**1.23**	**18.35**	**31.05**
S. D.	0.28	2.55	5.23

Table 18: Sample size prepared from the class C fly ash and used in nano-indentation. Note that, the diameter and height reported in this table belong to samples prepared for measurements and not to nanoparticles themselves.

Figure	Sample Diameter (μm)	Sample Height (nm)
4	8.63	975.00
5	7.42	692.30
6	6.89	392.00
7	3.87	368.40
8	5.46	300.50
9	6.90	445.00
10	3.25	245.90
11	5.26	270.10
12	4.77	287.10
13	4.98	300.40
Average	**5.74**	**427.67**
S. D.	1.68	232.06

Table 19: Sample size prepared from the class F fly ash and used in nano-indentation. Note that, the diameter and height reported in this table belong to samples prepared for measurements and not to nanoparticles themselves.

Figure	Sample Diameter (μm)	Sample Height (nm)
14	9.78	764.00
15	5.75	512.80
16	8.59	63.40
17	10.05	130.90
18	17.22	224.60
19	8.37	117.30
20	4.86	39.46
21	10.99	627.80
22	7.38	85.65
23	8.63	975.00
Average	**9.16**	**354.09**
S. D.	3.40	338.60

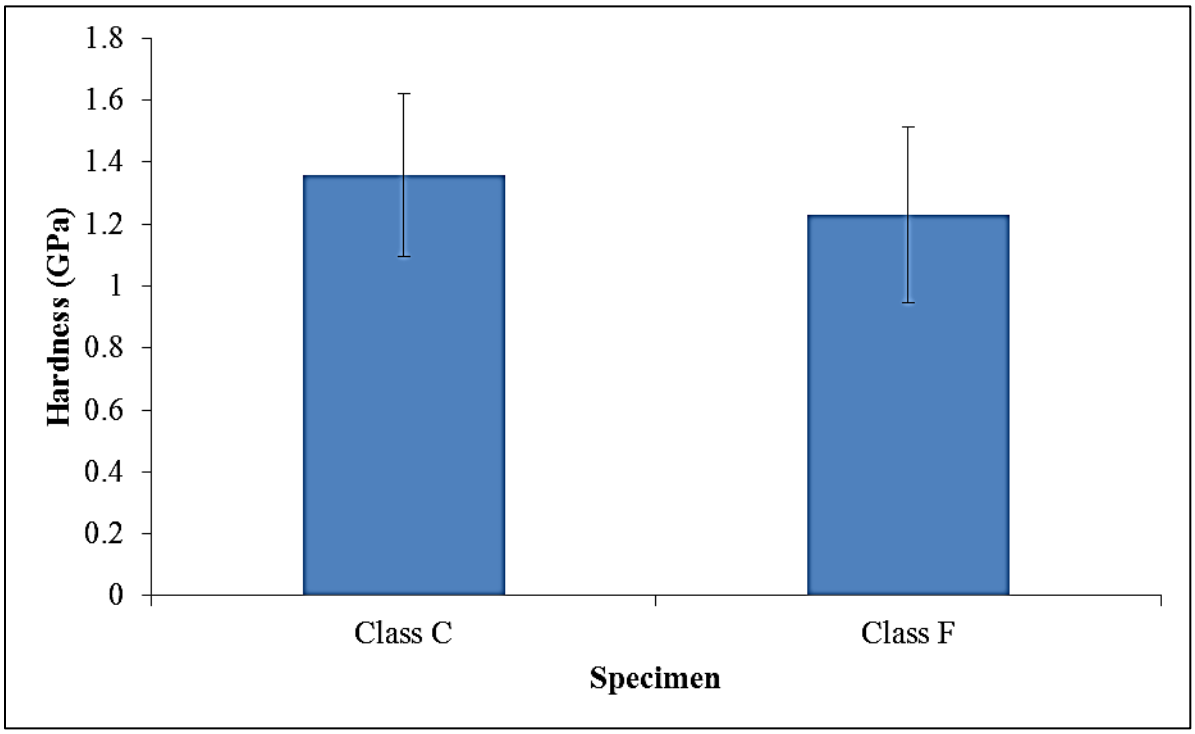

Figure 58: Average hardness for each tested specimen.

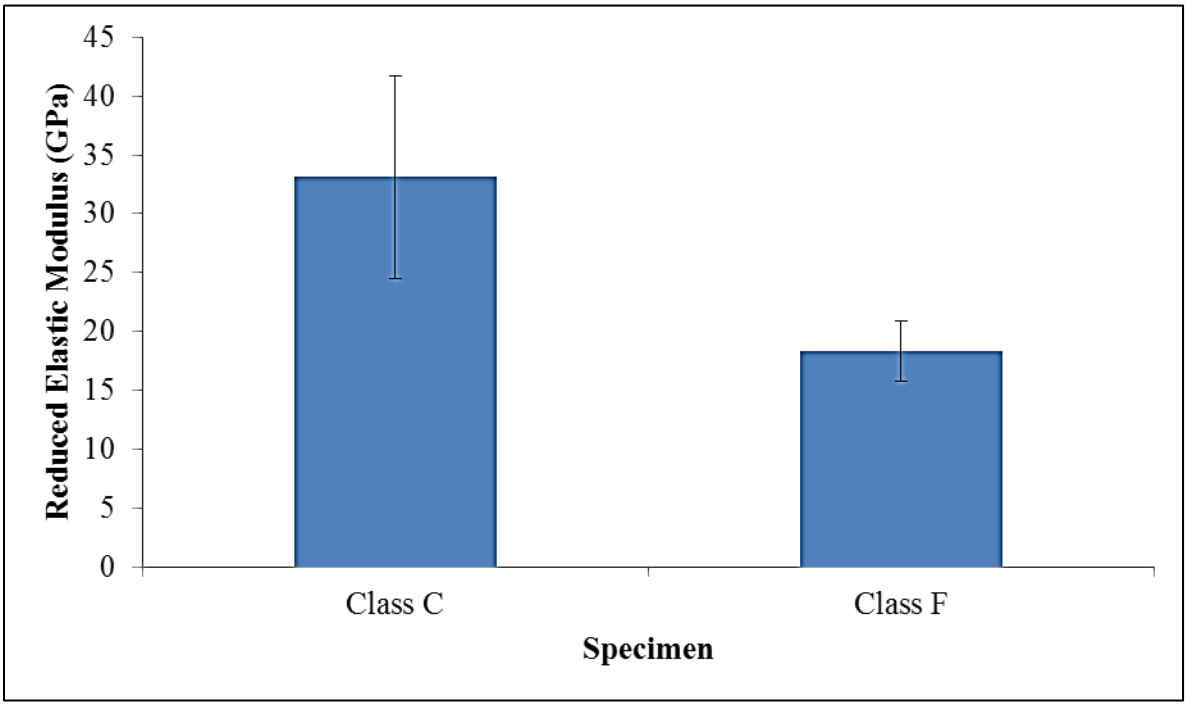

Figure 59: Average reduced elastic modulus for each tested specimen

Nano-scale quasi-static indentation was performed on both samples of fly ash particles by applying a force to an indenter tip while measuring tip displacement into the specimen. From the load-displacement curve, hardness and reduced elastic modulus values were determined by applying the Oliver-Pharr method using a pre-calibrated indenter tip area function and a pre-determined machine compliance value [14, 95].

Figure 58 and **Figure 59** show the average hardness and reduced elastic modulus, respectively, for all tested specimens. Class C fly ash nanoparticles showed higher hardness and modulus of 1.36 GPa ($1.9 * 10^5$) and 33.10 GPa ($48 * 10^5$) respectively. Class F fly ash nanoparticles showed hardness and modulus of 1.23 GPa ($1.8 * 10^5$) and 18.35 GPa ($26.6* 10^5$), respectively [12].

The measurement of the average value of reduced elastic modulus provides information about the extent of deformation that can happen to the proppants when subjected to stress. The conductivity of the fracture is adversely affected when the proppants get compressed. An average reduced elastic modulus of 33 GPa for class C and 20 GPa for class F shows the ability of the fly ash particles to withstand deformation. The conductivity of the fly ash proppant pack would be studied in the next section [12].

The hardness of a material is the measure of how resistant the material is to permanent deformation under the effect of a compressive stress. It is very important that the nano-proppants placed inside the fractures are able to withstand the effective minimum stress usually encountered in the horizontal direction, and the absolute vertical stress which is a function of their depth under the surface. A hardness value of 1.3 GPa for class C and 1.2 GPa for class F translates to 1.8×10^5 psi and 1.7×10^5 psi, respectively, which implies that these nano-proppants can withstand more than the maximum stresses encountered in typical shale formations [12].

5.2.3 API Static Fluid Loss Tests

Static fluid loss tests were conducted using class ‘F’ sample fly ash particles to investigate their potential fluid loss reduction capability. They were tested on both high permeability and low permeability cores separately.

5.2.3.1 Tests on High Permeability Indiana Limestone Cores (1-10 mD)

Fluid loss tests were conducted on Indiana limestone (IL) core samples having permeability values in the range of 1-10 mD. The results obtained from the first experiment, where the borate cross-

linked 5000 ppm Hydoxypropylguar (HPG) solutions were mixed in 2% KCl, were compared with that of the second experiment, where borate cross-linked 5000 ppm HPG solution was mixed with 1% fly ash samples in 2% KCl, and with the third experiment, where 1% fly ash mixed in 2% KCl was used as the test fluid. The final concentration of cross-linked guar was made to 3077 ppm in both the cases and the total volume of fluid was maintained constant at 234 ml so that the results could be compared with each other to study the effect of the addition of fly ash.

The volume of each fluid and their respective combinations used in all the fly ash experiments are given below [12].

- Case 1: 45 ml 2%KCL+ 144 ml HPG(5000 ppm) + 45 ml Borate cross-linker, the final concentration of HPG in the solution was 3077 ppm
- Case 2: 2.34 g of fly ash in 42.66 ml of 2%KCL + 144 ml HPG(5000 ppm) + 45 ml Borate cross-linker, the final concentration of HPG in the solution was 3077 ppm
- Case 3: 2.34 g of fly ash added to 231.66 ml of 2% KCl solution [12]

Table 20 summarizes all the core plugs used for API static fluid loss tests along with their porosity and permeability values.

Table 20: Porosity and Permeability of the cores used *[12]*

Core name	Porosity (%)	Permeability (mD)
IL#15	5.3	4.53
IL#16	5.49	4.7
IL#8	5.76	6.8

Table 21: Summary of fluid properties, measured fluid loss volumes and calculated fluid loss coefficients *[12]*

Core	Fluid	Total fluid loss volume, ml	C_w (ft./min$^{1/2}$)	Total time, minutes
IL#15	144 ml HPG+45 ml Borate + 45 ml 2% KCL	6.93	0.42	90
IL#16	144 ml HPG+45 ml Borate + 45 ml (fly ash+ 2% KCl)	4.07	0.31	90
IL#8	150ml 2%KCL+2.34 g fly ash class F	221.6	NA	90

Table 21 21 gives a summary of the fluids used for fluid loss testing using different cores. Total fluid loss volume and fluid loss coefficients related to each test have also been reported in **Table 21**. Fluid loss curve obtained when 1% fly ash solution was used with cross-linked HPG solution is shown in Appendix 9.3. **Figure 60** shows the cumulative fluid loss volume obtained for different tests using Indiana Limestone Cores.

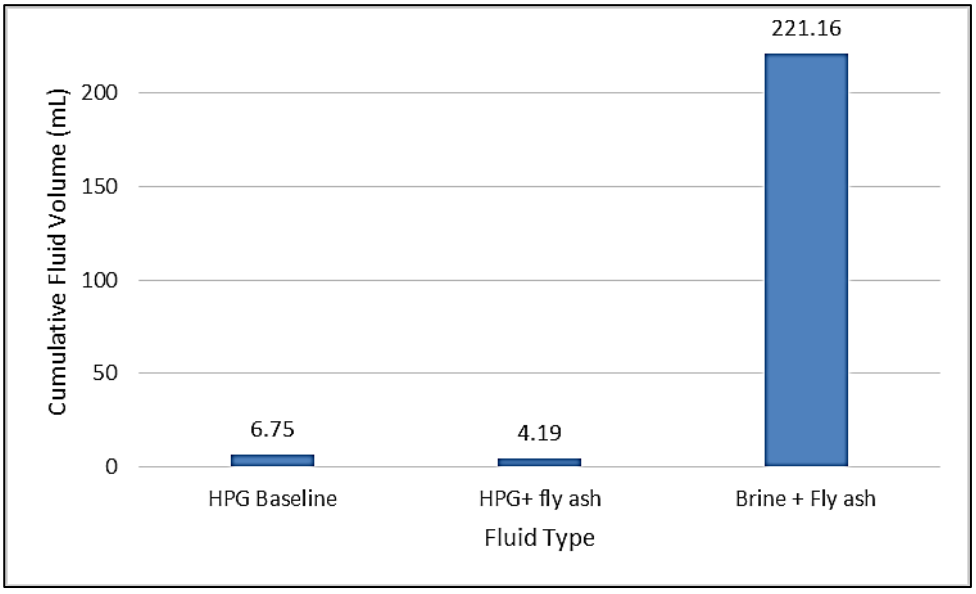

Figure 60: Fluid loss volume obtained for different fluid types using fly ash *[12]*

Fly ash nanoparticles performed as strong fluid loss control additives both by reducing the fluid loss coefficient and the total fluid loss volume. There was an increase in the mass of the external filter cake deposited on the surface of the core sample when the fly ash particles were used with cross-linked HPG solution. The mass of the external filter cake was found to be 1.6 g. The mass of the core sample after removing the external filter cake was still higher than the mass of the core

before the tests (by 0.2 g). This indicates that fly ash particles contributed to formation of internal filter cakes in the cores.

Figure 61: Filter cake formed with cross-linked HPG gel+ fly ash solution [13]

Figure 62: Filter cake formed with fly ash in 2% KCl solution [13]

Table 22: Core Permeability Before and After Fluid Loss Tests

Core	**K Before the test (mD)**	**Fluid (234 ml)**	**K After the test (mD)**
IL-15	5.58	144 ml HPG+45 ml Borate + 45 ml 2% KCL	5.73
IL-16	6.12	144 ml HPG+45 ml Borate + 45 ml (fly ash+ 2% KCl)	2.88
IL-8	6.61	150ml 2% KCL+2.34 g fly ash class F	6.44

The permeability reduction of the cores in experiments were fly ash particles were used shows the contribution of fly ash nanoparticles in forming an internal filter cake.

When fly ash particles were suspended in 2% KCl, fly ash particles tended to settle very quickly and non-uniformly. Due to the absence of a viscosifying agent (guar), there was no way to ensure a uniform distribution of fly ash in the solution. **Figure 62** shows that after the fluid loss, the filter cake that is formed using 1% fly ash solution in 2% KCl is not uniform. Even though there were no visible particles in the fluid that was lost, the filter cake that existed allowed the fluid to easily flow through, which resulted in a very high fluid loss volume. **Figure 61** shows that with the addition of cross-linked guar to the 2% KCl and class F fly ash, a uniform filter cake was formed which apparently reduced the fluid loss. This can help explain the significant difference in fluid loss volumes that were observed between the experiments where fly ash was used with only 2% KCl and where fly ash was used with cross-linked guar [12].

The tests were repeated for the two cases with cross-linked HPG solution to ensure the reproducibility of results (**Figure 64**). Fluid loss coefficient values obtained for different tests are shown in **Figure 63**.

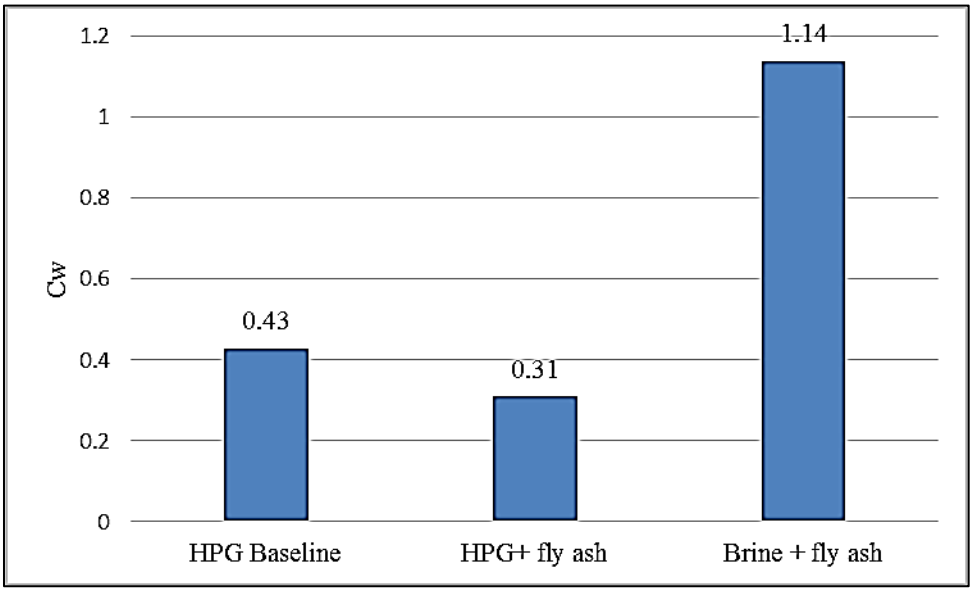

Figure 63: Fluid Loss Coefficients (C_w) Obtained for Different Fluids

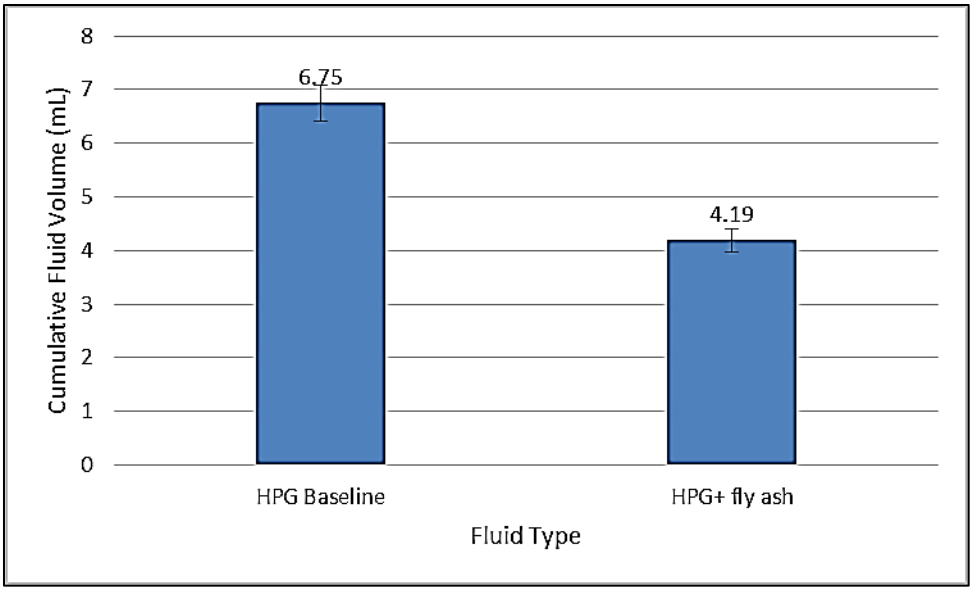

Figure 64: Fluid loss volume for multiple tests using fly ash- Standard deviation: n=2

A significant reduction in the fluid loss volume and coefficient was observed when fly ash particles were added to the cross-linked HPG gel solution compared to the case where there were not any fly ash particles in the solution. Fluid loss prevention capability of the fly ash nanoparticles has been thus proved for cores with 1-10 mD permeability range. This will prevent the loss of fracturing fluid to intermittent relatively higher permeability zones that usually exist in shale formations because of reservoir heterogeneity. Fluid loss prevention to such 'thief zones' will aid in the generation of longer fracture wings as well as in the extension of network of fractures during a hydraulic fracturing job for the same volume of injected fracturing fluids [14, 60].

5.2.3.2 Tests on Low Permeability Kentucky Core Samples (0.1-1 mD)

Fluid loss tests were carried out with fly ash nanoparticle tests on low permeability Kentucky core samples. Lower concentration of HPG solution (769 ppm) which was not cross-linked was used in these tests to simulate slickwater treatments in low permeability reservoirs. Despite showing favorable results in the initial tests, the results were found to be non-reproducible in the subsequent tests.

The fly ash nanoparticles were found to be highly successful as a fluid loss reduction additive when used with high permeability reservoirs. However, the results on low permeability cores could not be reproduced.

5.2.4 Hydraulic Fracture Conductivity Tests

Long term fracture conductivity tests complying with the API recommended procedures were conducted using Scioto sandstone cores with permeability values of approximately 0.01 mD. Fly

ash samples of class F were used as proppants between two core wafers placed under stress. With the prior knowledge of the fracture width generated by 3lbm/ft^2 of Carbo econoprop proppants, quantity of fly ash required to create an almost same fracture width was estimated by knowing the density of the material. Fracture conductivity of this proppant pack was measured at different overburden stress values and the results are shown in **Figure 65**. Results show the reduction of fracture conductivity as a function of closure stress.

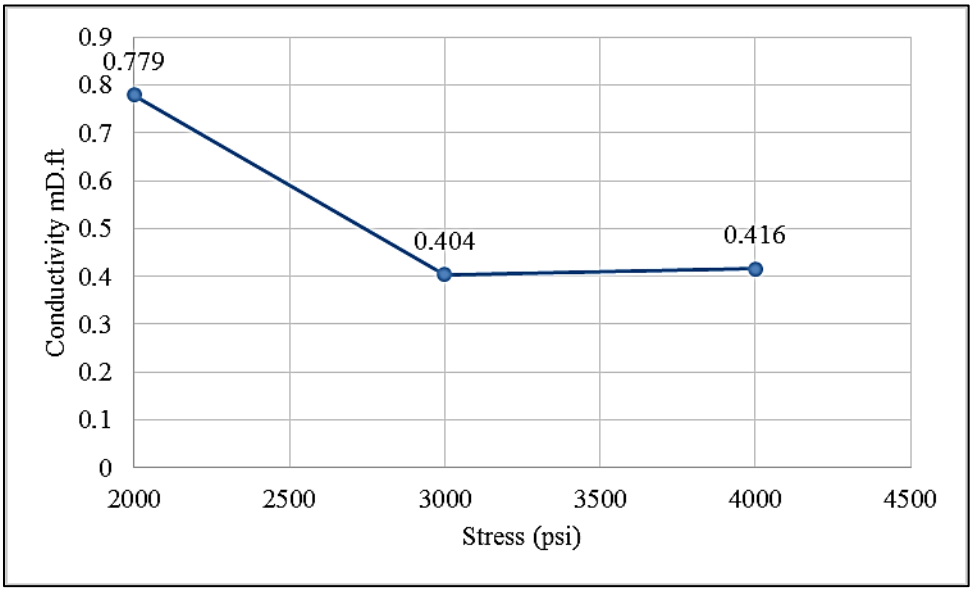

Figure 65: Proppant Conductivity (fly ash) vs Stress

Fracture conductivity of 0.779 mD.ft was obtained for class F fly ash sample at 2000 psi which translates to a dimensionless fracture conductivity value of 7.8, when the matrix permeability is 100 nD and effective fracture length is 1000 ft. [12].

Dimensionless fracture conductivity (F_{cd}) of a bi-wing vertical fracture is given by

$$Fcd = (K_f * W_f)/(K * X_f) \quad \text{Eq. 5}$$

Where:

K_f= fracture conductivity

W_f = fracture width

K= Matrix permeability

X_f= Effective fracture length

Prats [84] showed that a significant increase in production would not be caused because of an increase in the dimensionless conductivity beyond 10 or 20. This implies that the fly ash nanoparticles when injected as nano-proppants prior to the injection of conventional proppants, would prop and ensure a good fracture conductivity inside the micro-fractures [12].

5.2.5 Summary

For the shale formations, where the formation permeability is usually very low, injection of fly ash ahead of commercial proppants is recommended to pack the network of micro-fractures [85]. Fly ash particles were tested for their size, hardness, reduced elastic modulus, fluid loss prevention capabilities as well as for their induced fracture conductivity. All tests supported the application of fly ash nanoparticles as fluid loss additives and nano-proppants.

6. Conclusions

6.1 Polyelectrolyte Complex Nanoparticles (PEI-DS)

After conducting a series of experiments using PEC nanoparticles in the fracturing fluid, we arrived at the following conclusions.

1. The PEC nanoparticles acted as efficient fluid loss reducing agents for both high permeability and low permeability formations. The nanoparticles with close to 500 nm average particle size showed good results with both cross-linked as well as slick water fluids. This could significantly reduce the damage to the formation which normally occurs during hydraulic fracturing due to fluid leak-off. The reduction in fluid loss helps in creating longer fractures with the same volume of injected fluid and ultimately increase production.
2. From the results of the HPGNP long term fracture conductivity experiment, it was observed that the use of nanoparticles without breakers produced higher conductivity proppant pack than the HPG Baseline case.
3. The enzyme entrapped in the nanoparticles used in HPGEE gave the best conductivity results among all the tests carried out with fracturing fluids, which could be explained as a cumulative effect of enzymes and nanoparticles in breaking down the cross-linked gel.
4. A nanoparticle system with dual application is presented in this work which results in a system with multiple capabilities including delayed release and protection against high pH of enzymes [2], fluid loss reduction capabilities, as well as efficient fracture clean up results [52].

6.2 Fly Ash Nanoparticles

Fly ash nanoparticles were found to have the following properties:

1) High sphericity and nanometer dimensions of the fly ash nanoparticles as observed from the TEM images make them ideal candidates to prop micro-fractures in unconventional reservoirs.
2) Fly ash nanoparticles are inexpensive and possess good mechanical strength and reduced elastic moduli. Commercial proppants used in shale formations are usually tested between 4000 and 12,000 psi. Nano-indentation tests results show that fly ash nanoparticles can withstand stress values in this range without undergoing deformation.
3) When used with fracturing fluids, class F fly ash nanoparticles were found to be effective fluid loss additives for high permeability core samples (1-10) mD. This implies that they can reduce fluid loss to intermittent high permeable zones found in unconventional reservoirs when used with fracturing fluids.
4) Class F fly ash nanoparticles formed a conductive proppant pack when used as proppants in the long term fracture conductivity experiments.

The results of this study show that fly ash nanoparticles can potentially be used as both fluid loss reduction additives as well as nano-proppants for hydraulic fracturing in tight and ultra-tight formations. These particles can reduce fluid loss to high permeable formations (1-10 mD) during the propagation of hydraulic fractures while they pack the system of micro-fractures induced by propagation of hydraulic fractures.

7. Nomenclature and Abbreviations

cP: Centi Poise

C_W: wall building coefficient (ft. / $min^{1/2}$)

DS: Dextran Sulfate

FA: Fly ash

HPG: Hydroxy Propyl Guar

HPGE: HPG + Enzyme

HPGEE: HPG+ Enzyme Entrapped in Nano-particles

HPGNP: HPG + Nanoparticles

K: Permeability

K_f: Fracture permeability

mD: Milli-Darcy

NP: Nano-Particles

PEC: Polyelectrolyte Complex

PEI: Polyethylenimine

R.O: Reverse Osmosis

SRV: Stimulated reservoir Volume

TEM: Transmission Electron Microscope

8. References

[1] R. Barati, R. Hutchins, T. Friedel, J. Ayoub, M. Dessinges and K. England, "Fracture Impact of Yield stress and fracture-face damage on production with a three phase 2D Model," *SPE productions & operations*, 2009.

[2] R. B. Ghahfarokhi, "Fracturing Fluid Cleanup by Controlled Release of Enzymes from Polyelectrolyte Complex Nanoparticles-PhD thesis," University of Kansas, Lawrence, 2010.

[3] R. J. Smith, J. R. Loscutova, E. A. Whitsitt, C. E. Coker, A. R. Barron, M. Wiesner, S. A. Costantino and R. K. Bordia, "Composition and method for making a proppant," Oxane materials Inc. - Patent Application Number: US8603578 B2, 2012.

[4] "AGSCO Corporation Technical data".

[5] M. Economides and K. Nolte, Reservoir Stimulation. 3 ed., John Wiley & Sons, Inc:, 2000.

[6] D. Davies and T. Kulper, "Fracture Conductivity in Hydraulic Fracture Stimulation," *Journal of Petroleum Technology,* 1988.

[7] J. Ayoub, A. Hill, C. Montgomery and S. Scott, "Spotlight on R&D: Production Operations R&D- Optimizing Performance From Sandface to the Tanks," *JPT SPE Journal Paper*, vol. 4, pp. 36-39, 2004.

[8] R. Seright, R. Scharder, J. Hagstrom, Y. Wang, A. Al-Dhafeeri and R. Gary, "Conformance Improvements Using Gels-Report," New Mexico Petroleum Recovery Research Cent, Socorro, New Mexico, Sept 2002.

[9] J. Elbel and J. Ayoub, "Evaluation of Apparent Fracture Lengths Indicated From Transient Tests," *Journal of Canadian Petroleum Technology,* vol. 31, no. 10, December 1992.

[10] E. May, L. Britt and K. Nolte, "The Effect of Yield Stress on Fracture Fluid Clean-up," in *SPE Annual Technical Conference and Exhibition*, San Antonio, TX, Oct 5-8, 2007.

[11] O. Jaripatke, B. Grieser and K. Chong, "A Review Of Successful Approach Towards Shale Play Stimulation In The Last Two Decades - A Completions Road Map To Shale Play Development," in *SPE Deep Gas Conference and Exhibition*, Manama, Bahrain, 2010.

[12] C. Bose, T. J. B Fairchild, A. Gul and R. Ghahfarokhi, "Application of nanoproppants for fracture conductivity improvement by reducing fluid loss and packing of micro-fractures," *Journal of Natural Gas Science and Engineering,* Vols. 27, 424-431, November 30, 2015.

[13] J. Cai, M. Chenevert, M. Sharma and J. Friedheim, "Decreasing Water Invasion Into Atoka Shale Using Nonmodified Silica Nanoparticles," *SPE Drilling and Completion,* March, 2012.

[14] J. Ayoub, R. Hutchins, F. Van der bas, S. Cobianco, C. Emiliani, M. Glover, M. Kohler, S. Marino, G. Nitters, D. Norman and G. Turk, "New Findings in Fracture Cleanup Change Industry Perceptions," in *SPE International Symposium and Exhibition on Formation damage Control*, Lafayette, LA, 15-17 February 2006.

[15] J. L. Gidley, S. A. Holditch, D. E. Nierode and R. W. Veatch Jr, Recent Advances In Hydraulic Fracturing, SPE, 1990.

[16] P. C. Harris, "Fracturing-Fluid Additives," *Journal of Petroleum Technology*, vol. SPE Distinguished Author Series, 1988.

[17] C. Montgomery, "Fracturing Fluids," Free Article, 2013.

[18] M. Robert and Tjon-Joe-Pin, "Enzyme Breaker for Galactomannan Based Fracturing Fluid," US Patent 5201370, April 13, 1993.

[19] J. Weaver, E. Schmelzl, M. Jamieson and G. Schiffner, "New Fluid Technology Allows Fracturing Without Internal Breakers," in *SPE Gas Technology Symposium*, Calgary, Alberta, 2002.

[20] C. Montgomery, "Fracturing Fluid Components," Free Article, 2013.

[21] G. Schein, "The Application and Technology of Slickwater Fracturing," SPE Distinguished Lecture, 2004-2005 Season.

[22] M. Mayerhofer, E. Lolon, J. Youngblood and J. Heinze, "Integration of Microseismic Fracture Maping Results With Numerical Fracture Network Production Modelling in the Bernett Shale," in *SPE Annual Technical Conference and Exhibition*, San Antonio,TX,USA, 2006.

[23] "http://www.halliburton.com/public/pe/contents/Data_Sheets/web/H/H05667.pdf," Report Halliburton.

[24] R. Barati, "Personal communications between Reza Barati and top representatives of Schlumberger, Halliburton, and Baker Hughes about their fracturing jobs in Texas, North Dakota and Oklahoma," SPE Forum about Numerical Modeling in Unconventional Reservoirs," New Port Beach, California.

[25] S. Laramay, L. Norman, B. Carathers and H. Services, "The Effect of Delayed Enzyme Breakers on Filter Cake Cleaning in Southeastern New Mexico Stimulation Jobs," in *SPE Permian Basin Oil and Gas Recovery Conference*, Midland. Texas, March 18-20, 1992.

[26] A. Tayal, R. M. Kelly and S. A. Khan, "Viscosity Reduction of Hydraulic Fracturing Fluids through Enzymatic Hydrolysis," *SPE Journal*, vol. 2, 1997.

[27] J. Ayoub, R. Hutchins, F. Van der Bas, S. Cobianco, C. Emiliani, M. Glover, M. Kohler, S. Marino, G. Nitters, D. Norman and G. Turk, "New Results Improve Fracture Cleanup Characterization and Damage Mitigation," *SPE Productions & Operations*, vol. 3, no. 374-380, p. 24, 2006.

[28] G. C. Howard and C. R. Fast, "Optimum Fluid Characteristics for Fracturing Extension," in *Drilling and Production Practice*, 1957, pp. p. 261-270.

[29] J. Davis, J. J. Reynolds and H. F. Coffer, "Effect of Fluid Loss on Fracture Extension; AIME, Continental Oil & Co," in *496-G SPE conference paper*, 1955.

[30] R. Barati and J.-T. Liang, "A Review of Fracturing Fluid Systems Used for Hydraulic Fracturing of Oil and Gas Wells," *Journal of Applied Polymer Science*, 2014.

[31] H. D. Brannon and R. J. Pulsinelli, "Breaker Concentrations Required to Improve the Permeability of Proppant Packs Damaged by Linear and Cross-linked Fracturing Fluids," *SPE Production Engineering*, Vols. 7, (4), pp. 338-342, 1992.

[32] C. E. Cooke, "Conductivity of Fracture Proppants in Multilayers," *J. Pet. Tech,* pp. 1101-7, Sept. 1973.

[33] T. Palisch, R. Duenckel, L. Bazan, H. Heidt and G. Turk, "Determining Realistic Fracture Conductivity and Understanding Its Impact on Well Performance—Theory and Field Examples," in *Hydraulic Fracturing Technology Conference*, College Station, 2007.

[34] Inyang, Ubon; Fontenelle, Lucas; Schultheiss, Nate;, "Proppant Pack Permeability, Does it Matter? Field Case Histories of a Nearly Residue Free Cross-Linked System-SPE 168159," in *SPE International Symposium and Exhibition on Formation Damage Control*, Lafayette, Louisiana, 26-28, February, 2014.

[35] J. Tannich, "Liquid Removal from Hydraulically Fractured Gas Wells," *Journal of Petroleum Technology,* 1975.

[36] C. M. Kim and J. A. Losacano, "Fracture Conductivity Damage Due to Crosslinked Gel Residue and Closure Stress on Propped 20/40 Mesh Sand- SPE 14436," in *60 th Annual Technical Conference and Exhibition of the Society of Petroleum Engineers*, Las Vegas, Sept 22-25, 1985.

[37] L. Roodhart, T. Kuiper and D. R. Davies, "Proppant Rock Impairment During Hydraulic Fracturing-SPE 15629," in *61st Annual Technical Conference and Exhibition of the Society of Petroleum Engineers*, New Orleans, Oct 5-8, 1986.

[38] G. S. Penny, "An Evaluation of the Effects of Environmental Conditions and Fracturing Fluids Upon the Long-Term conductivity of the Proppants- SPE 16900," in *62nd Annual Technical Conference and Exhibition of the Society of Petroleum Engineers*, Dallas, Sept 27-30, 1987.

[39] S. Almond, "Factors Affecting Gelling Agent Residue Under Low Temperature Conditions- SPE 10658," in *SPE Formation Damage Symposium*, Lafayette, 1982.

[40] M. A. Parker and B. W. McDaniel, "Fracturing Treatment Design Improved by Conductivity Measurements Under In-Situ Conditions- SPE 16901," in *62nd Annual Technical Conference and Exhibition of the Society of Petroleum Engineers*, Dallas, Sept 27-30, 1987.

[41] G. W. Hawkins, "Laboratory Study of Proppant-Pack Permeability Reduction Caused by Fracturing Fluids Concentrated During Closure," in *63rd Annual Technical Conference and Exhibition of the Society of Petroleum Engineers*, Houston, Oct 2-5, 1988.

[42] J. Ayoub, R. Hutchins, F. Van der bas, S. Cobianco, C. Emiliani, M. Glover, M. Kohler, S. Marino, G. Nitters, D. Norman and G. Turk, "New Changes in Fracture Cleanup Change Industry Perceptions," in *SPE 98746*, 2008.

[43] K. G. Nolte and S. O. C. US4506734 A, "Fracturing Fluid Breaker System which is Activated by Fracture Closure," Patent, 1983.

[44] Elbel,J; Gulbis,J; King,M.T; Maniere,J;-Dowell Schlumberger Inc., "Increased Breaker Concentration in Fracturing Fluids Results in Improved Gas Well Performance," in *Production Operations Symposium-SPE*, Oklahoma City, Oklahoma, 1991.

[45] J. Koetz and S. Kosmella, Polyelectrolytes and Nanoparticles, Springet Laboratory, 2007.

[46] S. H. Hartig, R. R. Greene, M. M. Dikov, A. Prokop and M. Davidson, "Multifunctional Nanoparticulate Polyelectrolyte Complexes," *Pharmaceutical Research 2007,* pp. 24, (12), 2353- 2369, 2007.

[47] J. W. Waree Tiyaboonchai and C. R. Middaugh, "Formulation and Characterization of DNA-Polyethylenimine-Dextran Sulfate Nano-Particles," *European Journal of Pharmaceutical Sciences,* Vols. 19, 191-202, 2003.

[48] W. Tiyaboonchai, Development of a New Nanoparticle Delivery Vehicle Based on an Aqueous Polymer System: Polyethylenimine and Dextran Sulfate, University of Kansas, Pharmaceutical Chemistry, 2002.

[49] J. Waree Tiyaboonchai, R. C. Sims and C. R. Middaugh, "Insulin Containing Polyethylenimine-Dextran Sulfate Nanoparticles," *International Journal of Pharmaceutics,* Vols. 225, 139-151, 2003.

[50] M. Cordova, M. Cheng, J. Trejo, S. J. Johnson, G. P. Willhite, J.-T. Liang and C. Berkland, "Delayed Hpam Gelation Via Transient Sequestration of Chromium in Polyelectrolyte Complex Nanoparticles," *Macromolecules,* 41, (12), 4398-4404. 2008.

[51] S. Aldrich, "MSDS Sheet -Polyethylenimine".

[52] C. Bose, B. Alshatti, L. Swartz, A. Gupta and R. Barati, "Dual Application of Polyelectrolyte Complex Nanoparticles as Enzyme Breaker Carriers and Fluid Loss Additives for Fracturing Fluids”," in *SPE/CSUR Unconventional Resources Conference*, Calgary, Alberta, 2014.

[53] J. D. Hawsey and C. L. Jacocks, "The Use Of Fluid-Loss Additives In Hydraulic Fracturing Of Oil And Gas Wells," in *SPE California Regional Meeting*, Bakersfield, California, 1961.

[54] A. D. Taleghani, M. Ahmadi and J. Olson, "Secondary Fractures and Their Potential Impacts on Hydraulic Frcatures Efficiency," in *International Conference for Effective and Sustainable Hydraulic Fracturing*, Brisbane, Australia, May, 2013.

[55] C. Cipolla, N. Warpinski, M. Mayerhofer, E. Lolon, P. Technologies, M. Vincent and C. Ceramics, "Relationship Between Fracture Complexity, Reservoir Properties, and Fracture Treatment Design," in *SPE Annual Technical Conference and Exhibition*, Denver, Colorado, 21-24, September, 2010.

[56] M. J. Mayerhofer, E. Lolon, N. Warpinski, C. Cipolla, D. Walser and C. M. F. A. Rightmire, "What Is Stimulated Reservoir Volume?," *SPE Journal 119890-PA*, 2010.

[57] N. Warpinski, M. Mayerhofer, M. Vincent, C. Cipolla and E. Lolon, "Stimulating Unconventional Reservoirs: Maximizing Network Growth While Optimizing Fracture Conductivity. Paper SPE 114173," in *SPE Unconventional Reservoirs Conference*, Keystone, Colorado, 2008.

[58] L. Weijers, "The near-wellbore geometry of hydraulic fractures initi-ated from horizontal and deviated wells. PhD thesis," Delft University of Technology, Delft, The Netherlands, February 1995.

[59] L. Beugelsdijk, d. P. C. and K. and Sato, "Experimental Hydraulic Fracture Propagation in a Multi-Fractured Media. Paper SPE 59419," in *SPE Asia Pacific Conference on Integrated Modelling for Asset Management*, Yokohama, Japan, 2000.

[60] C. Cipolla, K. Hansen and W. and Ginty, "Fracture Treatment Design and Execution in Low Porosity Chalk Reservoirs. Paper SPE 86485," in *SPE International Symposium and Exhibition on Formation Damage Control*, Lafayette, Louisiana, USA, 2004.

[61] C. Cipolla, L. Jensen, W. Ginty and C. de Pater, "Complex Hydraulic Fracture Behavior in Horizontal Wells, South Arne Field, Danish North Sea. Paper SPE 62888," in *SPE Annual Technical Conference and Exhibition*, Dallas, Texas, Dallas, 1–4 October 2000.

[62] P. Gadde and M. Sharma, "The Impact of Proppant Retardation on Propped Fracture Lengths," in *SPE Annual Technical Conference and Exhibition*, Dallas, Texas, 9-12 October, 2005.

[63] P. Kaufman and G. S. Penny, "Critical Evaluations of Additives Used in Shale Slickwater Fracs," in *Shale Gas Production Conference*, Fort Worth, Texas, 16-18 November, 2008.

[64] S. A.Gaurav, S. E.K Dao, K. Mohanty and S.-U. o. T. a. Austin, "Ultralightweight Proppants in Shale Gas Fracturing," in *SPE Tight Gas Completions Conference*, San Antonio, 2010.

[65] H. D. Brannon, M. R. Malone, A. R. Rickards, W. D. Wood, E. J. R. and J. L. Bryant, "“Maximizing Fracture Conductivity with Proppant Partial Monolayers: Theoretical Curiosity or Highly Productive Reality?”," in *SPE Annual Technical Conference and Exhibition*, Houston, Texas, 26-29 September, 2004.

[66] A. Keshavarz, A. Badalyan, T. Carageorgos, R. Johnson and P. Bedrikovetsky, "SPE 167757 “Stimulation of Unconventional Naturally Fractured Reservoirs by Graded Proppant Injection: Experimental Study and Mathematical Model”," in *SPE/EAGE European Unconventional Conference and Exhibition*, Vienna, Austria, 25–27 February, 2014.

[67] M. Zou and D. Yang, "Nanoindentation of silica nanoparticles attached to a silicon substrate," *Tribology Letters*, vol. 22, no. 2, May 2006.

[68] EPRI (Project Manager K. Ladwig) , "Comparison of coal combustion products to other common materials - Chemical Characteristics," Electric Power Research Institute, Palo Alto, CA, 2010.

[69] ASTM, ""ASTM C618 - 08 Standard Specification for Coal Fly Ash and Raw or Calcined Natural Pozzolan for Use in Concrete".," ASTM International, 2008.

[70] "Recommended Practice Standard procedure for Evaluation of Fracturing Fluids," API Institute, 1983.

[71] J. McGowen and S. Vitthal, "Fracturing-Fluid Leakoff Under Dynamic Conditions Part 1: Development of a Realistic Laboratory Testing Procedure," in *SPE Annual Technical Conference and Exhibition*, Denver, USA, 6-9 Oct, 1996.

[72] "API Recommended Practices for Evaluating Short Term Proppant Pack Conductivity," API RP-61, Washington D.C, Oct 1, 1989.

[73] "Rhodia Product Data Sheet for Hydroxypropyl Guar Jaguar® 415 Houston, TX, 2008".

[74] http://www.carboceramics.com/attachments/wysiwyg/23/1001_67_C_Econoprop_.

[75] "Microscopy and Analytical Imaging Laboratory- University of Kansas".

[76] W. Oliver, ""“Measurement of hardness and elastic modulus by instrumented indentation: Advances in understanding and refinements to methodology”," *Journal of Material Science Research*, 2003.

[77] "Exponential Business And Technologies Company (EBATCO)".

[78] R. E. Hutchins, "Notes on the Schlumberger Static Fluid Loss Apparatus," 2010.

[79] J. M. McGowen and B. W. McDaniel, "Effect of Fluid Preconditioning and Test Cell Design on Measurment of Dynamic Fluid Loss Data," in *Annual Technical Conference and Exhibition of Society of Petroleum Engineers*, Houston, Texas, 1988.

[80] R. Hutchins, Interviewee, *Personal communication about the conductivity cell donated by Schlumberger*. [Interview]. 2010.

[81] M. Alhajari, "Weekly report#49," 2012.

[82] "Tele-Dyne Dual ISCO pump Manual".

[83] "Honeywell Pressure Transducer Manual".

[84] M. Prats, "Effect of Vertical Fractures on Reservoir Behavior - Incompressible Fluid Case," *SPE Journal*, vol. 1, pp. Number 2 pp105-118, 1961.

[85] R. Barati, "Personal communication with Reza Barati," Lawrence, Kansas, March 12, 2015.

[86] P. Rae and G. Lullo, "Fracturing Fluids and Breaker Systems – a Review of the State of the Art," in *SPE Eastern Regional Meeting*, Columbus, Ohio, 23-25 October 1996.

[87] T. Palisch, M. Vincent and P. Handren, "Slickwater Fracturing, Food for Thought," in *SPE ATCE*, Denver, Colorado, 2008.

[88] R. Horton, L. A. Moran, R. S. Ochs, J. D. Rawn and K. G. Scrimgeour, Principles of Biochemistry 2 Ed.; Prentice Hall, 1996.

[89] S. M. Moghimi, "Nanotoxicology of Synthetic Gene Transfer Vectors : Polyethylenimine and Polyfectin-Mediated Membrane Damage and Apoptosis in Human Cell Lines," *Nanomaterials for Medical Diagnosis and Therapy*, no. Kumar, C., Ed. Wiley-VCH, 2006.

[90] Y. Cheng and R. K. Prud'homme, "Enzymatic Degradation of Guar and Substituted Guar," *Biomacromolecules* , Vols. 1, (4), 782-788, 2000.

[91] R. S. Aboud and R. C. B. Melo, "Past Technologies Emerge Due to Lightweight Proppant Technology: Case Histories Applied on Mature Fields"," in *SPE Latin American and Carribean Petroleum Engineering Conference*, Buenos Aire, 2007.

[92] M. Ahmadi, A. Habibi, P. Pourafshary and S. Ayatollahi, "Zeta Potential Investigation and Mathematical Modeling of Nanoparticles Deposited on the Rock Surface to Reduce Fine Migration," in *SPE Middle East Oil and Gas Show and Conference*, Manama, Bahrain, 2011.

[93] A. Habibi, M. Ahmadi, P. Pourafshary and S. Ayatollahi, "Reduction of Fine Migration by Nanofluids Injection, An Experimental Study," in *SPE European Formation Damage Conference*, Noordwijk, 2011.

[94] D. Kundert and M. Mullen, "'"Proper Evaluation of Shale Gas Reservoirs Leads to a More Effective Hydraulic- Fracture Stimulation"," in *SPE Rocky Mountain Petroleum Technology Conference*, Denver, Colorado, 14-16 April, 2009.

[95] C. Ozyildrim and C. Zgetosky, "Laboratory Investigation of Nanomaterials to Improve the Permeability and Strength of Concrete," Virginia Transportation Research Council, Charlottesville, Virginia, 2010.

[96] M. J. Irwin and D. Muir, "Encapsulated Breaker Slurry Compositions and methods of Use-WO1999063199 A1,US Patent 6225262," 3M Innovative Properties Company, 1998.

[97] R. Barati, "Nano-Particles as Fluid Loss Additives for Hydraulic Fracturing of Tight and Ultra-tight Formations manuscript accepted (peer-reviewed) to e published in proceedings of ASME 2014 33rd International Conference on Ocean, Offshore and Arctic Engineering," in *OMAE 2014*, San Francisco, CA, USA, 2014.

[98] G. Voneiff, B. Robinson and S. Holditch, "The Effects of Unbroken Fracture Fluid on Gas Well Performance," *SPEPF,* vol. 11, no. 4, pp. 223-229, November 1996.

[99] D. Pope, L. Britt, V. Constien, A. Anderson and L. Leung, "Field Study of Guar Removal From Hydraulic Fractures," in *SPE Formation Damage Symposium*, Lafayette, LA, February 14-15, 1996.

[100] C. Cooke, "Effect of Fracturing Fluids on Fracture Conductivity," *JPT*, pp. 1273-1283, Oct 1975.

[101] R. Barati, S. Johnson, S. McCool, D. W. Green, G. P. Willhite and J.-T. Liang, "Fracturing Fluid Clean up by Controlled Release of Enzymes from Polyelectrolyte Complex Nanoparticles," *Journal of Applied Polymer Science,* vol. 121, no. 30, pp. 1292-1298, August 2011.

[102] A. R. Rickards, H. R. Brannon, W. D. Wood and C. J. Stephenson, "High Strength, Ultralightweight Proppant Lends New Dimensions to Hydraulic Fracturing Applications," in *SPE Annual Technical Conference and Exhibition*, Denver, Colorado, 5-8 October, 2003.

[103] R. Snellings, M. G. and E. J., "Supplementary cementitious materials Reviews in Mineralogy and Geochemistry 74: 211–278. doi:10.2138/rmg.2012.74.6," 2012.

[104] A. A. Khanna, "Stimulation of the natural fracture system by graded proppant injection," *Journal of Petroleum Science and Engineering,* 2013.

[105] J. Cai, M. Chenevert, M. Sharma and J. Friedheim, "Decreasing Water Invasion Into Atoka Shale Using Nonmodified Silica Nanoparticles," *SPE Drilling and Completion,* March 2012.

[106] W. Knight, "Lecture Notes : Fundamentals of Biochemistry," University of Montana, 2005.

[107] M. G. Much and G. S. Penny, "Long-Term Performance of Proppants under Simulated Reservoir Conditions," in *SPE/DOE Low Permeablity Reservoir Symposium*, Denver, Colorado, May 18-19 1987.

[108] G. Penny and M. Conway, "Fracturing Fluid leak-off and damage mechanisms in Coalbed," in *SPE rocky Mountain regional Low Permeability Reservoirs Symposium*, Denver, CO, USA, April 12-14,1993.

[109] "API Recommended Practise Standard Procedure for Evaluating of Fracturing," 1983.

[110] B. G. De Geest, N. N. Sanders, G. B. Sukhorukov, J. Demeester and S. C. De Smedt, "Release Mechanisms for Polyelectrolye Capsules," *Chemical Society Reviews*, pp. 36, 636-649, 2007.

[111] K. Industries-Products, "http://www.kocurekindustries.com/Core-sampling-services".

[112] A. C. -. 08, "Standard Specification for Coal Fly Ash and Raw or Calcined Natural Pozzolan for Use in Concrete".

9. Appendix

9.1 Calculating the quantity of proppant

Quantity of proppant can be calculated based on desired mass per unit area of proppant or the width of unstressed pack width as illustrated

Mass per unit area, expressed in lbs. per square ft. is defined as:

$$\boldsymbol{Mp = A * C}$$

A: the area of the proppant bed expressed in .

C: proppant loading expressed in pounds per square feet.

Mp: proppant mass expressed in pounds

For getting the concentration of $3\ ^{lb}/_{sq.ft}$ on the 0.9777 proppant bed of the fracture conductivity cell, 92.4 grams of proppant is required.

9.2 Calculating Fracture Conductivity

Fracture width created after the fracturing of the formation is very difficult to measure. Therefore, many researchers have used the term of fracture conductivity for representing the ability of flow in the fracture by keeping the term of permeability and width of the fracture together thus multiplying the permeability and the width of the fracture. This calculation of fracture conductivity is based on modified Darcy's law

$$k_f w = \frac{q\mu L}{1.127 w \Delta P}$$

Where:

$k_f w$ = Fracture conductivity (D.ft)

μ= viscosity of brine solution at room temperature (cP)

q= Flow rate (STB/D)

L=Distance between differential pressure measurement points (ft.)

w= width of the cell

ΔP= differential pressure recorded (psi)

9.3 Fly Ash Used as Fluid Loss Additive

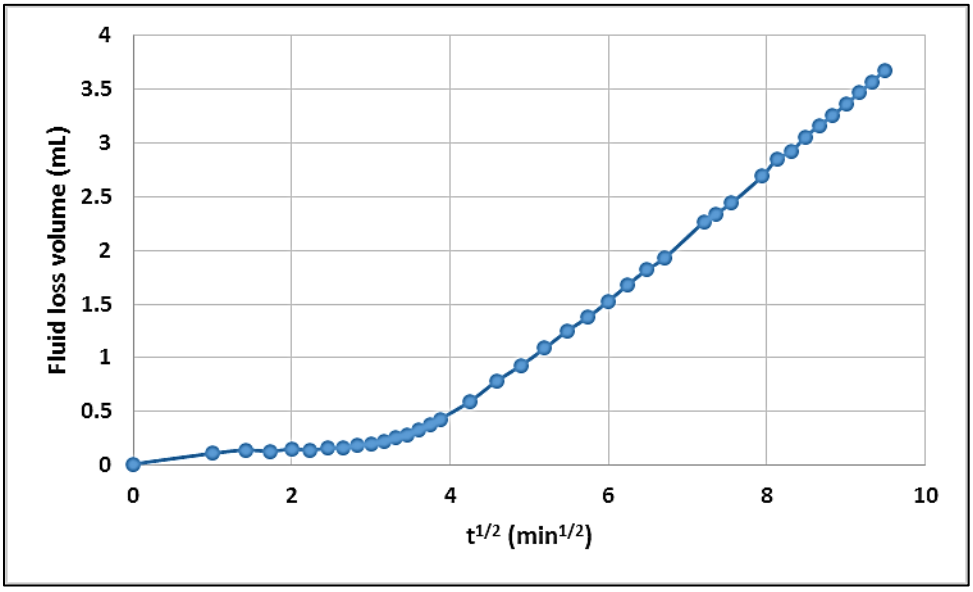

Figure 66: Fluid loss curve obtained when fly ash nanoparticles were used with cross-linked HPG solution

9.4 TEM Images of Fly Ash

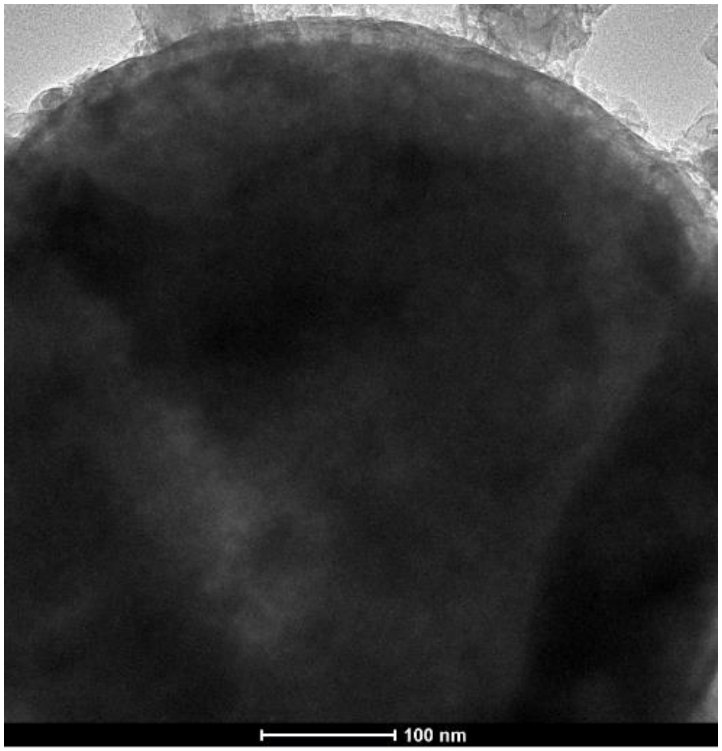

Figure 67: TEM Image of Fly Ash Nanoparticle

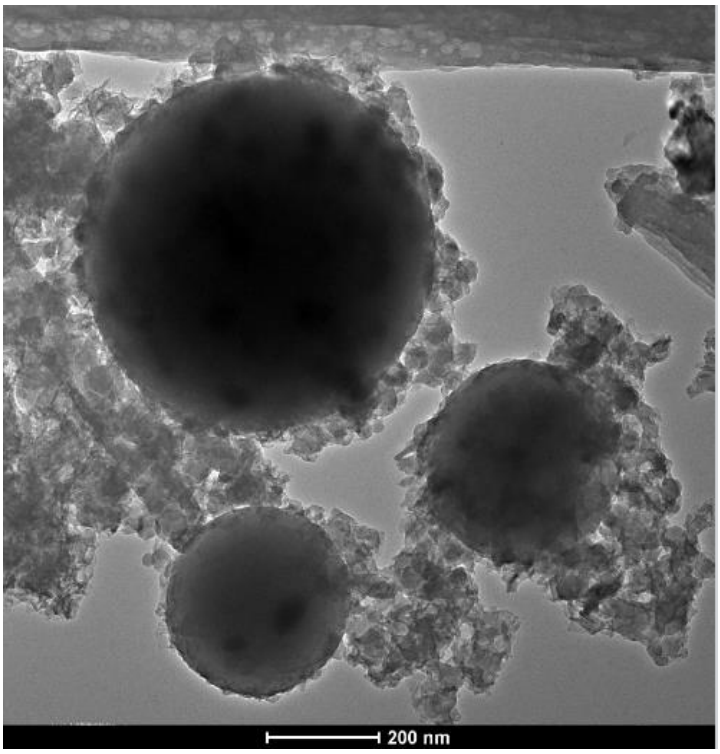

Figure 68: TEM Images of Multiple Fly Ash Nanoparticles

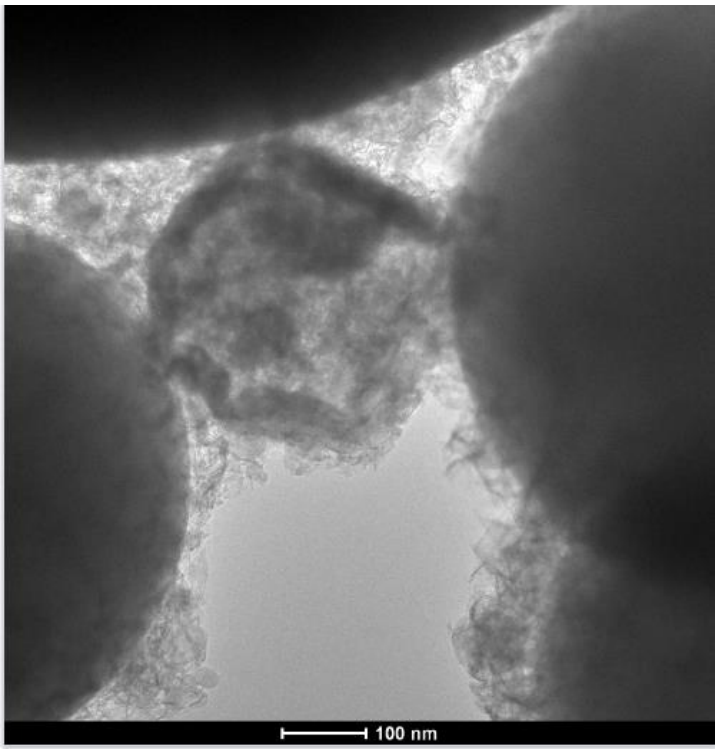

Figure 69: Fly Ash Nanoparticles and Residue